EXPERIMENTAL MEASUREMENT OF THERMAL-HYDRAULIC CHARACTERISTICS AT LOW REYNOLDS NUMBER IN WAVY FIN HEAT EXCHANGERS

FAISAL BARI AL MAHMUD

Experimental Measurement of Thermal-Hydraulic Characteristics at Low Reynolds Number in Wavy Fin Heat Exchangers

A thesis
submitted to the Memorial University of Newfoundland
in fulfilment of the requirements for the degree of

Master
In
Mechanical Engineering

2009

by

©Faisal Bari Al Mahmud

Abstract

Experiments were conducted to predict the thermal hydraulic characteristics for flow in wavy fin heat exchangers. Low Reynolds number ($0.1 < Re < 100$) and larger Prandtl number ($318 < Pr < 573$) were considered using high viscous oil. Experimental results were obtained for fifteen different fin specimens having various geometric parameters. The corrugation ratio ranged from 0.1 to 0.18, the aspect ratio ranged from 0.07 to 0.67, and spacing ratio ranged from 0.4 to 1.23.

Experimental results of heat transfer and fluid friction data for all the wavy fins exposed the presence of two flow regimes. These were: 1. the low Reynolds number regime where the flow behaviour is the same as that in rectangular ducts, 2. the laminar boundary layer regime where vortices induced in the wall waviness valley region with the increase of Reynolds number provided a higher heat transfer performance and pressure drop penalty. This could be due to the complex flow pattern in the wavy fin channels. Models for each regime were developed from fundamental solutions of fluid dynamics and heat transfer. Experimental results were compared with both models which suggested a new model.

Finally, an asymptotic model was developed by combining both analytical models for predicting the Fanning friction factor, f, and Colburn factor, j, which covered a wide range of Reynolds number. Most of the experimental data sets agreed with this model to within $\pm$ 25 %.

Acknowledgements

First and foremost, all Thanks to God!

I offer my sincerest gratitude to my supervisor, Professor Yuri Muzychka, for his invaluable support, encouragement, supervision, patience and useful suggestions throughout this research work. His friendly and positive approach made this work easier. This thesis would not have been completed or written without his guidance and assistance.

I am also highly thankful to Dr. M. M. Awad, for his helps and suggestions during the completion of this work.

I would also like to thank my parents, sisters, and brothers for their encouragement and support in my higher study.

This work was supported by Natural Sciences and Engineering Research Council of Canada (NSERC), and TAT Technologies Inc. I am very grateful to these two organizations.

To my parents and grandmother

Table of Contents

List of Tables

List of Figures

Nomenclature

A	area, m^2
$2A$	twice the wavy fin amplitude, m
c_p	heat capacity (J/kg.K)
D_h	hydraulic diameter
$E(\cdot)$	complete elliptic integral second kind
f	Fanning friction factor = $\tau_m/(0.5\rho_m u_m^2)$
F_L	effective fin conduction length, m
h	heat transfer coefficient, $W/m^2 \cdot K$
H	fin height, m
I	current, A
j	Colburn factor = $Nu_{D_h}/(Re_{D_h} Pr^{1/3})$
k	thermal conductivity, W/m·K
K	consistency index, $kg/m.s^{2-n}$
K_c	contraction loss coefficients
K_e	expansion loss coefficients
L	channel length, m
L_d	wavy fin length, m
L_e	effective length, m
L_{hy}	hydrodynamic entrance length
L^+	dimensionless hydrodynamic entrance length $= L/D_h Re_{D_h}$, m
m	fin parameter = $(2h/k_f t_f)^{0.5}$
$\dot{m}$	mass flow rate, kg/s
N_{ch}	Number of channels
Nu	Nusselt number, = h/k
p	pressure, Pa
Δp	differential Pressure, Pa

P	power, W
Pr	Prandtl number, $= \mu\, c_p / k$
Q	heat transfer rate, W
r_h	hydraulic radius, m
R	Result
Re	Reynolds number, $= D_h\, u_m / v$
RH	relative humidity
S	fin pitch, m
t	fin material thickness, m
T	temperature, K
ΔT	the temperature difference between inlet and outlet, K
u_m	average velocity, m/s
U	overall heat transfer coefficient, W/m^2·K
V	voltage, V
w_R	Uncertainty in results.
W	fin width, m
x_i	independent measure quantity

Greek symbols

α	cross-section aspect ratio = (S/H)
ε	wavy-fin-channel spacing ratio = ($S/2A$)
γ	wavy-fin-channel corrugation ratio = ($2A/\lambda$)
η_f	fin efficiency
η_o	overall surface efficiency
λ	wavy fin wavelength, m
μ	dynamic viscosity, N·s/m^2
θ	corrugation angle, $^\circ$
ρ	fluid density, kg/m^3
τ	wall shear stress, N/m^2

Subscripts

app	apparent
b	bulk value/spacing
corr	correlation
D_h	based on hydraulic diameter
f	fin
flow	flow
front	frontal
H1	constant heat flux boundary condition
i	inlet
liquid	liquid
m	mean
o	outlet
ref	reference
s	surface
T	thermal entrance region/constant wall temperature boundary condition.
total	total
w	at wall conditions
wavy	wavy fin

Acronyms

AER	area enhancement ratio (total area to basic (unenhanced) area)
ERR	entrance reduction ratio
FAR	fin area ratio (fin area to total area)
FPI	fin per inch
LBL	laminar boundary layer
LMTD	log mean temperature difference
OSF	offset strip fin
RMS	root mean square error

Chapter-1

Introduction

1.1 Introduction

This thesis is related to the experimental measurements and model development for predicting the thermal-hydraulic characteristics of compact wavy plate-fin heat exchangers. An asymptotic model has been developed for complex internal flows in wavy fins which is the combination of the asymptotic behaviour for the low Reynolds number & laminar boundary layer regions. The experiments have been conducted for fifteen different fin geometries (variable fin height, fin spacing and fin amplitude).

Previously both experimental and numerical studies have been performed on wavy fins. Most of them were predominantly with air (Pr ~ 0.7) as a working fluid, i.e. Kays & London (1984), Gschwind and Kottke (1999), Manglik (2005), Zang (2005), Muley et al. (2006), Junqi et al. [2007] etc. with tests performed for different geometric parameters. Only a few data sets are available for liquid as a working fluid, i.e. Ali and Ramadhyani (1992), O'Brien and Sparrow (1982), and Sparrow and Comb (1983), who obtained data using water in a wavy channel. Presently no data is available for high Prandtl number. The aim of the present work to obtain data for different geometrical wavy fins using 5W30 oil as a working fluid (Pr > 300) and to develop an asymptotic model for comparing and predicting the heat transfer & pressure drop characteristics.

1.2 Enhanced Heat Transfer

Heat transfer enhancement is defined as the improvement of heat transfer performance through surface and flow modification. The enhancement of heat transfer has concerned researchers and practitioners since the earliest documented studies of heat transfer,

Bergles (1998). In recent years, enhancement techniques have played an important role for the development of energy efficient heat exchangers due to increased the costs of energy and materials. The process industry is aggressively working to incorporate enhanced heat transfer surfaces in its heat exchangers, Webb and Kim (2005). At first heat exchangers were designed to use plain heat exchanger surfaces. But an enhanced surface is more efficient in transferring heat than plain surfaces. So, to fulfill a designer's objectives, an enhanced surface can be used to provide – (1) reduction in size and weight of a heat exchanger for the given heat duty and pressure drop which provide a smaller heat exchanger, (2) increase in heat exchange rate for a given fluid inlet temperatures and flow rate, (3) reduction in temperature differences which increase the thermodynamic process efficiency as well as decrease operating cost, (4) reduction of pumping power or pressure drop for a given size and heat duty. Depending on the requirement, one can chose any one or all of the above advantages of thermal enhancement.

The "enhancement ratio" (E_h) is a very important term in enhanced heat transfer. It is defined as follows, Webb and Kim (2005):

$$E_h = \frac{(hA)_{ENHANCED}}{(hA)_{PLAIN}} \qquad 1.1$$

Three basic principles are normally used to increase the "enhancement ratio" or 'hA' of enhanced surface include: (1) increase the heat transfer co-efficient 'h' without an appreciable physical area 'A' by improving the flow pattern near the heat transfer surfaces, (2) increase the heat transfer surface area 'A' without appreciably changing the heat transfer co-efficient 'h' by using extended surfaces or (3) increase both heat transfer co-efficient 'h' and heat transfer surface area 'A', i.e. heat exchanger which have extended surfaces like, louvers or corrugations which increase the heat transfer co-efficient by means of both mechanisms.

Thirteen enhancement techniques were identified by Bergles et al. (1983). These techniques may be categorized into two groups. One is 'passive' techniques which do not

need any direct application of external power but need to employ special surface geometries or fluid additives for enhancement such as extended surfaces, treated surfaces, rough surfaces, displaced enhancement devices, swirl flow devices, surface tension devices, additive for fluids and additives for gases. The other is 'active' techniques which need external power such as electric or acoustic fields, surface vibration, mechanical aids, fluid vibration and injection or suction. Passive techniques are the most commonly used technique due to their simplicity of manufacture and low cost. Extended surfaces or fins are the most reasonable passive techniques which are used in a compact heat exchanger to enhance heat transfer.

1.3 Compact Heat Exchangers

A heat exchanger having a surface area density greater than about 700 m^2/m^3 is quite arbitrarily referred to as compact heat exchanger, Kakac and Liu (1998). The hydraulic diameter for most compact heat exchangers is very small and usually at least one of the fluids is a gas. The overall heat transfer co-efficient is also generally higher than that of other types. Thus, both the large surface area density and high heat transfer co-efficient help to reduce the volume of a compact heat exchanger. Normally extended surfaces or fins are added to increase the surface area and compactness of the heat exchanger. In general addition of fins can increase the surface area by 5 to 12 times the primary surface area in general, depending on the design, Shah and Shekulic (2003). A variety of fin surfaces are available that can be used in compact heat exchanger. Special geometries of fin surfaces may provide heat transfer coefficients 50 to 150% higher than those given by plain extended surfaces, Webb and Kim (2005). In general the compact heat exchanger is classified as plate fin exchanger and tube fin exchanger. Each can contain different shapes and sizes of fins depending on the requirement. Cost and compactness are very important issues for selecting the compact heat exchanger types. The plate fin heat exchangers are cheaper and more compact than the tube fin heat exchangers per unit heat transfer surface area in general.

In plate fin heat exchangers, fins are sandwiched between two parallel plates and are joined with the plates by welding, brazing, soldering, mechanical fit or extrusion. Fluid streams flow along the passages are made by the fin corrugations between the parallel plates. The corrugations of fins act as secondary heat-transfer surfaces. It also makes a mechanical support for the internal pressures between layers. Flows through such a device are considered as laminar or low Reynolds number flows as the hydraulic diameter is very small, due to the presence of high density secondary surfaces or fins. The use of secondary surfaces provide appreciable enhancement for such low-Reynolds-number flows which is based on two basic concepts, Webb and Kim (2005), as follows:

1. special channel or surface shapes that promote fluid mixing by secondary flows. An example is the wavy channel, which provides mixing due to secondary flows and boundary layer separation within the channel.
2. repeated growth and wake destruction of boundary layers.

Fig. 1.1 shows the basic components of plate fin heat exchangers. Plate fin heat exchangers are generally designed for low pressure applications. But recently they have been used for very high pressure as a result of modern manufacturing technology.

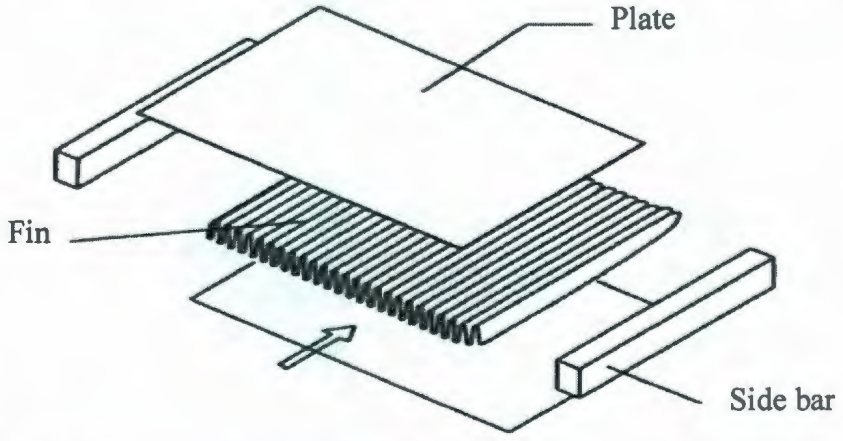

Fig. 1.1 - Basic components of plate fin heat exchangers (Kuppan, 2000).

The performance of the compact heat exchanger may vary, depending on extended or fin surface geometry, type of fin materials and other factors. These are discussed for plate-fin heat exchangers.

1) Different shapes and sizes. Such as (a) plain and straight fins, i.e. triangular and rectangular shape; (b) plain and wavy fin, i.e. corrugated or herringbone wave and

smooth wave; (c) interrupted fins, i.e. offset strip fins, louver fins, perforated fins and pin fins. Fig.1.2 shows different plate-fin exchanger geometries.

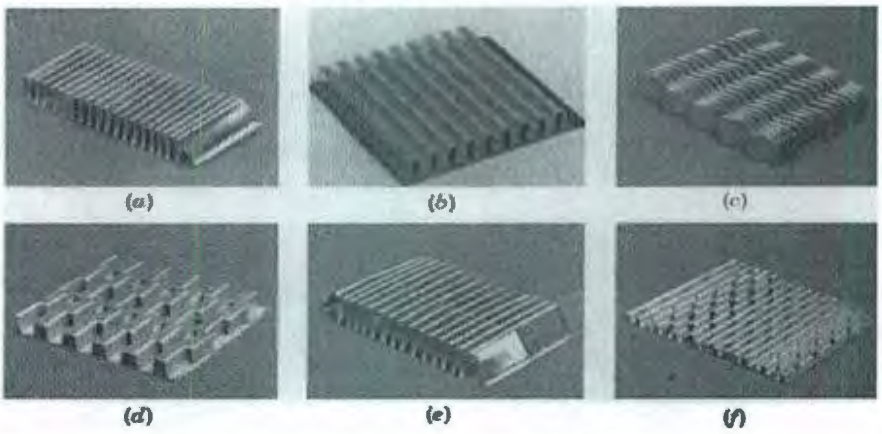

Fig. 1.2 - Plate fin exchanger surface geometries: (a) plain triangular fins, (b) plain rectangular fin, (c) wavy fins, (d) offset strip fins, (e) perforated fins, (f) louvered fins, shah and Webb (1983).

2) Number of fins per unit length. Normally these differ from 300 to 800 fins per meter, Webb and Kim (2005) and 120 to 700 fins/m, Kuppan (2000) and Gupta (1990).
3) Height of fins inside the core. Varies from 2 to 25 mm, Kuppan (2000).
4) Surface area density. Up to 6000 m^2/m^3, Shah and Sekulic (2003).
5) Thickness of the fins. Normally varies from 0.05 to 0.25 mm, Kuppon (2000) and Gupta (1990).
6) Hydraulic diameters. Varies from 1 mm to 10 mm, Zhang (2004).
7) Fin material. Generally Copper, brass, or aluminium.
8) Thermal-hydraulic characteristics as a function of the Reynolds number.

These days compact heat exchangers are used in a wide variety of applications. They are generally used in: condensers and evaporators in air-conditioning and refrigeration, aircraft oil coolers, automotive radiators, oil coolers, unit air heaters, inter coolers of compressors, and space applications etc. The demand for space-saving, light weight and economical heat exchangers has played an important role for the development of compact heat exchangers.

1.4 Wavy Fin Heat Exchanger

Figure 1-2 shows the different type of enhanced surfaces or fins which are used in compact heat exchangers according to a designer's requirement. Operating temperature, cost, bonding of fins to plates, choice of materials is the important factors to selecting fins for the heat exchangers. Wavy fins are particularly demandable for their simplicity of manufacture. Their performance is also competitive with that of most efficient offset strip fins. A wavy fin specimen is manufactured by placing a number of fins (same length and height) side by side and bonding with each other to form a number of equal spacing wavy channels. Fig. 1.3 - shows a wavy fin specimen. There are two basic types of wavy fin geometries. These are herringbone or corrugated passage and smooth passage. Fig. 1.4 - shows the two basic geometries of wavy fins. A lot of work has been done on the corrugated channel but only a few works have examined smooth wavy channels.

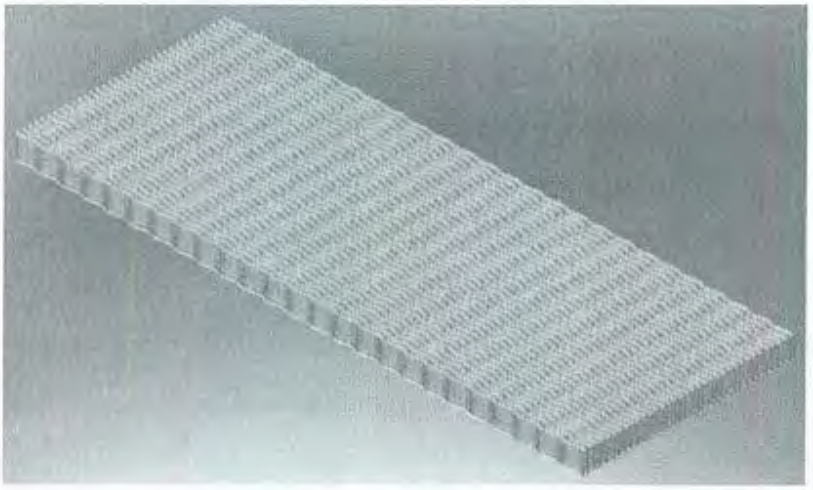

Fig. 1.3 - Wavy fin specimens

Fig. 1.4 - Two basic geometries of wavy fin; (a) herringbone or corrugated passage, (b) smooth passage.

Wavy fins have uncut surfaces in the flow directions that is why they are free from clogging or fouling and cheap to manufacture. They are wavy in the flow direction which provides effective interruptions to the flow and induces very complex flows. The augmentation is due to Goertler vortices, which form as the fluid passes over the concave wave surfaces. In this way, wavy fins can increase the heat transfer by about nearly three times as compared with the smooth wall channel, although they provide a larger pressure drop penalty.

1.5 Research Objectives

The motivation for the current research was provided by the Natural Sciences and Engineering Research Council of Canada (NSERC) and TAT Technologies Inc. TAT supplied fifteen different wavy fin specimens to test at high Prandtl number and very low Reynolds number having variable fin height H, fin spacing S and fin amplitude A.

The main objective of using wavy fin surfaces in plate-fin heat exchangers is that they can periodically interrupt the thermal boundary layer that forms on the heat transfer surfaces increasing the heat and mass transfer rate in laminar flow, although with a larger frictional penalty. Due to having uncut surfaces, these are free from fouling or clogging problems and carrying a lower manufacturing cost. As a result, many researchers have a attempted to measure and model the performance of the wavy fin heat exchanger.

Experiments are conducted to investigate the heat transfer and pressure drop characteristics through the various wavy plate-fin passages in flow regimes of Reynolds numbers from 0.1 to 100 and Prandtl numbers from 324 to 573 which are not available in any literature. To cover this range, each fin is tested at two different initial temperatures (50°C and 70°C). It is considered two dimensional flow for each case, as the ratio of fin spacing and fin height is less than 0.1. In order to show the comparative performance of wavy channel surfaces relative to bare channel, bare channel experiments are conducted at the same initial temperatures.

To predict the heat transfer and pressure drop characteristics of wavy fin channels, the experimental results are compared with both the 'low Reynolds no' and the 'laminar boundary layer region' asymptote individually. An asymptotic model by combining these two asymptotic characteristics through non linear transitions according to fundamental theory which agreed very well with the experimental data. Such a model is a robust model as it includes geometric variables (H, S, A), Reynolds number (Re) and Prandlt number (Pr). From this study, it is clear that the asymptotic behaviour is present in wavy fin data which has not been addressed in any of the literature.

The new experimental results for high viscous liquid and the newly developed asymptotic model can provide useful guide for the design and modification of wavy plate-fin surface and also for design of related compact heat exchanger.

1.6 Thesis Outline

This thesis contains six chapters. These are

- Chapter 1 which introduces the principles and techniques of enhanced heat transfer, and brief discussions of compact and wavy fin heat exchangers and current research objectives.
- Chapter 2 which reviews the current available models and experiments on wavy fin heat exchangers.
- Chapter 3 which explains the experimental measurement procedure for wavy fins being examined in this thesis.
- Chapter 4 which presents the reduction of experimental data into standard non-dimensional forms.
- Chapter 5 which provides the development of the wavy fin model and comparisons with the experimental data.
- Chapter 6 which summaries the present work and make recommendations for future work.

Chapter-2

Literature Review

2.1 Introduction

This chapter reviews the current available experimental and numerical investigations on wavy fin heat exchangers. Results from both investigations are related to the thermal-hydraulic characteristics of different geometric wavy channels and performance evaluations with comparisons to straight channels. Only the most general and similar studies to the present work are reviewed. Experimental and numerical studies are discussed separately.

2.2 Experimental Studies on Wavy Channel

Kays and London (1984) provided data on wavy fin geometries for three sets of geometric parameters using air as a test fluid. These geometries had (fins per inch) FPI = 11.4, 11.5 and 17.8, respectively, with a wavelength, λ = 0.375 in (9.525 mm).

Goldstein and Sparrow (1977) performed experiments on a corrugated wall channel to determine the local and average heat/mass transfer characteristics for laminar, transitional and low Reynolds number turbulent flow regimes range from Re=150 to Re=8550 by using a naphthalene sublimation technique. The flow channels were not sinusoidal but triangular as fig. 1.4 which had two corrugation cycles (corrugation angle=21 degrees). The flow behaviour is almost similar in both sinusoidal and triangular wavy channels. They measured the local mass transfer both in spanwise (i.e., cross steam) and streamwise directions. They also determined the overall mass transfer rates. They observed different types of complex transfer processes and related fluid flow phenomena in their experiment such as secondary flows with associated span wise mass transfer

variations, suppression of secondary flow effects by a counteracting centrifugal force, destruction of the secondary flow by the onset of turbulence, the coexistence of turbulent and nonturbulent flows in different part of the channel and the respective suppression and augmentation of the mass transfer rates by separation and by reattachment. Finally, they concluded that corrugated channels act as effective augmented heat transfer devices for low-Reynolds-number turbulent flows. Since they experimentally found moderately larger average mass transfer co-efficients in the laminar flow range (Re=1000-1200) but nearly three times larger average transfer co-efficient in low-Reynolds-number turbulent regimes (Re=6000-8000) due to wall corrugation. However, a greater pressure drop penalty was found in that turbulent flow regime.

O'Brien and Sparrow (1982) studied similar flow geometry as Goldstein and Sparrow (1977) to determine the forced convection heat-transfer coefficients and friction factors. But the corrugation angle was 30 degrees and the interwall spacing was equal to the corrugation height in their experiment. Fully developed conditions were not attained due to having only two corrugation facets, owing to the difficulty of fabricating a long corrugated duct using naphthalene in the previous experiment Goldstein and Sparrow (1977). But the authors O'Brien and Sparrow (1982) did their experiments in a corrugated duct using water (Pr = 4 to 8 by varying the temperature level) as a working fluid and the Reynolds number ranged from 1500 to 25000 based on the duct hydraulic diameter. A highly complex flow pattern, including large zones of recirculation adjacent to the rearward-facing corrugation facets was found by using the oil-lampblack flow visualization technique. They obtained the following correlation of heat transfer for corrugated duct surface:

$$Nu_{D_h} = 0.409\, Re_{D_h}^{0.614}\, Pr^{0.34} \qquad 2.1$$

In equation 2.1, the value (0.614) of the exponent of Reynolds number is lower than the value (0.8), the exponent of Reynolds number for a standard turbulent duct-flow situation. To match the dimensionless parameters of Goldstein and Sparrow (1977), they used the vertical inter-wall spacing as the characteristic dimension and obtained tabulated forms of Nusselt, Sherwood and Reynolds numbers. From tabulated results, they found that the values obtained by Goldstein and Sparrow (1977) were 50 % lower at the lowest

Reynolds number and 27% lower at highest Reynolds number than their study. They proposed that this type of disagreement must be due to the differences in geometry, degree of flow development, and boundary conditions. Finally they found from their experiment that heat transfer rates were approximately 2.5 times larger than that for the straight channel. But the average magnitude of the friction factor was 0.57, which was very high when compared to conventional pipe flows.

Sparrow and Comb (1983) did the same experiment in a similar geometry except with a wider inter-wall spacing. They considered a 2.6 mm wider inter-wall spacing than in O'Brien and Sparrow (1982). Also, they examined the role of the non-corrugated side walls in the evaluation of the heat transfer coefficient. Using a least-square fit of the experimental data, they obtained the following correlation for the Nusselt number for corrugated wall:

$$Nu_{D_h} = 0.491 Re_{D_h}^{0.632} Pr^{0.3} \qquad 2.2$$

They carried out performance evaluations for different constraints - fixed pumping power, fixed pressure drop, and fixed mass flow. They observed that the heat transfer was increased approximately 30 % and pressure drop was more than doubled than O'Brien and Sparrow (1982). They proposed that it was due to the wider inter-wall spacing channel where the recirculation zone became larger.

Sparrow and Hossfeld (1984) conducted experiments to determine the forced convection heat transfer, pressure drop, and flow field responses to the rounding of the peaks of a corrugated-wall duct. They considered two different degrees of corrugation-peak roundedness and also tasted the sharp corrugation peak channel for comparison. The experiments were carried out over the Reynolds number ranged from 2000 to 33000 and for Prandtl numbers between 4 to 11 by using water as test fluids. They observed that both the heat transfer and friction factor were decreased with the increase of the rounding of the corrugation peaks at a fixed Reynolds number. In the lower portion of the investigated Reynolds number range ($2000 \leq Re \leq 10000$), the rounding related reduction was moderate (not more than 8%) but larger reductions (up to 18%) were followed at higher Reynolds numbers (at 30,000). The pressure drop was also reduced to 40% of the

sharp-peak corrugation valley in the case of more-rounded corrugations. They also compared on the basis of equal pumping power. But any sensible reduction of Nusselt number was not found due to rounding of the corrugation peaks except 5-6% decrease for very large Reynolds numbers. Flow visualization experiments showed that rounding reduced the size of the separated region that was spawned at each corrugation peak.

Ali and Ramadhyani (1992) also conducted experiments to study flow visualization and convective heat transfer in the entrance region of corrugated channels. Two different channel spacing were considered having 20 degrees corrugation angle in both cases. Water was used as working fluid and the flow rate was varied over the range $150 \leq Re \leq 4000$. They made a comparison of the geometric conditions of previous studies with their study which is given below.

Table-2.1

Comparison of Geometric Conditions of Wavy Fin

Investigators	Spacing, b (mm)	wavelength, L_c (mm)	Corrugation, degree	No. of cycles
O'Brien and Sparrow (1982)	5.9	20.3	30	10
Sparrow and Comb (1983)	8.5	20.3	30	10
Sparrow and Hossfeld (1984)	8.5	20.3	30	10
Molki and Yuen (1986)	5.5, 8, and 11	19	30	20
Goldstein and Sparrow (1977)	1.65	9.3	21	2
Beloborodov and Volgin (1971)	5	20	26.6	58
Ali and Ramadhyani (1992)	6.9 and 10.3	45.7	20	5

Flow visualization studies indicated that the presence of streamwise vortices or longitudinal vortices at low flow rate and spanwise vortices at higher flow rate in both the corrugated channels. By testing both corrugated channels, they proposed that there were no benefits at steady and laminar flow ($Re < 500$) because no moderate augmentation of heat transfers were found but increase of pressure drop were observed in that ranges. The performance evaluation indicated that both the corrugated channels are superior to the parallel-plate channel under equal mass flow rate, equal pumping power, and equal pressure drop for $1750 \leq Re \leq 2000$.They also reported that the corrugated channel with larger spacing performed much better than the channel with smaller spacing, although a larger pressure drop penalty was involving with larger spacing channel.

Rush et al. (1998) investigated the local heat transfer and flow behaviour for laminar and transitional flows in sinusoidal wavy passages. The experimental sinusoidal channels were 12 to 14 wavelengths long and channel aspect ratio was 10:1 with varying amplitude, phase angle and wall to wall spacing. Flow visualization studies showed that the flow was characterized as steady or unsteady including the detection of the onset of macroscopic mixing in the flow, which depended on the flow rate and channel geometry. The full channel exhibited unsteady flow at moderate Reynolds number ($Re \sim 800$) but instabilities were present near the channel exit at low Reynolds number ($Re \sim 200$), and moved toward the channel entrance with an increase in Reynolds number. Finally they proposed that the onset of flow mixing is directly correlated to the increase of local heat transfer.

Lin et al. (2002) also performed an experimental study to obtain the airside performance of the herringbone geometry in wet conditions. Two different angles, θ =15 degree and 25 degree and spacings, S=2.6mm and 8.4mm were considered. Flow visualization showed that a locally dry spot occurred in the wavy channel for the corrugation angle 15 degree and a fin spacing of 8.4 mm. This phenomenon was related to the recirculation of the airflow across the apex. On the other hand that phenomenon was not clearly visible for fin spacing of 2.6 mm. Based on their results, they reported that higher heat transfer

co-efficients and larger pressure drops were obtained for larger corrugation angle and smaller fin spacing and they proposed the following correlations:

$$Nu_{D_h} = 0.02656\, Re_{D_h}^{0.92333} \left(\frac{S}{D_h}\right)^{2.5906} \theta^{0.47028} RH^{0.07773} \qquad 2.3$$

$$f = 0.02403\, Re_{D_h}^{-0.41543} \left(\frac{S}{D_h}\right)^{-0.096529} \theta^{1.3385} RH^{-0.13035} \qquad 2.4$$

Where, RH and D_h were relative humidity and hydraulic diameter respectively. The mean deviations of the proposed correlations of Esq. (2.3) and (2.4) were: 2.52% and 4.81%, respectively.

Junqi et al. (2007) conducted experiments which reported the air side thermal hydraulic performance of 11 different types wavy fin and flat tube heat exchangers. A number of tests were carried out for air side Reynolds numbers in the range of 600 – 8000 to determine the effects of various geometrical parameters such as fin pitch, fin height and fin length on the thermal hydraulic performance at a constant tube-side water flow rate. From the experimental data, they found that the colburn j-factor and the fanning friction factor f decrease with the increase of Reynolds number .They also proposed that the j factor was increased with an increase in fin spacing and fin height but the f factor only increased with fin spacing at constant Reynolds number. Correlations of f and j factor were also provided in their studies which were in good agreement with their data. The correlations are given below

$$j = 0.0836\, Re_{D_h}^{-0.2309} \left(\frac{S}{H}\right)^{0.1284} \left(\frac{S}{2A}\right)^{-0.153} \left(\frac{L_d}{\lambda}\right)^{-0.326} \qquad 2.5$$

$$f = 1.16\, Re_{D_h}^{-0.309} \left(\frac{S}{H}\right)^{0.3703} \left(\frac{S}{2A}\right)^{-0.25} \left(\frac{L_d}{\lambda}\right)^{-0.1152} \qquad 2.6$$

The mean deviations of the correlations for j and f factors were 4.4% & 5.1% and the average deviations were -0.4% and -0.3%, respectively.

2.3 Numerical Studies on Wavy Channel

Amano et al. (1985) numerically investigated thermal-hydraulic characteristics in a periodically corrugated wall channel for both laminar and turbulent flows which vary in the range of Reynolds number from 10 to 25,000. He reported the effects of channel height, H and fins spacing or channel width, W on f and j factors. He solved the governing transport equations based on the modified hybrid scheme. From his computations he found that the mechanisms of heat transfer were related to the flow phenomena of separation, deflection, recirculation, and reattachment. Finally, it was observed that the effect of the ratio between H and W (called step ratio) was generally minor on the local Nusselt number. But significant effects of the step ratio were found in the case of average Nusselt number and friction factor. In addition, it was observed that both the flow and heat transfer patterns were changed drastically from laminar to turbulent.

Amano and Bagherlee (1987) did further work numerically on the same flow channel where complex turbulent flows were created. They applied the Reynolds stress model to analyze these turbulent flows because these were highly nonisotropic. They made computations for several different corrugation periods and for different Reynolds numbers. Their results showed good agreement with experimental data for mean velocities, the Reynolds stresses, and average Nusselt numbers.

Asako and Faghri (1987) developed a finite volume methodology to predict two dimensional ($\alpha \rightarrow 0$) fully developed heat transfer coefficients, friction factors, and streamlines for flow in a corrugated duct. The numerical solutions were performed for laminar flow (the Reynolds number range between 100 and 1500) and the thermal boundary condition of uniform wall temperature. The calculations were carried out for three different corrugation angles such as 15°, 30°, and 45° and a number of interwall spacings. The heat transfer results were parameterized by Prandtl numbers of 0.7, 4, and 8. Highly complex flow patterns, including large recirculation zones were found from the streamlines. The pressure drops and friction factor results were higher than the corresponding values for a straight duct. Finally, small differences were found in the heat

transfer rate ratios from a performance analysis model under the different constraints-fixed pumping power, fixed pressure drop, and fixed mass flow rate.

Later Asako and Nakamura (1988) determined numerically the periodic, fully developed heat transfer and fluid flow characteristics of a corrugated duct with rounded corners. The channel geometries were same as Asako and Faghri (1987) except that rounded corners which were approximated by a cosine function. Computations were carried out for a Prandtl number of 0.7 in the Reynolds number range from 100 to 1000. They found that the Nusselt number and friction factor were decreased by rounding of the corners. The pressure drop for the round cornered duct was up to 80% less than that for the sharp cornered duct. The heat transfer rate for rounded corner duct were also found up to 20% and 35% less and 20% greater than that for the sharp corner duct under fixed pumping power, fixed mass flow and fixed pressure drop, respectively. They also compared with the straight duct and observed that the heat transfer rate for the rounded corner duct was greater than that for the straight duct under all constraints at higher Reynolds number.

Metwally and Manglik (2000) numerically investigated forced convection heat transfer for laminar ($10 \leq Re \leq 2000$), incompressible, single phase, and periodically developed, constant property fluid flow in sinusoidal corrugated channels with uniform wall temperature. They obtained results for a wide range of corrugation aspect ratio ($0 \leq \gamma \leq 1$) and three different values of Prandtl number (Pr = 5, 35, 150) of viscous fluids. Flow separation and reattachment in the corrugation troughs generated transverse vortex cells that grow with the increase of Re and γ in the swirl flow regimes including transition to this regimes. The heat transfer was found to be enhanced by up to thirty four times that in a flat parallel plate cannel having only seventeen times higher friction factor penalty depending on γ, Re and Pr. They also studied the same geometries for power-law non Newtonian fluids for three different fluid shear-thinning index (n=0.5, 0.8, 1). Recirculations were found to be generated in wavy-wall valleys due to corrugations which were grew with the increase of γ and Re but with a decrease in n. Enhanced thermal-hydraulic performance was obtained at the beginning of swirl regime. In this case, the heat transfer effectiveness (*j/f*) was found to be enhanced by up to 3.3 times that

in a flat parallel plate cannel depending on γ, Re and Pr. They finally proposed that the performance of shear-thinning fluid was better than the previous one.

Muley and Manglik (2002) also presented an experimental and numerical investigation of thermal-hydraulic performance for single phase laminar flows in a novel corrugated-wall compact heat exchanger core. They considered the corrugation aspect ratio ($\gamma = 2A/\lambda$) of 0.15, and duct aspect ratio ($\alpha = S/H$) of 0.4533 for their test geometry and obtained their experimental result for laminar flows ($70 \leq Re \leq 830$), using water as a working fluids ($Pr \sim 6$). A CFD model was also developed for their numerical study using control volume based on commercial code FLUENT to determine fully developed laminar flows. They found a good agreement (±10%) between the numerical prediction and experimental data. They correlated the numerical prediction and experimental data by the following two equations for $Re > 100$:

$$f = 3.051\, Re_{D_h}^{-0.6365} \tag{2.7}$$

$$j = 0.173\, Re_{D_h}^{-0.385} \left(\frac{\mu_b}{\mu_w} \right)^{0.14} \tag{2.8}$$

It should be noted that their f and j correlations were valid only for the wavy duct with γ of 0.15, and α of 0.4533 used in their study. Finally, they reported that the wavy channels provided 1.40 to 2.35 times higher j/f compared to an equivalent straight duct, and up to 4.3 times higher heat transfer for the fixed geometry and pumping power constraint.

Zhang et al. (2003) investigated enhanced laminar flow heat transfer in 3-D sinusoidal wavy-plate-fin channels computationally and experimentally. The computational study was performed using finite volume techniques to determine the complex flow behaviour, and the associated frictional loss and enhanced heat transfer in the steady laminar regime at the uniform heat flux condition. They modeled the wavy-fin by its two asymptotic limits of 100% fin efficiency and zero fin efficiency. Air flow rate in the range of $10 \leq Re \leq 1500$ was considered to obtain the computational results for fanning friction factor f and colburn factor j. To obtain the effect of fin density on flow behaviour, they considered four different fin geometries having constant corrugation aspect ratio (0.267) and variable

aspect ratio, α and spacing ratio, ε. The experimental study was also performed for two geometries ($\alpha = 0.637$ and $\varepsilon = 0.803$; $\alpha = 0.241$ and $\varepsilon = 0.303$). An excellent agreement was found between the computational and experimental results. They observed that the f and j were increased with the increase of ε but decreased with the increase of α. They obtained the optimum performance (j/f) when $\varepsilon = 0.470$. The effect of flow rate was also followed on flow behaviour. Viscous forces dominated and the flow behaviour was similar to that in a straight rectangular channel at low flow rate (Re < 100) but swirl flows consisting of multiple pairs of counter-rotating helical vortices were observed at higher flow rate (Re> 100), which result in higher momentum and energy transport. Finally they proposed that the overall heat transfer performance was improved in compare to the straight channel with the same cross-section under swirl flow conditions including a relatively smaller increase in the pressure drop penalty.

Vyas et al. (2004) performed a visualization experiment and computational simulation to study the swirl flow and enhanced heat transfer in a 2-D (plate separation to width = 0.067) sinusoidal channel having corrugation aspect ratio, $\gamma = 0.25$ and spacing ratio, $\varepsilon =$ 1. They carried out the computational work using finite-volume techniques for a non-orthogonal non-staggered grid which agreed very well with experimentally visualized flow fields. They observed that the flow was essentially streamline and contoured to the wall waviness at low $Re < 200$ but lateral recirculation was produced in through regions of the wavy channel due to wall curvature with increasing Re > 200. Finally they reported that the swirl strength and spatial flow coverage increased with Re to produce temperature field which had sharper gradients at the wall with considerable thinning of the boundary layer and enhanced heat transfer.

Zhang et al. (2004) also investigated numerically the laminar forced convection of air (Pr=0.7) in 2-D (aspect ratio, $\alpha \rightarrow 0$) sinusoidal wavy-plate-fin channels considering same assumptions as their previous work for different flow rates ($10 \leq Re \leq 1000$). They obtained velocity and temperature fields, isothermal Fanning friction factor (f), and Colburn factor (j) for different wall-corrugation severity ($0.125 \leq \gamma \leq 0.5$), and fin spacing ($0.1 \leq \varepsilon \leq 3.0$). They followed that the re-circulation was induced in the near-wall

axial flow separation bubble, and it's spatial growth is governed by Re, γ, ε. The consequent local fluid mixing and core flow acceleration resulted in enhanced convection heat transfer, though the associated flow friction also increased. They suggested two flow regimes: 1) A low Re (Re→ 10) regime with fully developed flows and 2) A high Re (Re→ 1000) swirl regime. The peak heat transfer performance was found in the swirl regime (Re~600) for all γ and $1.0 \leq \varepsilon \leq 1.2$ when compared with the (*j/f*) performance in flat plate. But for low flow rates, much higher fin waviness severity ($\gamma > 0.5$) was needed to achieve significant enhancement.

Manglik and Zhang (2005) again performed a numerical study of steady forced convection for the same flow of air in 3-D wavy-plate-fin cores using finite-volume techniques. They considered four geometrical attributes having constant fin waviness ratio, γ =0.2667 and variable aspect ratio, α and fin separation ratio, ε. They found that the wall waviness produced a secondary flow pattern that was made up of multiple counter-rotating vortices in flow cross-section of the trough region which was increased with Re and ε. As a result, high local heat transfers near the recirculation zones were found due to periodic interruption of thermal boundary layer. At low flow rate (Re < 100), suppress or diminish the extent of swirl was followed but at higher flow rate (Re > 100), higher momentums and energy transportations were obtained. Finally, they reported that wavy channel was superior than a straight channel to enhance the overall heat transfer co-efficient as well as pressure drop penalty and the relative surface area compactness as measured by the (*j/f*) performance increased with the fin density.

Webb and Kim (2005) summarized briefly much of the significant work in wavy channel analysis.

Muley and Manglik (2006) did further work to obtain the effect of corrugation severity numerically, using control-volume techniques and also experimentally. In this case they were considering the corrugation aspect ratio γ=0.0667, 0.1333 and 0.2667 with constant ε=0.803 and α =0.1677. The experimental study was performed in the range 500 < Re < 5000 and resulted in an excellent agreement with numerical results. Finally they proposed

that the relative enhancement was highest for γ =0.0667 as measured by the Area Goodness Factor.

Recently, Tao et al. (2007) studied the air side performance of 3-D wavy fin surface using body-fitted coordinates numerically. Results for local Nusselt number distributions on the whole wavy fin and plain plate fin surfaces showed that the local Nusselt number decreased quickly along the flow direction and the values at the upstream were about 10 times of those at the downstream. They proposed a new type of the fin surface pattern with a wave located only in the upstream part (fin B) which was compared with the whole wavy fin (fin A) and whole plain plate fin (fin C). The Nusselt number for fin B was found only about 4% lower than for fin A and about 45% higher than for fin C while the friction factor of fin B was found about 18% lower than for fin A and only about 26% higher than for fin C within the range of the Reynolds number studied. Fin B had the best comprehensive performance among the three types of fins, followed by fin C and fin A under identical Reynolds number. Finally they reported that Fin B had the best *Nu/f* performance in compare to Fin A and Fin C under identical pressure drop and the identical pumping power constraint.

2.4 Limitations of Previous Works

The data and models or correlations found in the previous two sections have some limitations. Most of the experiments are conducted only for air (Pr = 0.7) as a working fluid and few for water. There are no data available for high viscous liquid such as oil at very low Reynolds number and over a wide range of Prandtl numbers. Metwally et al (2002) did some numerical investigation for large Prandtl numbers which were no more than 150.

Goldstein and Sparrow (1977) developed a correlation for the Nusselt number using mass transfer tests which is very specific. O'Brien and Sparrow (1982) also developed a correlation based on their test in a corrugated channel geometry using water. But these correlations are only valid for the specific geometries tested, and thus do not account for

changes in corrugation pitch and angle. Manglik and Zhang (2005) numerically predicted the thermal performance of wavy fin geometries using computational fluid dynamics (CFD). Though their simulation results agreed very well with the experimental data and the asymptotic behaviour are easily seen for low Reynolds number .This aspect has not been addressed in any of the literature. Recently, Junqi et al. (2007) also provided simple correlations for f and j factor for corrugated wavy fin which cover only the range of Reynolds number 600 to 8000.

No general model exist for friction factor, f and Colburn factor j which covers all geometrical variables such as (fin pitch or spacing, fin thickness, fin height, and wavelength of convolutions), Reynolds number (Re) and Prandtl number (Pr).

Chapter 3

Experimental Method

3.1 Introduction

This chapter discusses the experimental setup and method to measure the heat transfer characteristics and pressure drop of various wavy fins. Experimental objectives, experimental apparatus, the method of doing experiment, experimental procedure and, experimental uncertainty are presented here.

3.2 Experimental Objectives

The main objectives of the experiment are to determine the Fanning friction factor f and Colburn factor j from experimental measurements on fifteen fins. These data are compared with the model which is developed by combining the asymptotic behaviour for the low Reynolds number and laminar boundary layer regions. Fin dimensions for fifteen fin specimens are summarized in Table 3-1 which were supplied by TAT Technologies Inc.(TAT Technologies, Ltd. is a diversified technology-based engineering and industrial company specializing in design, development and manufacture of Heat Exchangers, Cooling Systems, Air Conditioning Systems, Fuel Systems, etc.). For data reduction, surface characteristics of each fin are calculated by using idealised formulas and summarized in Table 3-2.

Before conducting the main experiment for each different geometry, the test cells are benchmarked. Five test cores and one common cover plate were machined to test the fifteen fins. The test loop consists of a test section with flexible Silicone Rubber Heaters, test fluid loop, a shell and tube heat exchanger and data acquisition system. A schematic diagram and photo of the experimental setup are shown in fig. 3.2 & 3.3, respectively.

Next geometrical parameters of the test core and various components of test loop are discussed.

3.3 Geometrical parameters

Geometrical parameters of the test section are important for data reduction. It consists of flow and frontal area, surface area, fin area, fin length, hydraulic diameter etc, actually depend on the length (L) of the fin in the flow direction, thickness (t) of the fin material (which is neglected for very small values), the spacing (S) between two adjacent fins, channel height (H) and channel width (W), the number of channels (N_{ch}) in fin specimens, and amplitude (A) of the fin waviness.

These parameters are defined here and shown in figure 3-1.

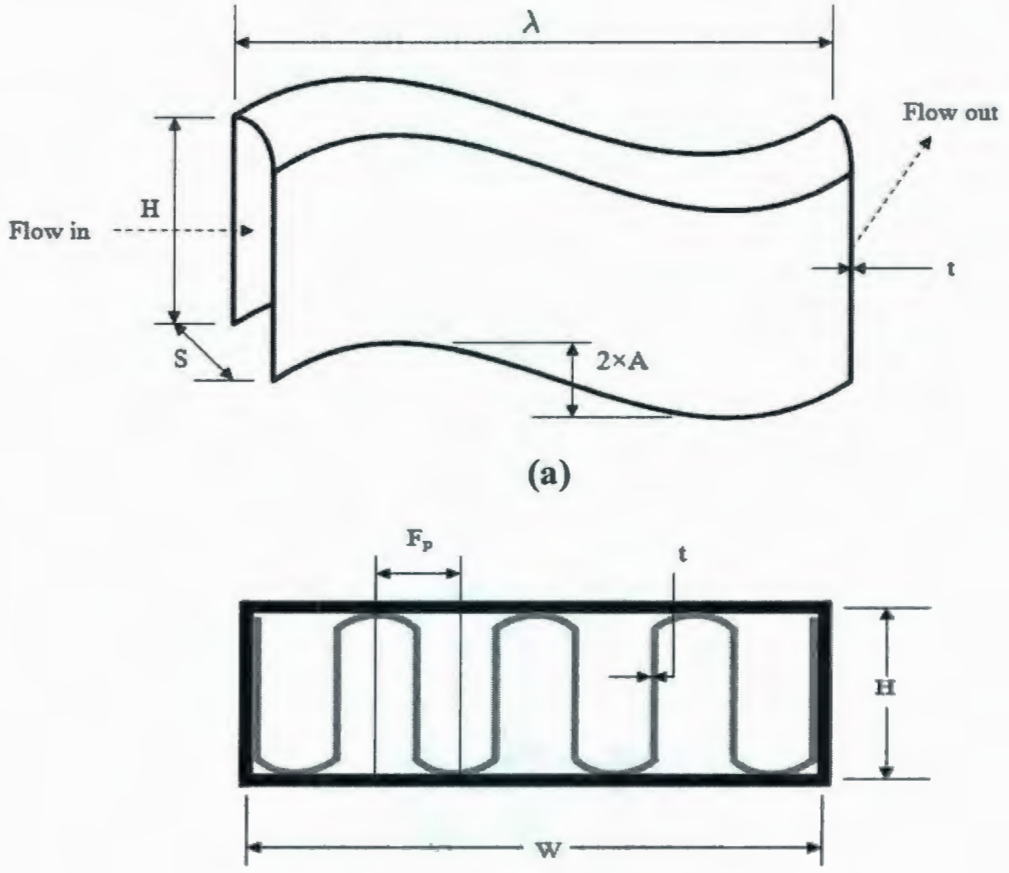

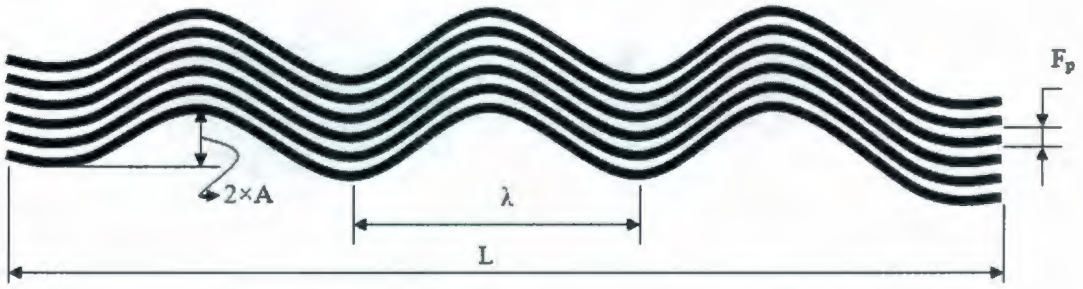

(b)

Fig. 3.1 - Wavy Fin: (a) geometrical description, (b) two dimensional representation of the inter-fin flow channel- front & top view.

3.3.1 Frontal and Flow Area

The frontal area (A_{front}) and the flow area (A_{flow}) are defined by the following equations.

$$A_{front} = WH \tag{3.1}$$

$$A_{flow} = WH - N_{ch}t(H + S) \tag{3.2}$$

The ratio of A_{front} and A_{flow} is called entrance reduction ratio and represented by *ERR*. The ratio between fin spacing (S) and height (H) is called aspect ratio and represented by α.

$$ERR = \frac{A_{flow}}{A_{front}} = 1 - \frac{N_{ch}t}{W}(1 + \alpha) \tag{3.3}$$

$$\alpha = \frac{S}{H} \tag{3.4}$$

These parameters are needed to calculate the velocity (u_m), Reynolds number (Re) and Fanning friction factor (f) of the experiment.

3.3.2 Surface Area

The total heat transfer surface area (A_{total}) and the reference surface area (A_{ref}) are defined by the following equations.

$$A_{total} = \left(\frac{L_e}{\lambda}\right) L_{ch}(H + S)2N_{ch} \tag{3.5}$$

$$A_{ref} = (WL)_{ch} \tag{3.6}$$

The ratio of A_{total} and two times of A_{ref} are called area enhancement ratio and represented by AER:

$$AER = \frac{A_{total}}{2A_{ref}} = \left(\frac{L_e}{\lambda}\right)\left(\frac{H}{W}\right)(1+\alpha)N_{ch} \tag{3.7}$$

These parameters are needed to calculate the Colburn factor j of the experiment.

3.3.3 Fin Area

Fin area (A_f) is defined by the following equation:

$$A_f = \left(\frac{L_e}{\lambda}\right)L_{ch}(H+S)2N_{ch} - 2(WL)_{ch} \tag{3.8}$$

The ratio of A_f and A_{total} is called fin area ratio and represented by FAR.

$$FAR = \frac{A_f}{A_{total}} = 1 - \frac{1}{AER} \tag{3.9}$$

This is used to calculate the surface efficiency.

3.3.4 Fin Length

Assuming good thermal contact exists between the fin and wall, the fin length is represented in the definition of the fin efficiency by the following equation

$$F_L \approx \left(\frac{H}{2} + \frac{S}{2}\right) \approx \frac{H}{2}\left(1 + \frac{S}{H}\right) \approx \frac{H}{2}(1+\alpha) \tag{3.10}$$

For two dimensional flow $\alpha \rightarrow 0$. So,

$$F_L \approx \frac{H}{2} \tag{3.11}$$

3.3.5 Hydraulic Diameter

Hydraulic diameter is defined as four times the hydraulic radius by Kays and London (1984). But as the model also utilizes fully developed flow Nu_{Dh} numbers and fRe_{Dh}, for channel. The hydraulic diameter is defined as follows:

$$D_h = \frac{4S(H-t)}{2S+2(H-t)} \tag{3.12}$$

Neglecting the thickness of the fins as it is thin, it becomes

$$D_h = \frac{4SH}{2(S+H)} = \frac{2S}{(\alpha+1)} \tag{3.13}$$

For two dimensional flow $\alpha \rightarrow 0$. So,

$$D_h = 2S \tag{3.14}$$

The relationship between the fin spacing and the *FPI* is presented by the following equation when spacing is considered in inches.

$$S(in) = \frac{1}{FPI} \tag{3.15}$$

There is little difference in the hydraulic diameter using the present definition than the definition of the Kays and London (1984).

Table 3-1

Fin Surface Dimensions

Serial No	Tool number	Length	Width	Height	Thickness	FPI	Pitch(Wavy length)	2×Amplitude(A)
-	-	*inch*	*inch*	*mm*	*inch*	-	*inch*	*inch*
1	83P0163-47-0719	11.8	5.5	6.35	0.006	13	0.375	0.063
2	92P0519-35-0719	11.76	5.5	6.35	0.006	18	0.375	0.067
3	92P0519-35-0719	11.79	5.6	6.35	0.006	30	0.375	0.067
4	92P0519-35-0719	11.9	5.57	6.35	0.006	32	0.375	0.067
5	8329109-10719	12	5.57	2	0.006	19	0.375	0.067
6	92P0512-35-0719	11.9	5.74	2	0.006	31	0.375	0.067
7	92P0512-35-0719	11.9	5.67	2	0.006	28.5	0.375	0.067
8	78205180-0719	11.8	5.2	10.8	0.006	21	0.375	0.05
9	78205180-0719	11.77	5.52	10.8	0.006	27	0.375	0.05
10	78205180-0719	11.82	5.5	10.8	0.006	30	0.375	0.05
11	1091111100-40-0719	11.79	5.57	8.26	0.006	24	0.375	0.05
12	8287111-1,-2,-4	11.9	5.57	8.26	0.006	27.5	0.375	0.04
13	8287111-1,-2,-4	11.8	5.7/6.1	8.26	0.006	26	0.375	0.04
14	7201-016-1,-2,-3	11.8	5.5	4.7	0.006	30	0.375	0.05
15	7201-016-1,-2,-3	11.8	5.58	4.7	0.006	20	0.375	0.05

Table 3-2

Surface Characteristics of Fins

Serial No	Tool number	ERR	AER	FAR	F_L	D_h
-	-	-	-	-	*mm*	*mm*
1	83P0163-47-0719	0.89943	4.4685	0.77621	4.15E-03	2.99E-03
2	92P0519-35-0719	0.86934	5.8512	0.82909	3.88E-03	2.31E-03
3	92P0519-35-0719	0.79721	9.0803	0.88987	3.60E-03	1.49E-03
4	92P0519-35-0719	0.78522	9.6177	0.89603	3.57E-03	1.41E-03
5	8329109-10719	0.81160	2.6572	0.62366	1.67E-03	1.60E-03
6	92P0512-35-0719	0.73933	3.6763	0.72799	1.41E-03	1.16E-03
7	92P0512-35-0719	0.75438	3.4642	0.71133	1.45E-03	1.23E-03
8	78205180-0719	0.86117	10.256	0.90250	6.01E-03	2.18E-03
9	78205180-0719	0.82507	12.924	0.92262	5.87E-03	1.73E-03
10	78205180-0719	0.80707	14.254	0.92984	5.82E-03	1.57E-03
11	1091111100-40-0719	0.83877	9.1098	0.89023	4.66E-03	1.88E-03
12	8287111-1,-2,-4	0.81774	10.151	0.90149	4.59E-03	1.66E-03
13	8287111-1,-2,-4	0.82677	9.6480	0.89635	4.62E-03	1.75E-03
14	7201-016-1,-2,-3	0.78887	6.7878	0.85268	2.77E-03	1.43E-03
15	7201-016-1,-2,-3	0.84894	4.8567	0.79410	2.99E-03	2.00E-03

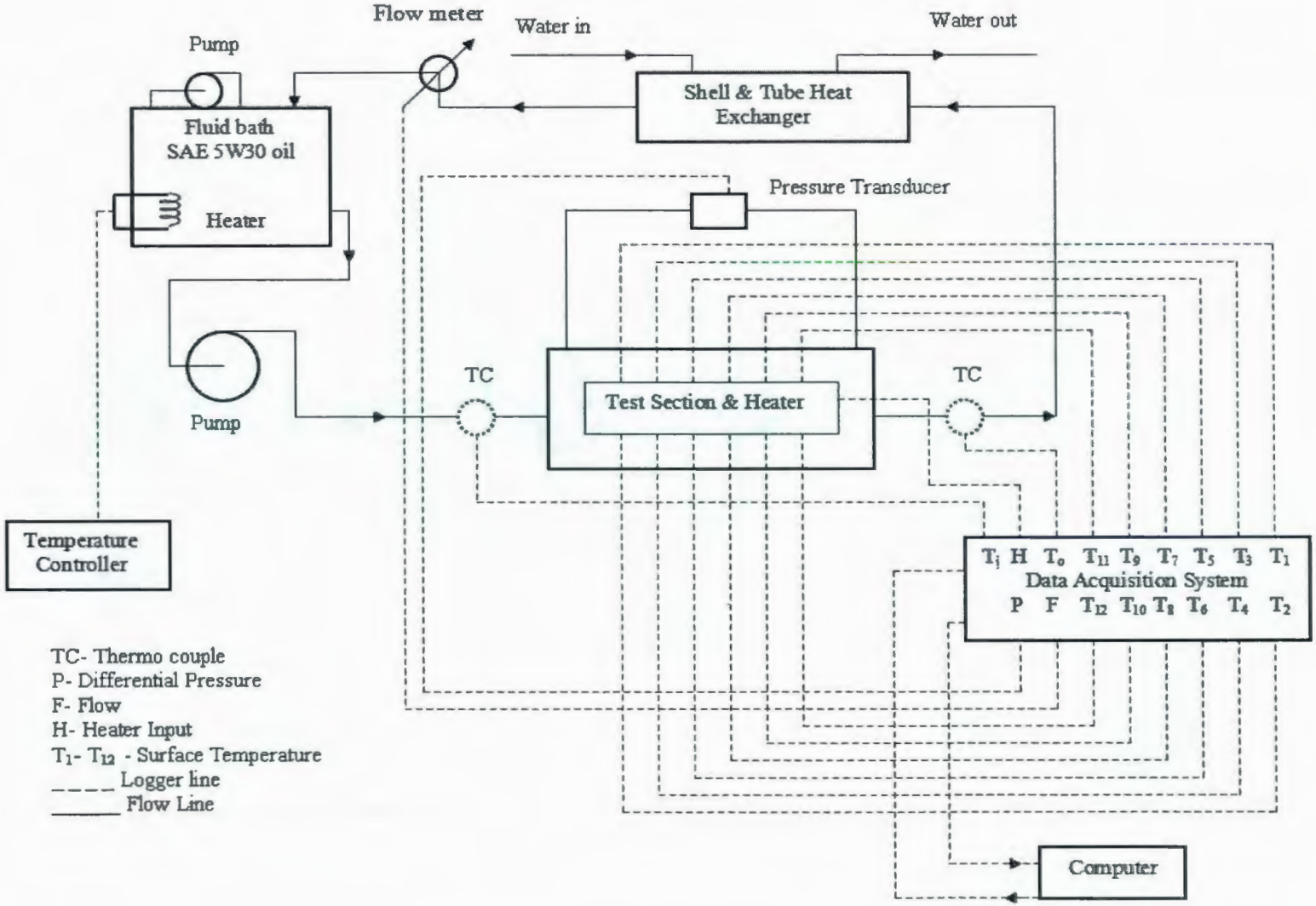

Fig. 3.2 - Schematic diagram of experimental setup

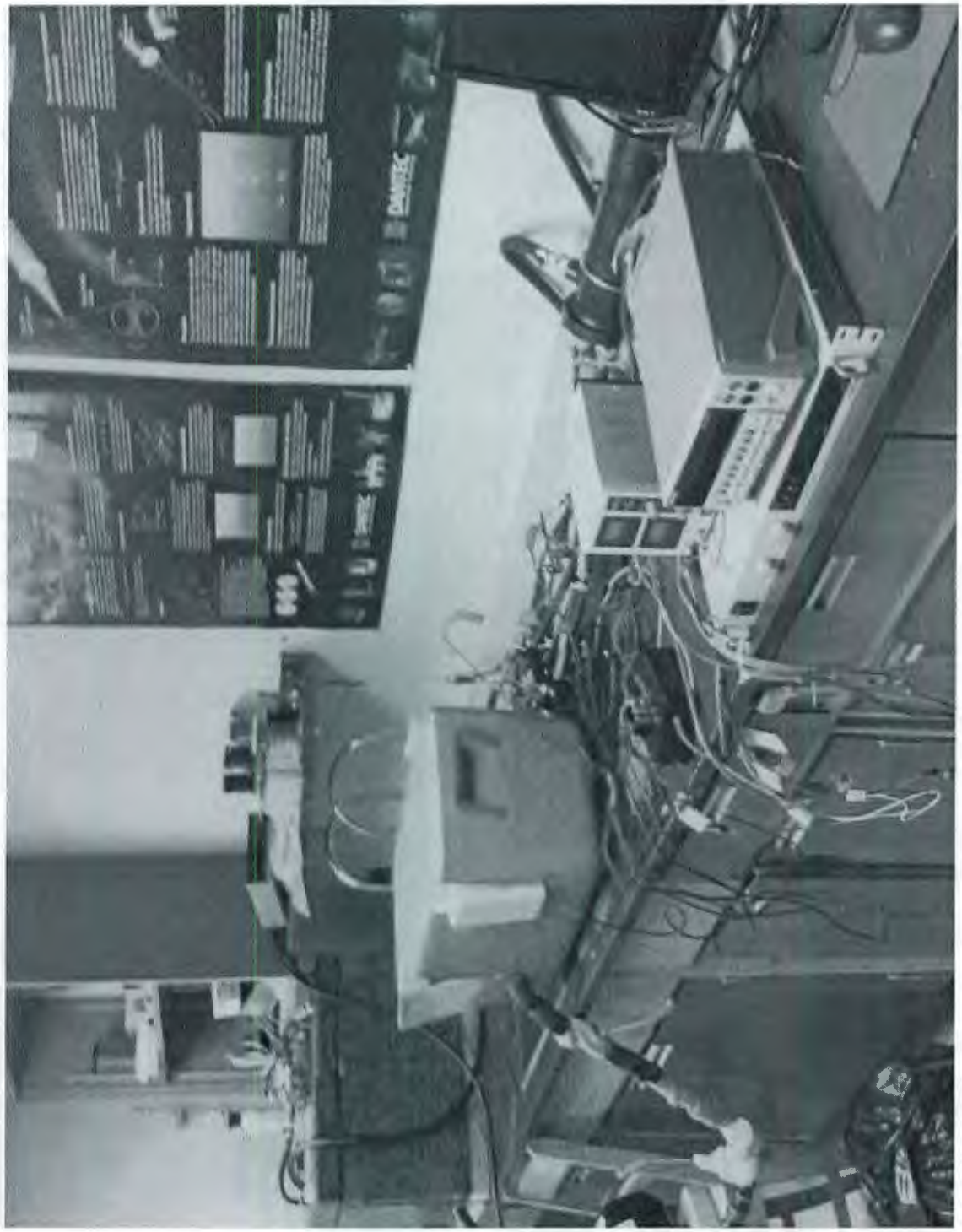

Fig. 3.3 - Photo image of experimental setup

3.4 Measurement Facility

The measurement facility consists of a test fluid bath, temperature controller, pump, test section, flexible silicon rubber heaters, pressure transducer, thermocouples, flow meter, shell and tube heat exchanger, and data acquisition system. In this section these are discussed in details.

3.4.1 Test Fluid Bath

One fluid bath is installed with the experimental setup to store the test fluid and for recycling the fluid flow. The bath is well insulated which is maintained at constant temperature but variable flow rate. The volumetric capacity of the fluid bath is 30L. The fluid bath is equipped with a 3000W heater to heat the fluid to the required initial temperature. Maximum capacity of the heater provides up to 150°*C*. One small pump is installed at the top of the bath. This pump is used to mix the fluid to maintain uniform temperature in the bath.

Test Fluid

The experimental test fluid was SAE 5W30 oil which was manufactured by Quaker State. Data provided in the technical specifications for SAE 5W30 oil included two values of viscosity at 40 °C (64.1 centistokes) and 100 °C (10.7 centistokes). These results were compared with correlations of this oil test data that were previously obtained from a automotive heat exchangers manufacturer, Lemczyk and Molloy (1996). Excellent agreement between the technical specification data and the correlations was found, with values at 40 °C and 100 °C being predicted to be: 60.4 centistokes and 11.1 centistokes, respectively. This yields a 3.6 % to 6.1% difference in reported versus correlated properties. Further, comparisons of the measurements for a plain channel with theory support the use of the property correlations within the realm of the experimental measurement errors. The correlated properties for 5W30 oil which were used for data reduction are:

$$\log_{10}(\mu) = 9274 - 2437.83T^{0.5} + 256.145T - 13.4449T^{3/2} + 0.352491T^{2} - 0.00369285T^{5/2} \quad 3.16$$

$$k = 0.183482 - 0.00123141T^{0.5} - 0.0000613542T \quad 3.17$$

$$\rho = 1021.18 + 4.2243T^{0.5} - 0.703867T \quad 3.18$$

$$c_p = 1286.63 - 71.4665T^{0.5} + 6.20997T \quad 3.19$$

Where T in Eqs. (3.16 to 3.19) is given in the absolute [K] scale. The units for other properties are μ [$kg/m.s$], ρ [kg/m^3], k [$w/m.K$] and C_p [$J/kg.K$]. Fluid properties were evaluated at the mean bulk value of the inlet and outlet temperatures.

3.4.2 Temperature controller

A temperature controller R/S (advanced model) is used to maintain the constant, pre-set inlet temperature of the oil before entering into the test section. It is connected with the heater which is equipped with the oil bath and with a temperature sensor which is also placed inside the oil bath. It detects the temperature of the oil bath by using the sensor and adjusts the heater by varying the output duty cycle. It is a single loop controller. It can control load up to 15 amperes and 1750 W.

3.4.3 Pump

Flow of the oil from the fluid bath to the test section is done by a pump having a capacity of 1.5 HP and 3450 RPM. The pump is controlled by an *XFC* Series micro-Inverter to make the necessary amount of oil flow to the test section. The frequency range was used from 10 Hz to 70Hz for obtaining that particular oil flow rate. The pump is rated for 1 gpm open flow at zero head loss.

3.4.4 Test Section

To determine the heat transfer co-efficients five different test cores have been machined which allow five different plate fin heights to be tested. Both the test core and wavy fin specimens are constructed from aluminium. Each test core has 14.5inch×5.5 inch channel in which 12inch×5.5inch wavy fin specimen can be placed. One common top cover plate

of aluminium of 16inch×7inch has also been machined. Two manifolds are also constructed allow the oil to flow into the channel and to exit from the channel. One O-ring groove (*Ø 2.5mm*) is made inside the cover plate around the channel position and also one O-ring groove is made in both manifolds around the oil passage slot to prevent the oil leakage from the test section. Two 1/8-27 NPT fittings are placed on the outer surface of the cover plate to connect the pressure transducer with the test section. Total twelve narrow grooves are machined at equal distance on the outer surface of the cover plate to place the thermocouple wire accurately. Two Flexible Silicone Rubber Heaters (12"×5") are used on the outer surface of the channel plate and the cover plate to heat the test section. Thermocouple wires are placed inside the grooves using adhesive. Details of the test section are provided in Appendix A. Fig. 3.4 shows only the position of the thermo couples and the heaters which is given below.

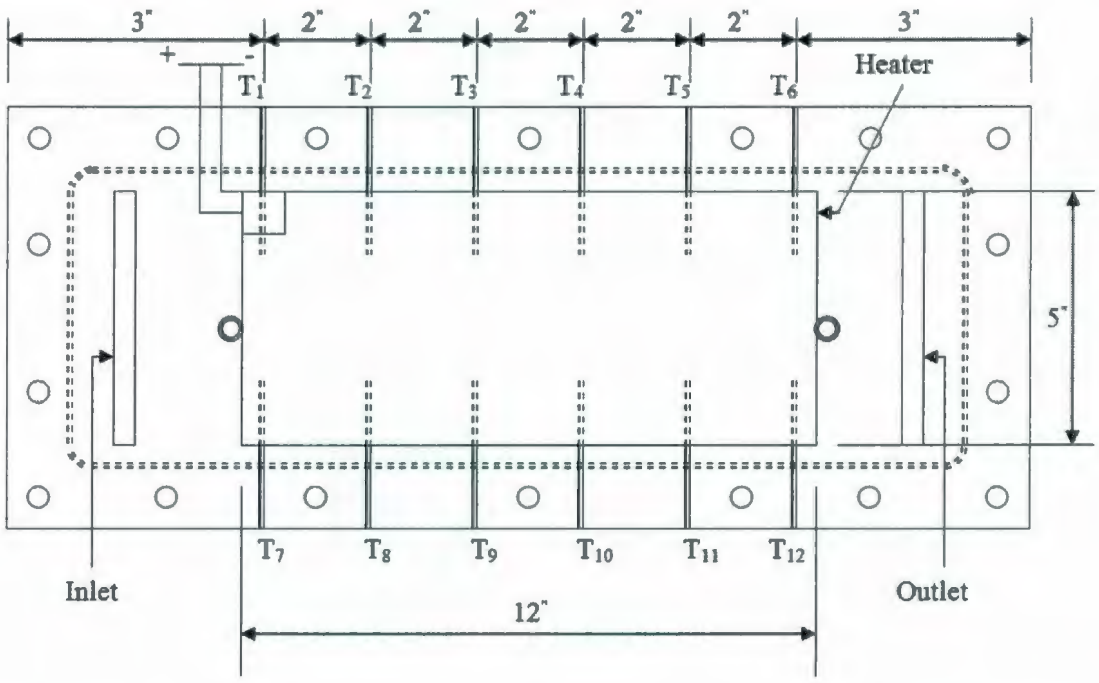

Fig. 3.4 - (a) Top surface (cover plate)

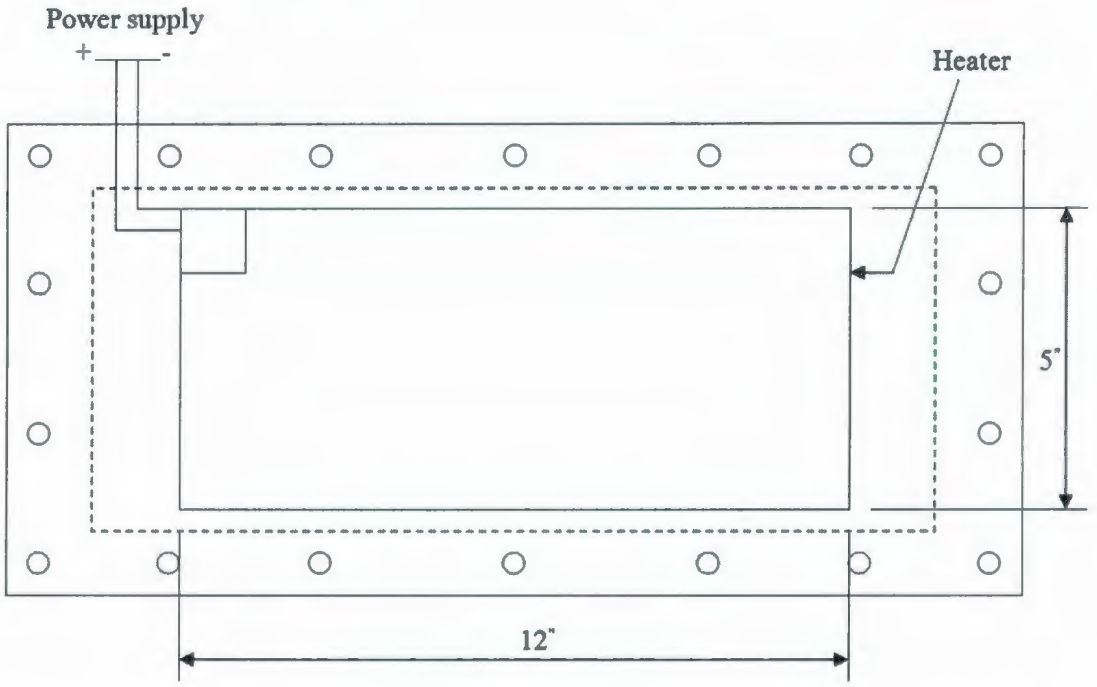

Fig. 3.4 - (b) bottom surface

3.4.5 Flexible Silicone Rubber Heaters

Heating of the test section is accomplished using two Omega Inc. *SRFG/SRFG* series flexible silicone rubber heaters at the top and bottom surface. These heaters can improve heat transfer and speed warm-ups where controlled heating is required in confined areas. The heaters were 12 inch in length & 5.5 inch in width and very thin. The maximum capacity of each heater cold produce 250°F (120°C) with pressure sensitive adhesive (PSA) which was provided on the heater to produce good contact with the metal surface. Maximum operating voltage of each heater was 115 V and W density of 5 W/in^2.

Power Supply

The *XFR* Series of variable DC output power supply device is used to supply required power in both heaters. Maximum power supply capacity was 1200 watt having a model of voltage 0-150 volt and current 0-8 amp. The top and bottom heaters are connected in parallel with power supply device. The circuit diagram is shown in fig. 3.5.

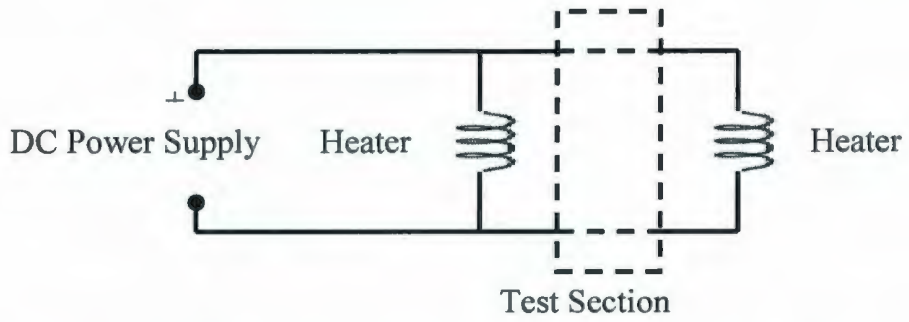

Fig. 3.5 - Circuit diagram of power supply in heaters

3.4.6 Thermocouples

Two copper constant thermocouples are used to measure the inlet and outlet temperature of the oil and one is used to measure the heat exchanger (shell & tube) outlet. They are positioned in such a way that the probes do not touch the wall of the flow pipe. Also twelve thermocouples are used to measure the surface temperature of the test section which is needed for data reduction of the experiment. All these thermocouples were pre-calibrated and checked at various temperatures using a constant temperature bath and ice/water mixture which have an accuracy of ± 0.05° *C*.

3.4.7 Pressure Transducer

One *PX81D0-050DI* pressure transducer is used to measure the differential pressure between the entrance and exit of the test section. Pressure transducer is rated for 0-50 PSD. Electrical excitation was 15 Vdc. An *Extech* 382200 series of variable DC output power supply device is used to supply required power in pressure transducer. Maximum power supply capacity was 30 watt having a model of voltage 0-30 volt and current 0-1 amp. The calibration of the transducer was performed by OMEGADYNE INC. using instruments and standards that are traceable to the United States National Institute of Standards Technology (NIST). The results of calibration were then fit using a linear regression analysis. Deviation of predicted result from the measured result is less than ±1%.

3.4.8 Flow Meter

A turbine flow meter with OMEGA signal conditioners was used to measure the flow rates of the test fluids. Flow meter was installed between the shell and tube heat exchanger and the fluid bath. The calibration of the transducer was performed by an OMEGA Technologies company and then the results of calibration were then fit using a linear regression analysis. The performance of the flow meter was not in acceptable range for all data points and was only used to predict the flow rate during the experiments. Actual flow rate was calculated from the heat supplied by the surface heaters to the test section using the enthalpy balance.

3.4.9 Shell and Tube Heat Exchanger

One small shell and tube heat exchanger was used to cool the oil exiting from the test section before retuning back to the fluid bath. It is very important to prevent test fluid from overheating and to maintain constant inlet temperature. Test oil was flowing through the tube side and cold water was flowing through the shell side of the heat exchanger. City water was used as coolant which was controlled by a valve.

3.4.10 Data Acquisition System

Data collection is carried out using a *KEITHLEY 2700* data acquisition system having a capacity of 25 Channels. It is fully automated which is connected to a personal computer. Programming software Lab View 8.2 is used to control the experiment and to display all measurements at all time through the data logger. Data logger also displayed the instantaneous output of all thermocouple as well as heat transfer rate of oil to determine when the steady state condition is reached. This device can scan and record at any desired rate. A total of 10 data points are collected over a certain interval in one minute. Average values of the 10 data points are then used in the data reduction procedures.

3.5 Fin Specimen Preparation

There were three specimens of every fin geometry. The best one was selected and was cut into 12"×5.5" to place inside the test channel. Cutting was done very smoothly by using a sharp knife. The plate channel was also machined very smoothly to ensure good contact of the fin surface with the channel wall.

3.6 Test Method

Prepared fin specimens were placed inside the test channel and closed with the top cover plate. Manifolds were also placed in the inlet and outlet positions. O-rings were used to make the system leak resistant. Before starting the experiment the test section was checked for leaks. Then it was insulated by using an insulating box. Two experiments were conducted for each specimen. One was at 50° *C* inlet temperature and another at 70°*C*.

The temperature was preset in the temperature controller and the oil flow was set to a flow rate a little higher than the starting flow rate. The starting power supply was between 150 to 250 watt depending on the fin density. When the oil bath was reached at required initial temperature the oil flow was set to a starting flow rate. It was approximately 0.5 L/s as the experiment was conducted for low Reynolds number. When it reached in steady state condition, the first data was collected for that flow rate. The oil flow rate was then increased by a certain interval of increment using the inverter which was connected with the pump and this procedure repeated until the maximum oil flow rate was reached. Power supply was also increased to maintain certain temperature difference (approximately more than 1.5°C) between the inlet and outlet. During the whole experiment the inlet temperature was maintained constant as much as possible. A thermocouple was installed at the outlet of the shell and tube heat exchanger by which it was easily determined that approximately how much water flow is needed to decrease the oil temperature.

3.7 Experimental Uncertainty

The experimental uncertainty in the Colburn factor, *j*, and Fanning friction factor, *f*, depends on the uncertainty in the experimental measurement of temperature, pressure, flow rate, supplied power on the system and uncertainty in the thermal and fluid properties of test fluids. The experimental uncertainty in f and j are generally within ± 5% when the temperatures and pressures measurement accuracy are within ±0.1°C and ±1% respectively. The uncertainty in the Reynolds number is generally ±2% if the flow measurement accuracy is within ±0.7%, shah (1985). Experimental uncertainties for this experiment were determined using the root sum square method outlined by, Moffat (1988) which is discussed briefly in Appendix-B.

The uncertainty analysis for this experiment was carried out at two different ΔT (temperature differences). The uncertainty in the experimental measurements of temperature, pressure, and heat transfer or power input to the heaters are provided in table 3.3.

Table 3.3

Uncertainty in Measurements

Measurement	Uncertainty
Temperature – T [*C*]	±0.05*C*
Differential Pressure – p [Pa]	±1%
Power–[Watt]	±1%

The accuracy of the micrometer used to measure the geometrical parameters was ±0.001 per 6 inch. The uncertainties of all the fluid properties such as density, ρ [kg/m^3] , dynamic viscosity, μ [*kg/m. s*], specific heat capacity, C_p [*J/kg. k*], conductivity, k [W/m^2. *K*] are assumed within ±0.5% assuming that the correlations (3.16 – 3.19) are valid for the fluids used in the experiment. If the test fluid properties are not exactly similar to those predicted by the correlations, there will be an increase in overall uncertainty.

As the flow rate are measured from the supplied heat as well as power input, the flow rate measurements depend on the temperature difference between the inlet and outlet. So, the uncertainty for Reynolds number and friction factor also vary at different ΔT as Colburn factor and Nusselt number. Two different data samples are considered having maximum and minimum possible temperature differences in the experiment. The same data samples are considered to determine the uncertainty in Log Mean Temperature Difference. The uncertainty is considered ±0.1% for temperature differences. The Results of the uncertainty analysis are given in Table 3.4.

Table 3.4

Uncertainty in *f, j,* and *Re*

Parameter	Uncertainty at ΔT = 1.5	Uncertainty at ΔT = 4.5
f	9.81 %	4.14 %
j	5.05 %	2.24 %
Nu	1.31 %	2.54 %
Re	4.87 %	1.99 %
Pr	0.87 %	0.87 %

3.8 Summary

This chapter represented the details of the experimental facilities and procedure for the experiments. All of the geometrical parameters of test fixture were determined which will be needed for the data reduction. The specifications of all equipment used in the experiments are also stated. The experimental uncertainty in *Re, f,* and *j* were found to be 4.87 /1.99, 9.81 /4.14, 5.05 /2.24 percent, respectively.

Chapter 4

Experimental Results

4.1 Introduction

Data reduction procedures to determine the Colburn factor j and Fanning friction factor f from various experimental measurements are discussed in this chapter. Experimental results for fifteen fin specimens are also represented by obtaining simple correlations. Heat transfer coefficients for bare channels are also determined here, to benchmark the facility. Experimental results for all specimens and bare channels are presented graphically.

4.2 Data Reduction

The Colburn factor j for this experiment depends on two dimensionless parameters, the Reynolds number and the Prandtl number. These two parameters are determined from the measurement of inlet and outlet temperature, surface temperature and the amount of power supplied by the silicone heaters, as well as mass flow rate. On the other hand the Fanning friction factor f is obtained from the measurement of mass flow rate and total pressure drop across the heat exchanger core. All the steps for obtaining these parameters are discussed in the next sections. The Colburn factor and the Friction factor data are usually plotted against the Reynolds number. The data reduction has been programmed using the symbolic programming language of the Maple V10 mathematics package. The data reduction code is provided in Appendix-C.

4.2.1 Reynolds Number

The Reynolds number for this experiment is defined by the following equation.

$$Re_{D_h} = \frac{\rho D_h u_m}{\mu} \quad 4.1$$

Where D_h is the hydraulic diameter which is defined in the previous chapter, ρ is the density and μ is the dynamic viscosity of the oil. All of the thermo-physical properties of oil are calculated at the average bulk mean temperature T_m. u_m is the mean flow velocity which is obtained using channel mass flow rate and entrance reduction ratio (ERR) as follows:

$$u_m = \frac{\dot{m}}{\rho_m WH(ERR)} \quad 4.2$$

where W is the width, and H is the height of the channel. ERR is the channel flow area reduction factor and m is the mass flow rate, which is obtained, form the following equation:

$$\dot{m} = \frac{Q}{c_p \Delta T} \quad 4.3$$

where c_p is the specific heat of the oil, ΔT is the temperature difference between outlet and inlet of the test section and Q is the heater power input which is supplied to two silicone rubber heaters to produce a heat flow of the surface of the test section. It is defined as follows:

$$Q = P = V \cdot I \quad 4.4$$

Where P is the supplied power, V is the voltage and I is the current.

4.2.2 Prandtl Number

The Prandtl number is defined by the ratio of the momentum diffusivity and the thermal diffusivity:

$$\mathrm{Pr} = \frac{c_p \mu}{k} \quad 4.5$$

It is solely a fluid property modulus. All the oil properties are evaluated at average bulk temperature. The Prandtl number is evaluated at the average bulk-mean temperature defined by:

$$T_m = \frac{T_i + T_o}{2} \qquad 4.6$$

where T_i and T_o are the inlet and outlet temperature of the test section which were measured with thermocouples placed at the entrance and exit of the test section respectively. The range of Prandtl number for oil is usually 50 to 10^5. For this experiment it was $324 < Pr < 573$.

4.2.3 Temperature Distribution

Temperature distributions through both walls of the test sections are very important to obtain the heat transfer coefficient as well as the Colburn factor. The mean surface temperature is calculated by the following equation:

$$T_s = \frac{T_1 + T_2 + T_3 + T_4 + T_5 + T_6}{6} \qquad 4.7$$

Where T_1 to T_6 are the temperatures which obtained from the thermocouples placed on the top surface of the test section. It is assumed that both walls had same temperature distributions during the experiment because the specifications of the heaters were same. The locations of the thermocouples are clearly shown in Fig. 3.3 (a).The variation of temperatures from entrance to exit at different position on the test core surface for fin-3 is shown graphically in Fig. 4.0. Four experimental runs have plotted for different Reynolds number, Re and power input, Q. The temperature should be gradually increased from entrance to exit but it was not followed. The mean surface temperature is considered in data reduction. The temperature gradients and variations from the mean are small and as a result of the high conductivity of aluminium, it may be assumed a "constant wall temperature".

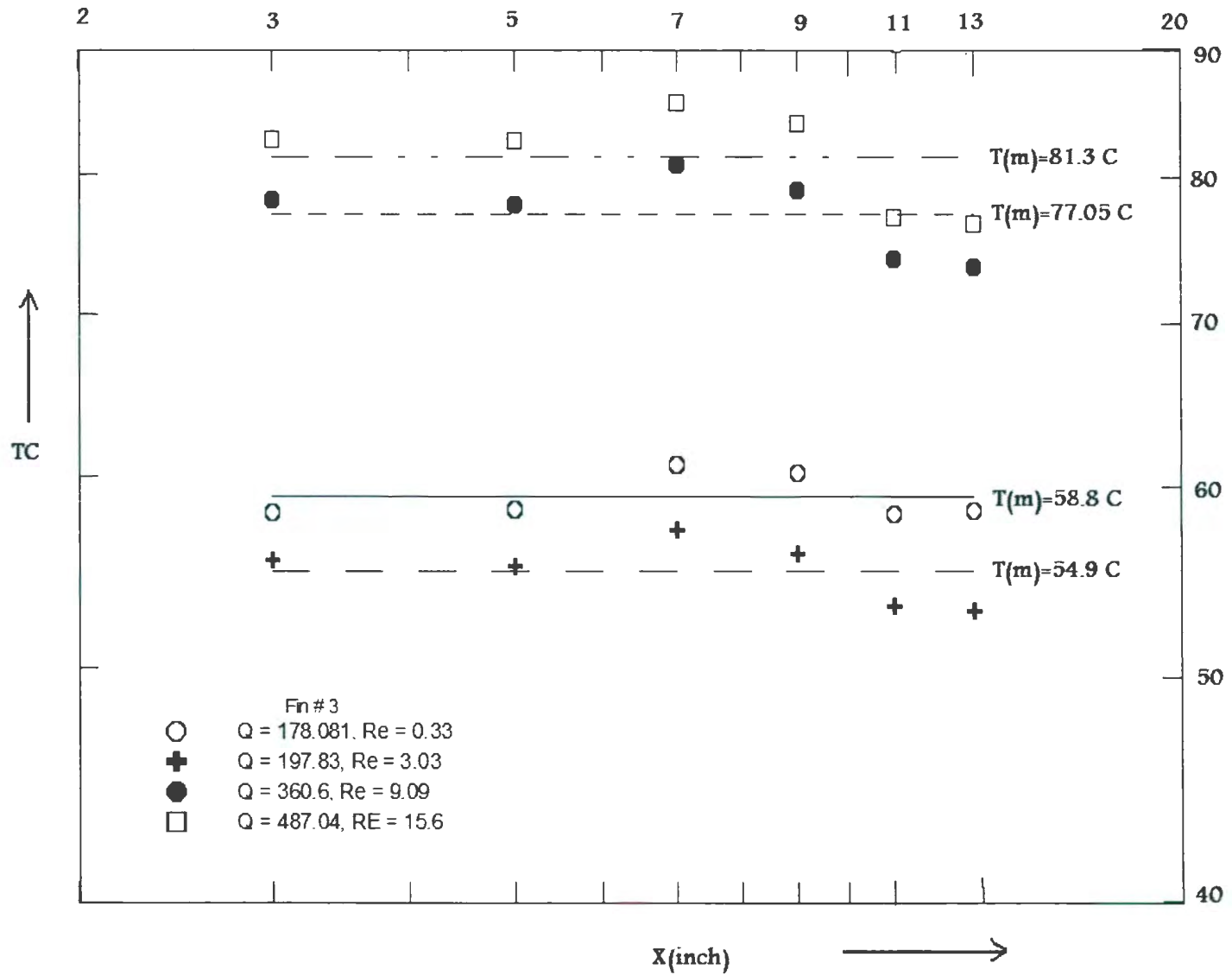

Fig. 4.1- Temperature distribution at various location of the test wall

4.2.4 Nusselt Number and j-Factor

The overall heat transfer coefficient may be obtained using the log mean temperature difference (LMTD) method. The *UA* product is obtained from the heat transfer rate *Q* and LMTD. The heat transfer rate *Q* is considered to be equal to the power supply in the two silicone rubber heaters. So, the UA product may be expressed as

$$UA = \frac{Q}{\Delta T_{LMTD}} = \frac{P}{\Delta T_{LMTD}} = \frac{VI}{\Delta T_{LMTD}} \qquad 4.8$$

The log mean temperature difference (ΔT_{LMTD}) is calculated using the mean surface temperature T_s and local inlet/outlet surface temperatures T_i/T_o as follows:

$$\Delta T_{LMTD} = \frac{(T_s - T_i) - (T_s - T_o)}{\ln\left(\frac{T_s - T_i}{T_s - T_o}\right)} \qquad 4.9$$

The average heat transfer coefficient for the enhanced surface is related to the *UA* product by the following expression:

$$\frac{1}{UA} = \frac{1}{\eta_o h A_{total}} + \frac{t_w}{k_w A_w} \qquad 4.10$$

where, $\frac{t_w}{k_w A_w} \approx 0$, t_w is the thickness of the channel wall, k_w is the thermal conductivity of the channel material. So the eq. 4.10 can be expressed as follows:

$$UA = \eta_o h A_{total} = \eta_o h (2WL) AER \qquad 4.11$$

Where *AER* is the area enhancement ratio which is defined in chapter-3 and η_o is the overall surface efficiency of the wavy fin which is defined by

$$\eta_o = 1 - FAR(1 - \eta_f) \qquad 4.12$$

The fin efficiency (η_f) may be computed using the definition for a straight fin

$$\eta_f = \frac{\tanh(mF_L)}{mF_L} \qquad 4.13$$

$$m = \sqrt{\frac{2h}{k_f t_f}} \qquad 4.14$$

This approach to compute the heat transfer coefficient h was achieved using Maple software with the measured data.

Once h is determined from Eq. (4.11), experimental results for the average heat transfer coefficient are obtained in terms of the Nusselt number which is one of the dimensionless representations of the heat transfer coefficient. It is defined as the ratio of the convective conductance h to the pure molecular conductance k/D_h as follows:

$$Nu_{D_h} = \frac{hD_h}{k} \tag{4.15}$$

It may be also represented by the Colburn factor which is given below

$$j = \frac{Nu_{D_h}}{Re_{D_h} Pr^{1/3}} \tag{4.16}$$

4.2.5 Fanning Friction Factor

The experimental determination of flow friction characteristics of compact heat exchanger surfaces is relatively straight forward. It is usually presented in terms of the Fanning friction factor f which is expressed by the following equation (Shah 2003):

$$f = \frac{D_h \rho_m}{4L}\left[\frac{\Delta p}{\frac{1}{2}\rho_m u_m^2} - \frac{1}{\rho_i}\left(1-\sigma^2+K_c\right) - 2\left(\frac{1}{\rho_o}-\frac{1}{\rho_i}\right) + \frac{1}{\rho_o}\left(1-\sigma^2-K_c\right)\right] \tag{4.17}$$

Where Δp is the pressure drop in the test core, L is the length, u_m is the average velocity, K_e and K_c are the expansion and contraction loss coefficients at the entrance and exit of the core respectively, $\sigma = A_{flow} / A_{front}$. Entrance and exit losses are significant for low values of σ and L and at high Reynolds numbers, for liquid at low Reynolds numbers the entrance and exit losses are negligible, Shah (2003). It may be considered that the fluid densities are approximately equal to the mean density for the isothermal pressure drop data which means the temperature difference between the inlet and outlet is very small. So eq. 4.15 can be written as follows:

$$f = \frac{D_h \rho_m}{4L}\left[\frac{\Delta p}{\frac{1}{2}\rho_m u_m^2} - K_c - K_e\right] \qquad 4.18$$

For obstructed flow applications such as flow through an interrupted surface, entrance and exit loss effects are not taken in consideration while calculating friction factor (Kays and London 1984). So, the eq. 4.17 simplifies to:

$$f = \frac{D_h}{4L}\left[\frac{\Delta p_{core}}{\frac{1}{2}\rho_m u_m{}^2}\right] \qquad 4.19$$

where Δp_{core} is the total pressure drop across the heat exchanger core excluding losses due to inlet/outlet manifolds and pipe fittings. Δp_{core} was measured using a differential pressure transducer with an accuracy of ±1 percent of the line of best fit.

4.3 Bare Channel Heat Transfer Co-efficient

The average heat transfer coefficient for three test cells without a fin specimen was also determined. The main purpose of these experiments was to benchmark the test cells. The test cells were benchmarked only for the Colburn j factor measurements, because the channel heights for the wavy fins produced pressure drops too small to measure the friction factor with the available differential gage in this experiment. Recently Muzychka and Kenway (2009) obtained good accuracy for both f and j characteristics from a benchmarking measurement for offset strip fin array at large Prandtl number using the same facility.

In Shah and London (1978), the hydrodynamic entrance lengths for a parallel plate channel is defined by the following equation:

$$L_{hy} = D_h(0.3125+0.011Re_{Dh}) \qquad 4.20$$

Using the above equation the hydrodynamic entrance length for the test fixture was determined for the region leading up to the test channels. It was found for the range of volumetric flow rates and inlet conditions that the velocity profile is nearly fully developed shortly after entering the heat exchanger core. Therefore the experimental data

for three bare channels are compared with the solution for thermally developing flow obtained from Shah and London (1978). The mean Nusselt number for the thermal entrance region ($Nu_{m,T}$) in a plane channel may be computed from the following expression obtained from (Stephan, 1959) for a parallel plate channel for simultaneously developing flow with constant wall temperature:

$$\mathrm{Nu}_{m,T} = 7.55 + \frac{0.024\left(\frac{L}{D_h \mathrm{Re}\,\mathrm{Pr}}\right)^{-1.14}}{1 + 0.0358\left(\frac{L}{D_h \mathrm{Re}\,\mathrm{Pr}}\right)^{-0.64} \mathrm{Pr}^{0.17}} \qquad 4.21$$

Which is valid for $0.1 < Pr < 1000$.

The comparison between the experimental and theoretical results for three different test cells is shown in Fig. 4.1, 4.2 and 4.3 respectively. Percentage of RMS error is found around +/- 25%. RMS errors for channel-1, channel-2 and channel-3 are found 26.09%, 17.58%, and 26.07% respectively. A comparison of all the bare channels is also provided in fig. 4.4. The surface area under the manifold inside the core and an effective flow length from entrance to exit was considered during the data reduction of bare channels. But this additional heat transfer surfaces were not counted when the fin specimen was present because it has an insignificant effect on the large heat transfer coefficient of wavy fin experiment, given the large value of AER. The dimensions of plain channels are provided in Table – 4.1.

Table - 4.1

Dimensions of Plain channels

Channel No	Length (inch)	Width (inch)	Height (mm)	Hydraulic diameter(mm)	% of RMS
1	14	5.5	6.35	12.12	26.09
2	14	5.5	2	3.94	17.58
3	14	5.5	10.8	20	26.07

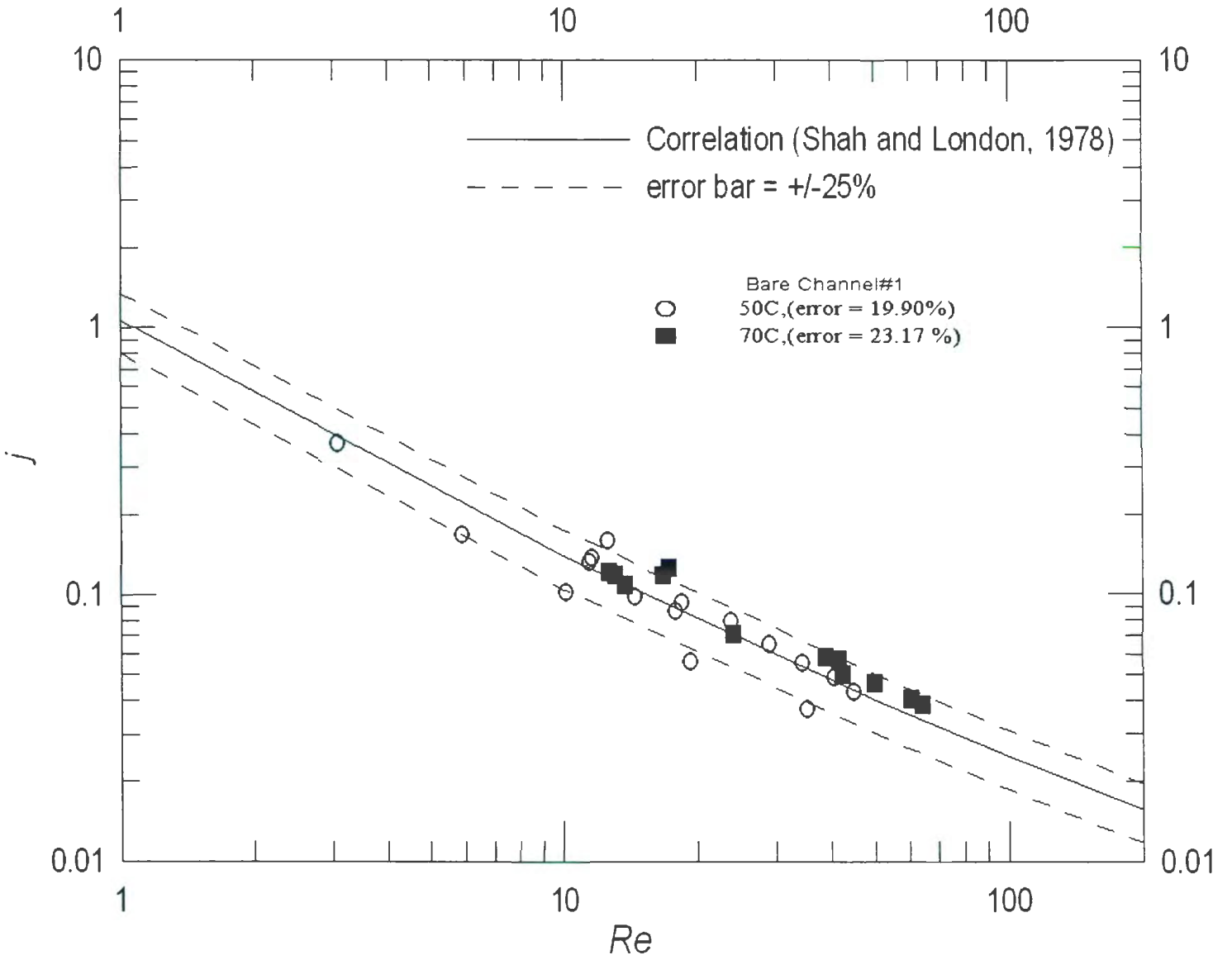

Fig. 4.2- Comparison of experimental results with thearitical for channel-1

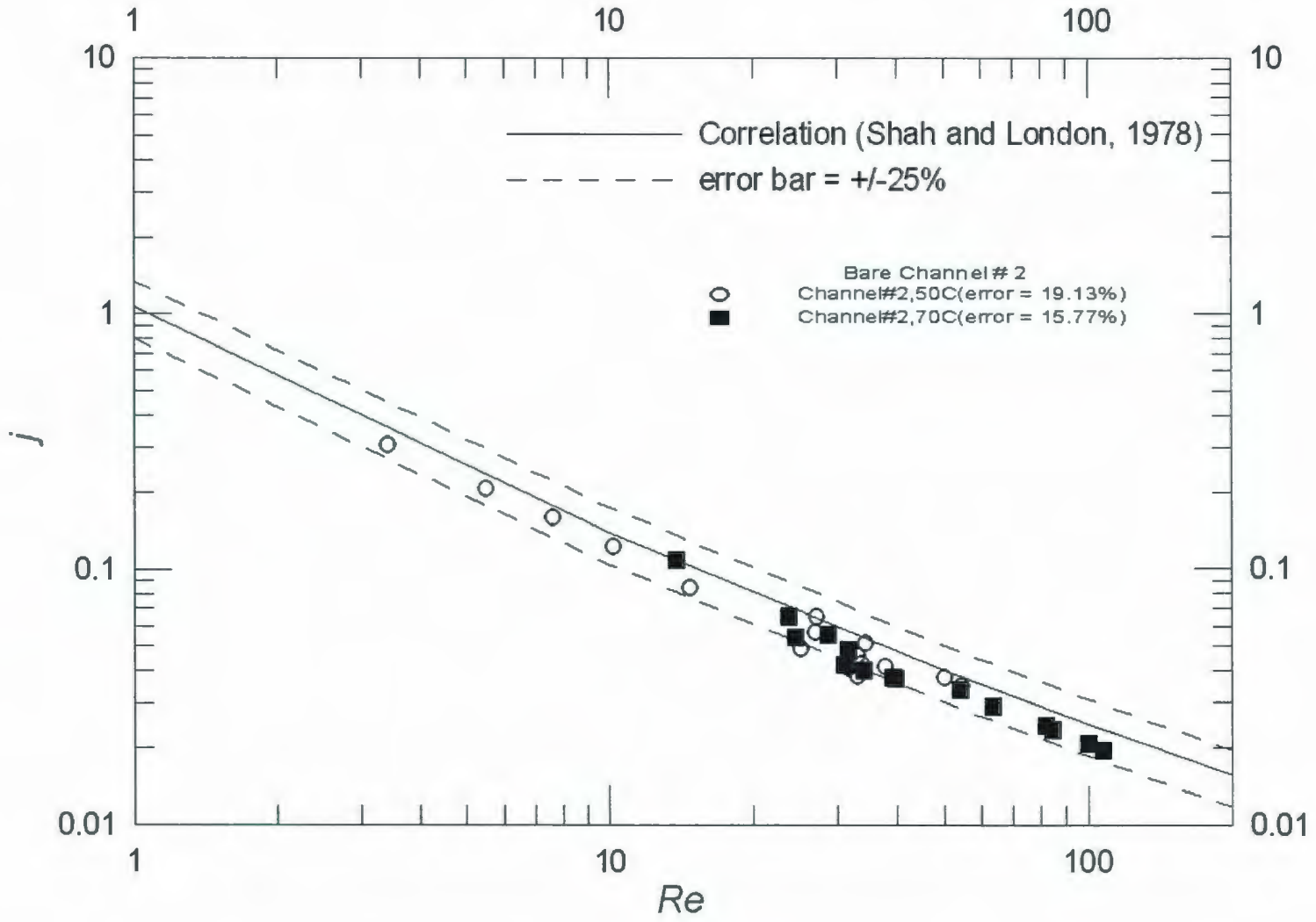

Fig. 4.3- Comparison of experimental results with thearitical for channel-2

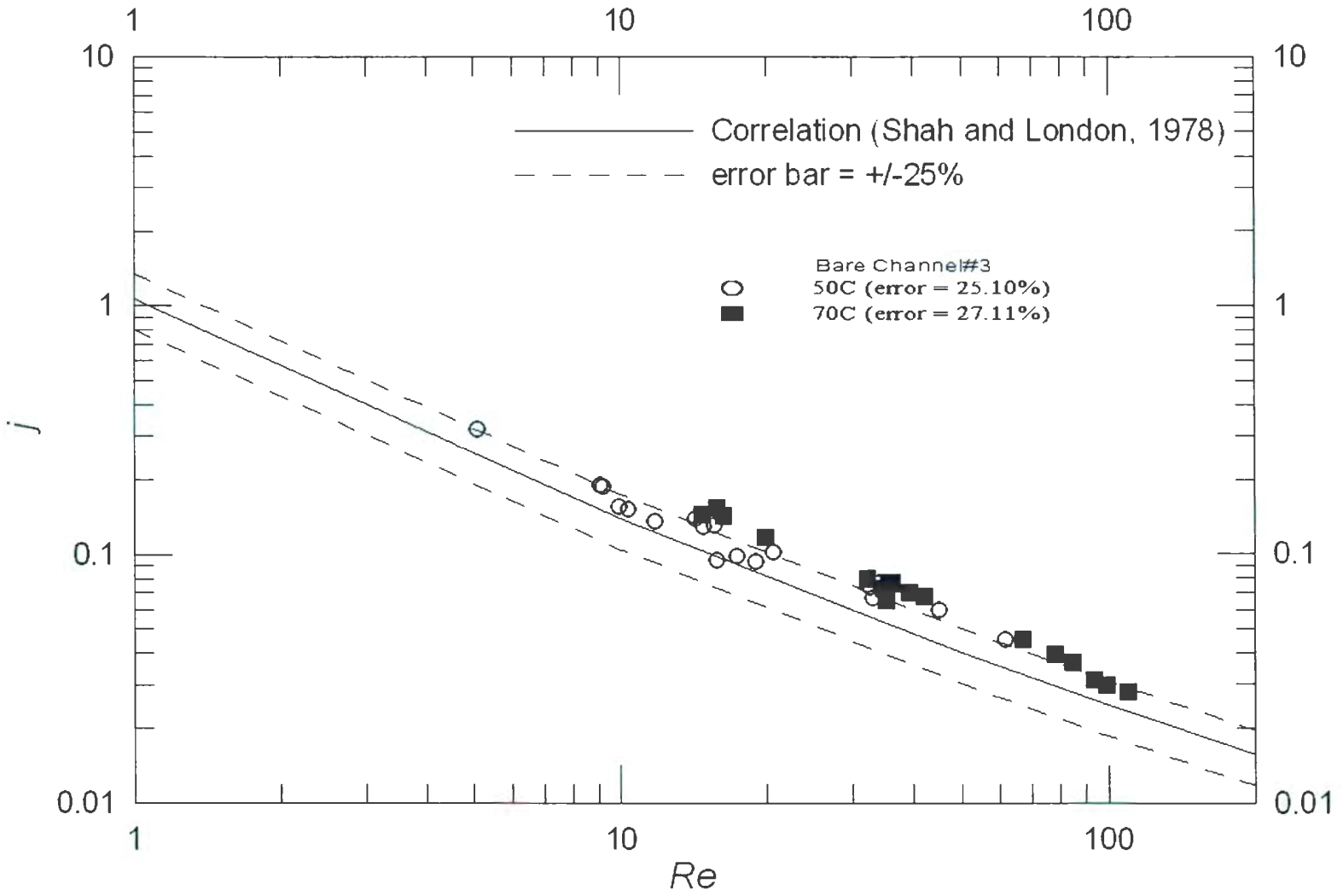

Fig. 4.4- Comparison of experimental results with thearitical for channel-3

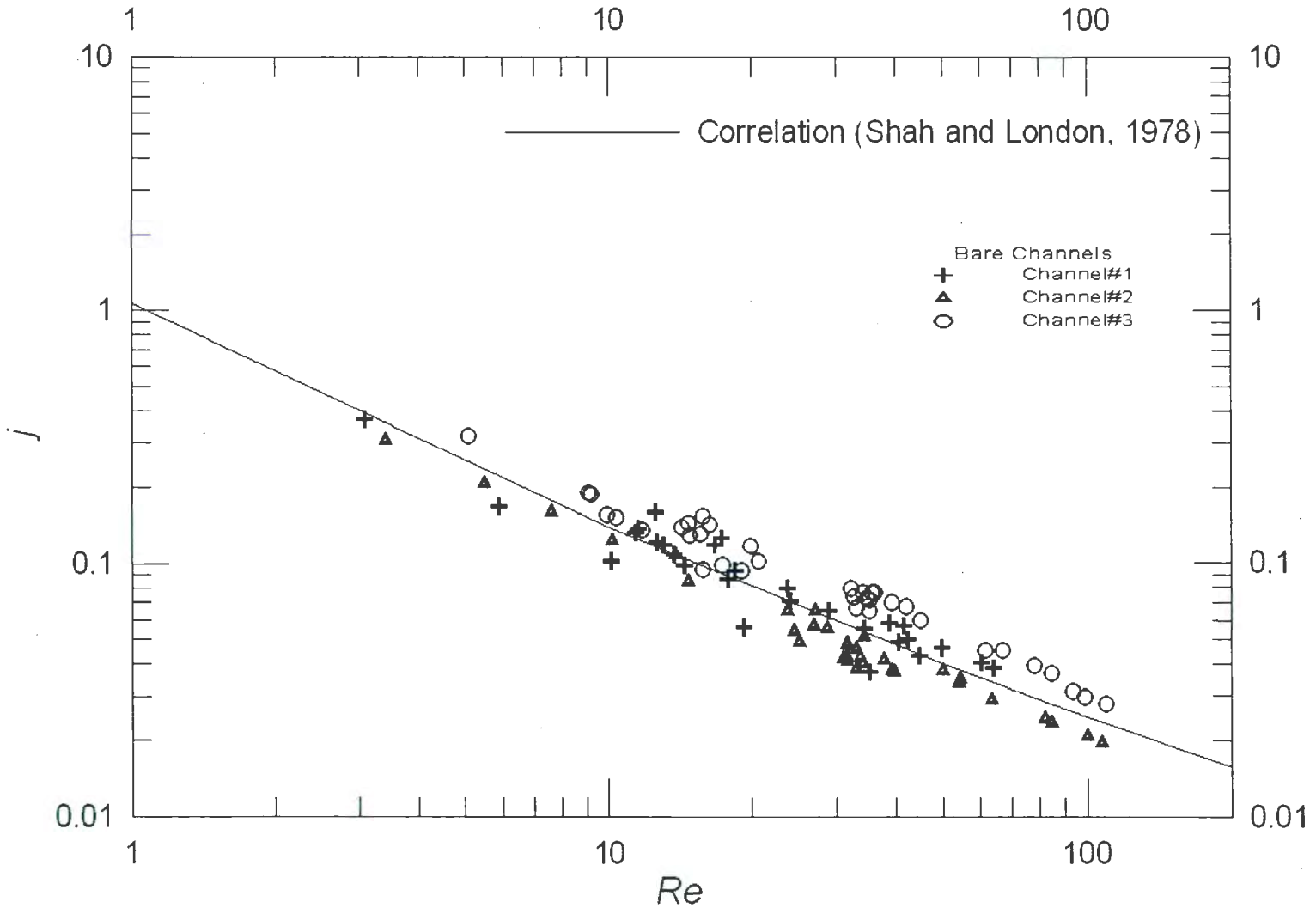

Fig. 4.5- Comparison between all bare channels data

4.4 Experimental Results for Wavy Fin

Experimental results for 15 wavy fins are shown using simple correlations are provided in Table 4.2. The experimental data has been correlated using the following two equations:

$$j = X\, Re_{D_h}^{x} \qquad 4.20$$

$$f = Y\, Re_{D_h}^{y} \qquad 4.21$$

Where X, x, Y, and y are constant for each fin. The values of these constants for each fin are provided in Table 4.2.Only the graphical representation of experimental result for fin # 1 has shown in this chapter. The rests would be provided in appendix-D.

Table 4.2

Coefficients for correlations

Fin No	X	x	Y	y
Fin-1	0.256548	-0.87034	21.91865	-1.08329
Fin-2	0.094273	-0.6173	18.86797	-1.03174
Fin-3	0.06981	-0.66117	23.61287	-0.98061
Fin-4	0.076491	-0.63885	19.39274	-1.01763
Fin-5	0.212813	-0.57618	7.499452	-0.90359
Fin-6	0.223554	-0.75715	13.40896	-1.00851
Fin-7	0.437043	-0.89463	13.19525	-1.02843
Fin-8	0.1077	-0.95641	29.50656	-1.18867
Fin-9	0.077537	-1.00847	26.7692	-1.09815
Fin-10	0.068227	-1.02016	26.00693	-1.0196
Fin-11	0.118332	-1.02131	21.44317	-0.96147
Fin-12	0.094945	-1.00322	19.57299	-1.06156
Fin-13	0.088656	-0.96615	23.4793	-1.0977
Fin-14	0.088382	-0.83752	16.9438	-0.95729
Fin-15	0.128118	-0.77255	13.88985	-0.99271

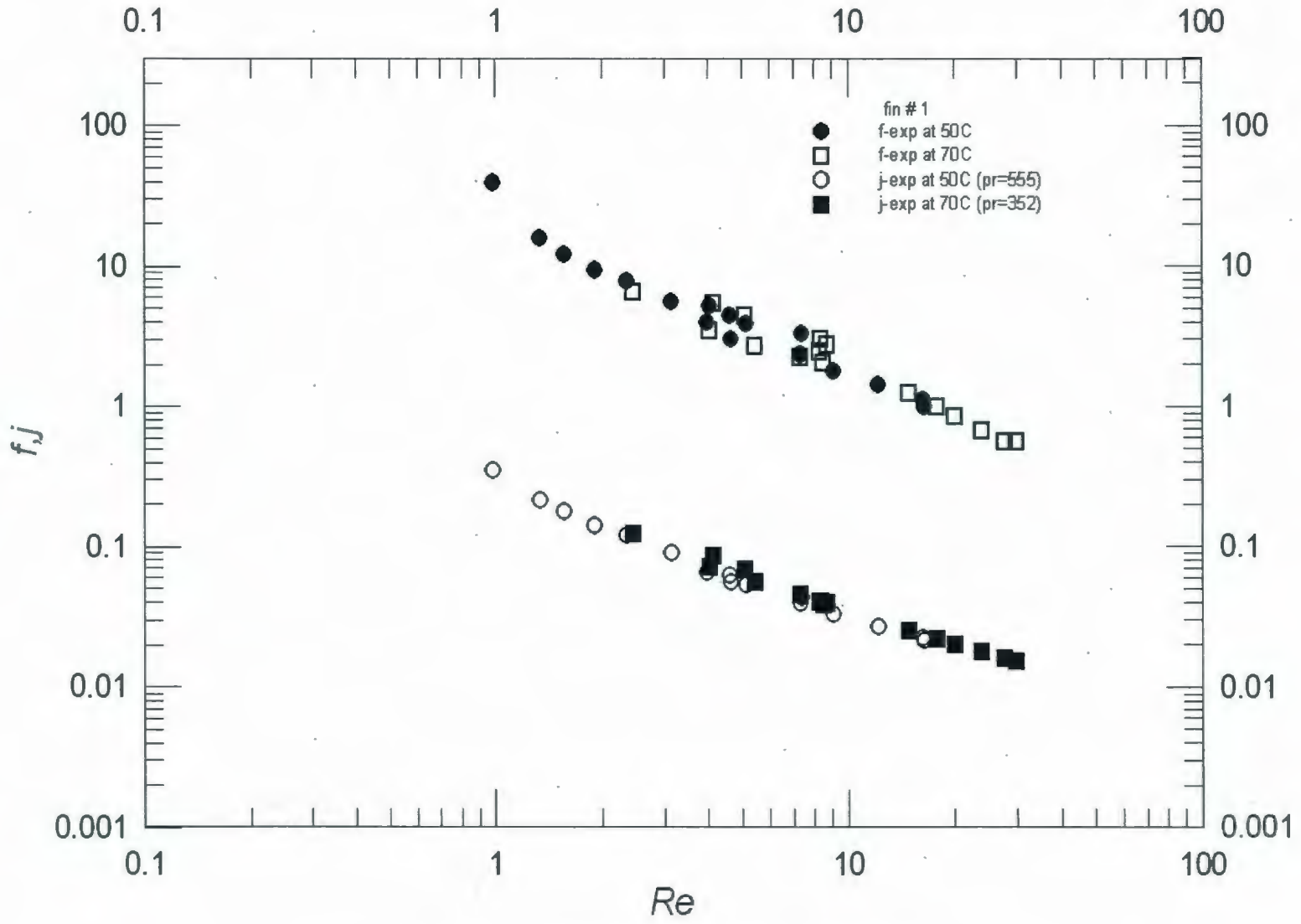

Fig. 4.6- Fin # 1 Experimental Data

4.5 Summary

Data reduction procedures for fifteen wavy fin specimens were discussed briefly in this chapter. A simple correlation was also obtained for a very low Reynolds number range such as Re < 60 for all the experiments. Each experimental result was plotted separately and also the comparison between the fin data having same height was depicted graphically. The procedure to obtain heat transfer co-efficient for a bare channel experiment was also discussed briefly for benchmarking. The experimental results for each bare channel were compared with a theoretical value which was around ± 25% RMS error.

Chapter 5

Modelling and Analysis

5.1 Introduction

Details of the analytical modelling of complex internal flows in wavy fins are presented in this chapter. A robust model is developed using fundamental theory of heat transfer and fluid mechanics. This model is robust because geometric variables (fin height, fin spacing and fin amplitude), Reynolds numbers (Re) and Prandtl number (Pr) are included in this model.

It has already mentioned in Chapter-2 that the presence of asymptotic characteristics in the wavy fin data, obtained by Manglik and Zang (2005), has not been addressed in any of the literature. The results of present experiments using high viscosity oil SAE 5W30 have also revealed this behaviour in the previous chapter. Taking advantage of these limiting characteristics enables the development of an analytically based model.

First, asymptotic and scaling principals are used to determine the limiting behaviour of the flow and then simple theoretical models are developed using fundamental theory, to link the asymptotic characteristics through non-linear transitions. This methodology was applied by Muzychka (1999) for the OSF system with air as a working fluid. He considered three distinct regions or flow regimes such as low Reynolds number flow, laminar boundary layer flow and turbulent boundary layer and/or inertial flow to develop the model using the asymptotic correlation method proposed by Churchill and Usagi (1972). He found good agreement between the model and experimental data. Recently Muzychka and Kenway (2009) also used the same methodology for the OSF system with high viscous liquid and found a good agreement.

The asymptotic model for wavy fins is developed by considering two flow regimes. These are low Reynolds number flow and laminar boundary layer flow. For both models Colburn *j* factor are modified by dividing it by the area enhancement ratio (*AER*) because this correction was observed experimentally. The high Prandtl number suppression in the wavy fin is very similar to that observed in the offset strip fin array with very viscous liquids (SAE 5W30 motor oil) by Muzychka and Kenway (2009). Finally, models combined using the asymptotic correlation method proposed by Churchill and Usagi (1972) and compared with the experimental data for fifteen wavy fins. The comparison of experimental data with both flow regimes are also shown separately.

5.2 Modeling the *f* and *j* Characteristics of Wavy Fin Geometry

Several fundamental solutions from the heat transfer and fluid dynamics are used to develop the present model. These solutions represent ideal flow conditions as well as fin geometries. The model of the *f* and *j* characteristics of wavy fin is developed assuming the fin configuration as a sinusoidal wave. This allows the effective flow length to be determined which in turn leads to the enhanced surface area. The geometrical attributes of the sinusoidal wave are shown in Figure 5.1.The sinusoidal wave can be expressed by the following equation:

$$f(x) = A\sin\left(\frac{2\pi x}{\lambda}\right) \tag{5.1}$$

where A is amplitude and λ is the wave length. The derivative of equation (5.1) is

$$f'(x) = \frac{2A\pi}{\lambda}\cos\left(\frac{2\pi x}{\lambda}\right) \tag{5.2}$$

The length of the sinusoidal wave can be determined by the following expression:

$$L_e = 2\int_0^{\lambda/2}\sqrt{1+[f'(x)]^2}\,dx = 2\int_0^{\lambda/2}\sqrt{1+\left[\frac{2A\pi}{\lambda}\cos\left(\frac{2\pi x}{\lambda}\right)\right]^2}\,dx \tag{5.3}$$

Equation 5.3 can be easily solved using Maple mathematic software. The final form of effective flow length is

$$L_e = 2\frac{\sqrt{\lambda^2 + 4A^2\pi^2}}{\pi} E\left(\frac{2A\pi}{\sqrt{\lambda^2 + 4A^2\pi^2}}\right) \quad 5.4$$

The wavy-fin-channel corrugation ratio (γ) may be defined as the ratio of Amplitude and wavelength which is given below.

$$\gamma = \frac{2A}{\lambda} \quad 5.5$$

Equation 5.4 can be written as:

$$L_e = 2\lambda\frac{\sqrt{1+\gamma^2\pi^2}}{\pi} E\left(\frac{\gamma\pi}{\sqrt{1+\gamma^2\pi^2}}\right) \quad 5.6$$

The ratio between the effective flow length and the wavelength is very important to calculate various surface area of wavy fin geometry in Chapter-3. This ratio is given by the following equation:

$$\frac{L_e}{\lambda} = 2\frac{\sqrt{1+\gamma^2\pi^2}}{\pi} E\left(\frac{\gamma\pi}{\sqrt{1+\gamma^2\pi^2}}\right) \quad 5.7$$

In this equation, the ratio, L_e/λ approaches unity when γ approaches zero.

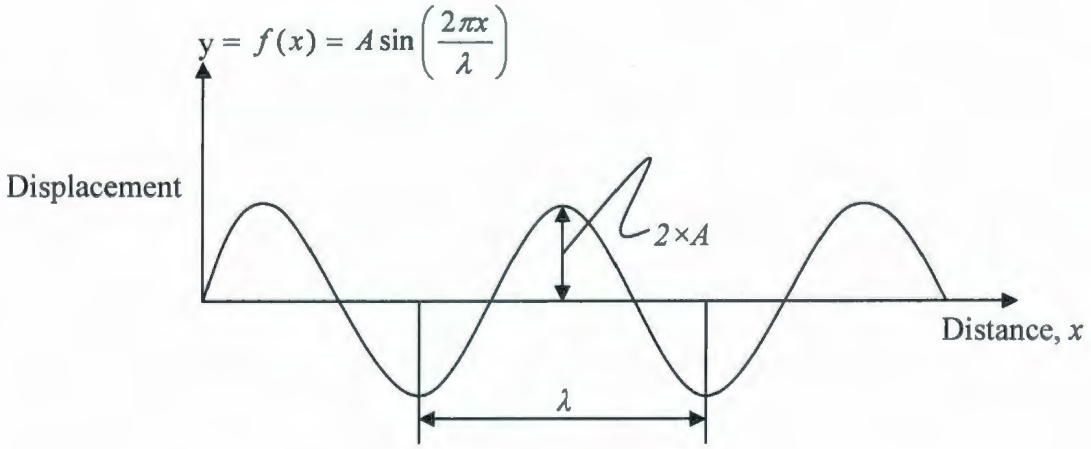

Fig. 5.1- Sinusoidal Model

5.3 Low Reynolds Number Asymptote

High viscous fluid flow inside the wavy fin passages is direct consequence of the dominant viscous effect in low inertia flows. At low Reynolds number, the flow

behaviour is the same as that in rectangular ducts with the wavy surface simply providing a longer flow path or residence time. The fluid simply adopts the wavy contour of the channel without exhibiting significant swirl, Zhang and Manglik (2003). As a result, the higher heat transfer coefficient and friction losses are due to the larger effective area of wavy surfaces.

Many researchers have verified the analytical correlations for frictional loss and heat transfer in a single flow channel which provided a excellent guideline for heat exchangers that may employ many such channels in parallel, i.e wavy channels. However, passage to passage flow non uniformity could result in significant deviation in *Nu* and *f* from the analytical predictions, Shah and Sekulic (2003). The analytical correlations for Friction factor and Colburn factor at low flow region are discussed here.

5.3.1. Friction *f* Factor

Friction factor at low Reynolds number flow in wavy fins may be determined from the wavy surface geometries and *f*-factor for the rectangular channel as the *f-Re* behaviour of wavy fin is similar to that in a straight rectangular duct except larger surface area. Thus, *fRe* for laminar flow forced convection in wavy fins is equal to *fRe* for laminar flow forced convection in rectangular ducts multiplied by the ratio of the length of the sinusoidal wave (L_e) to the wavy fin wavelength (λ) which is given below.

$$fRe_{wavy} = f\,Re_{channel}\left(\frac{L_e}{\lambda}\right) \qquad 5.8$$

There is a strong influence of flow passage geometry on *fRe* and *Nu*. *fRe* and *Nu* are a function of channel aspect ratio for laminar flow forced convection in rectangular channels. Shah and London (1978) gave the following relation between *fRe* and aspect ratio (α).

$$fRe = 24(1 - 1.3553\alpha + 1.9467\alpha^2 - 1.7012\alpha^3 + 0.9564\alpha^4 - 0.2537\alpha^5) \qquad 5.9$$

Aspect ratio (α) is already defined in Chapter-2 as S/H. Now from equation 5.7, 5.8 and 5.9, *fRe* may be obtained the following relationship:

$$fRe_{wavy} = 48\frac{\sqrt{1+\gamma^2\pi^2}}{\pi}E\left(\frac{\gamma\,\pi}{\sqrt{1+\gamma^2\pi^2}}\right)\begin{pmatrix}1-1.3553\alpha+1.9467\alpha^2-1.7012\alpha^3\\+0.9564\alpha^4-0.2537\alpha^5\end{pmatrix} \quad 5.10$$

5.3.2 Colburn *j* Factor

Nusselt numbers also depend on thermal boundary conditions and aspect ratio. Shah and London (1978) gave the following relations of heat transfer for laminar flow forced convection in rectangular ducts at the constant wall temperature boundary condition and the constant heat flux boundary condition.

$$Nu_T = 7.541(1-2.610\alpha+4.970\alpha^2-5.119\alpha^3+2.702\alpha^4-0.548\alpha^5) \quad 5.11$$

$$Nu_{H1} = 8.235(1-2.0421\alpha+3.0853\alpha^2-2.4765\alpha^3+1.0578\alpha^4-0.1861\alpha^5) \quad 5.12$$

The Nusselt number (*Nu*) for laminar flow forced convection in wavy fins at the constant wall temperature boundary condition and the constant heat flux boundary condition will be the same as they are assumed to be based on the total surface area and not nominal surface area. The Colburn factor can be determined by using the appropriate correlation of *Nu*.

5.3.3 Comparison of Models with Data

The low Reynolds number analytical model for friction factor and Colburn factor are compared with fifteen sets of experimental data to predict the thermal-hydraulic characteristics of wavy fin. Only the comparison for fin # 1 has shown in this chapter. The rests would be provided in appendix-D. From all the comparisons, it is clearly found that the experimental data agreed very well at low Reynolds number regimes but the data were under predicted from the model with the increase of Reynolds number. Some discrepancy was found between data and model predictions at higher Reynolds number due to presence of asymptotic characteristics in wavy fin data. Particularly for j-factor comparison, larger bias errors were found in most sets of data at larger Reynolds number although there was a great fit at low Reynolds number. Thus, it is not possible to obtain a great fit between the data and the Low Reynolds number asymptote for a wide range of Reynolds number.

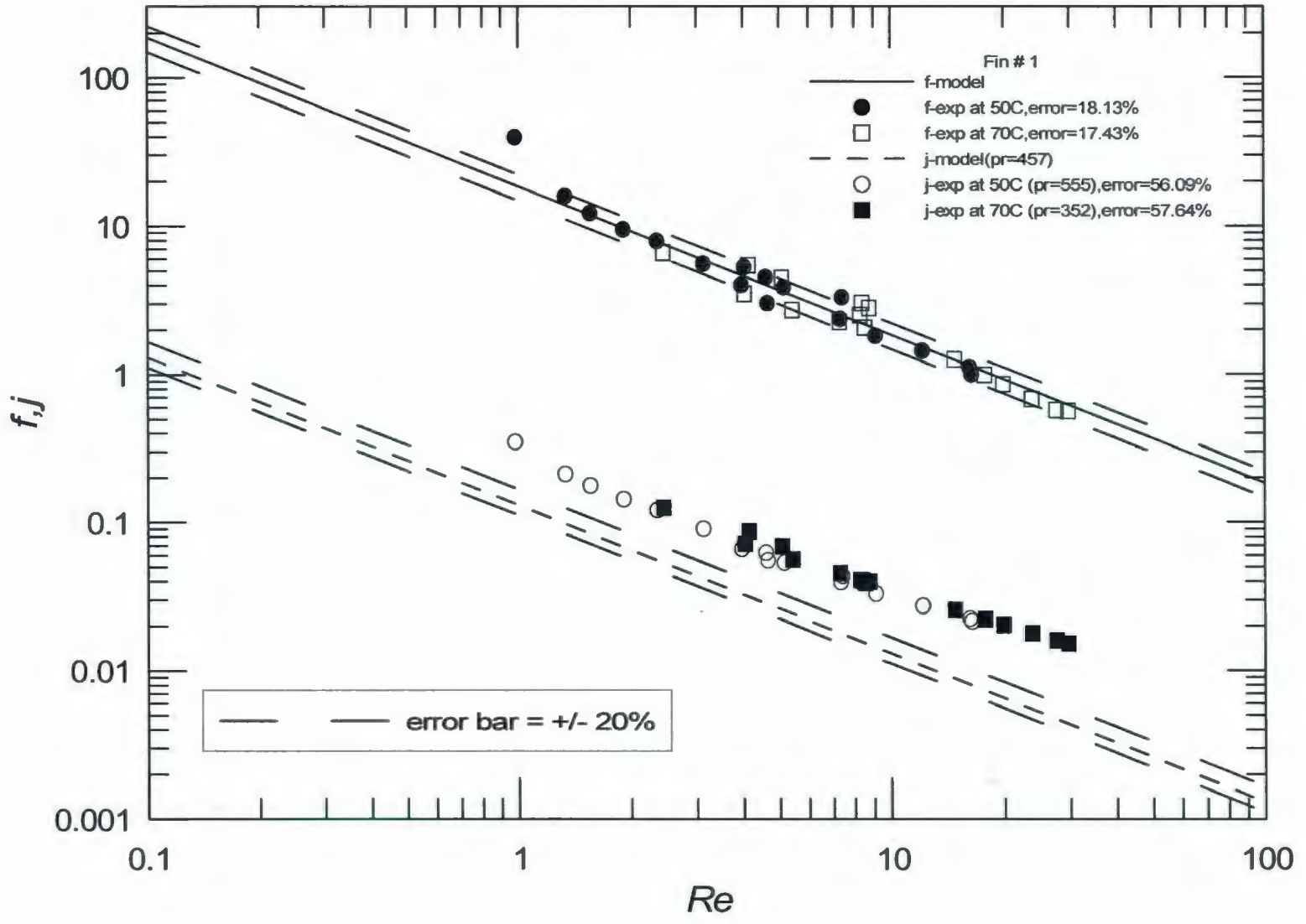

Fig. 5.2 - Comparison of Fin # 1 data with low Reynolds number Asymptote

5.4 Laminar Boundary Layer (LBL) Asymptote

The flow develops within each small sub channel of wavy fins are similar to plain channel in the laminar region. A boundary layer is created on the sub channel walls and starts to grow. As the Reynolds number increases, fluid inertia dominates and the spatial coverage of wavy-surface-curvature induced vortices or swirl recirculation increases, which initiated a higher momentum and energy transport and wall frictional loss.

5.4.1 Friction *f* Factor

In the entrance region where the boundary layer thickness is similar for all different geometrical ducts. Shapiro et al. (1954) derived an analytical result for the apparent friction factor in the entrance region of the circular duct using several methods. The leading term in the solution for any characteristic length D_h is given by

$$f_{app}\, Re_{D_h} = \frac{3.44}{\sqrt{L^+}} \quad L^+ = L/(D_h\, Re_{D_h}) < 0.001 \tag{5.13}$$

Where L is defined by the following equation:

$$L = \frac{L_e}{2} = \lambda \frac{\sqrt{1+\gamma^2\pi^2}}{\pi} \mathrm{E}\left(\frac{\gamma\,\pi}{\sqrt{1+\gamma^2\pi^2}}\right) \tag{5.14}$$

The length, L in Eqs. 5.14 is the half length of the sinusoidal wave ($L \sim 0.5L_e$) because it is from the top to the bottom of the sinusoidal wave.

This solution in Eqs. 5.13 is not depend on duct shape and may be used to compute the apparent friction factor in the entrance region of wavy fin passages.

5.4.2 Coulburn *j* Factor

In the laminar region, the colburn j factor should posses characteristics of laminar duct flow. For laminar boundary layer flow, the Nusselt number (*Nu*) may be defined as

$$Nu = 0.664 Re_L^{1/2} Pr^{1/3} \quad 5.15$$

Using Eq. 4.15 and Eq. 5.15, j factor for wavy fin channel can be predicted by the following expression:

$$j_{LBL} = \frac{0.664}{\mathrm{Re_L}^{1/2}} = \frac{0.664}{\mathrm{Re_{D_h}}^{1/2}} \left(\frac{D_h}{L} \right)^{1/2} \quad 5.16$$

Where L is defined in Eq. 5.14.

5.4.3 Comparison of Models with Data

All the data of present experiment are also compared with the laminar boundary layer asymptote. Only the comparison for fin # 1 has shown in this chapter. The rests would be provided in appendix-D. In this case, the data are under predicted at low Reynolds number regimes but an excellent agreement is found with the models with increase of Reynolds number for most of the data sets. For that reasons, larger bias errors were found for both comparisons. The friction factor data were drawn away more from the LBL flow prediction at low Reynolds number flow although the data agreed very well at higher Reynolds number. From these comparisons, it is also clear that a great fit is not possible between the wavy fin data and laminar boundary layer asymptote for a wide range of Reynolds number.

Fig 5.4 and 5.5 show the comparison of both asymptotic solutions with the data for friction factor and Colburn factor respectively. The enhanced heat transfer performance and increased pressure drop penalty are observed at LBL flow regimes due to induce vortices in the wall waviness valley region with the increase of Reynolds number at those regimes.

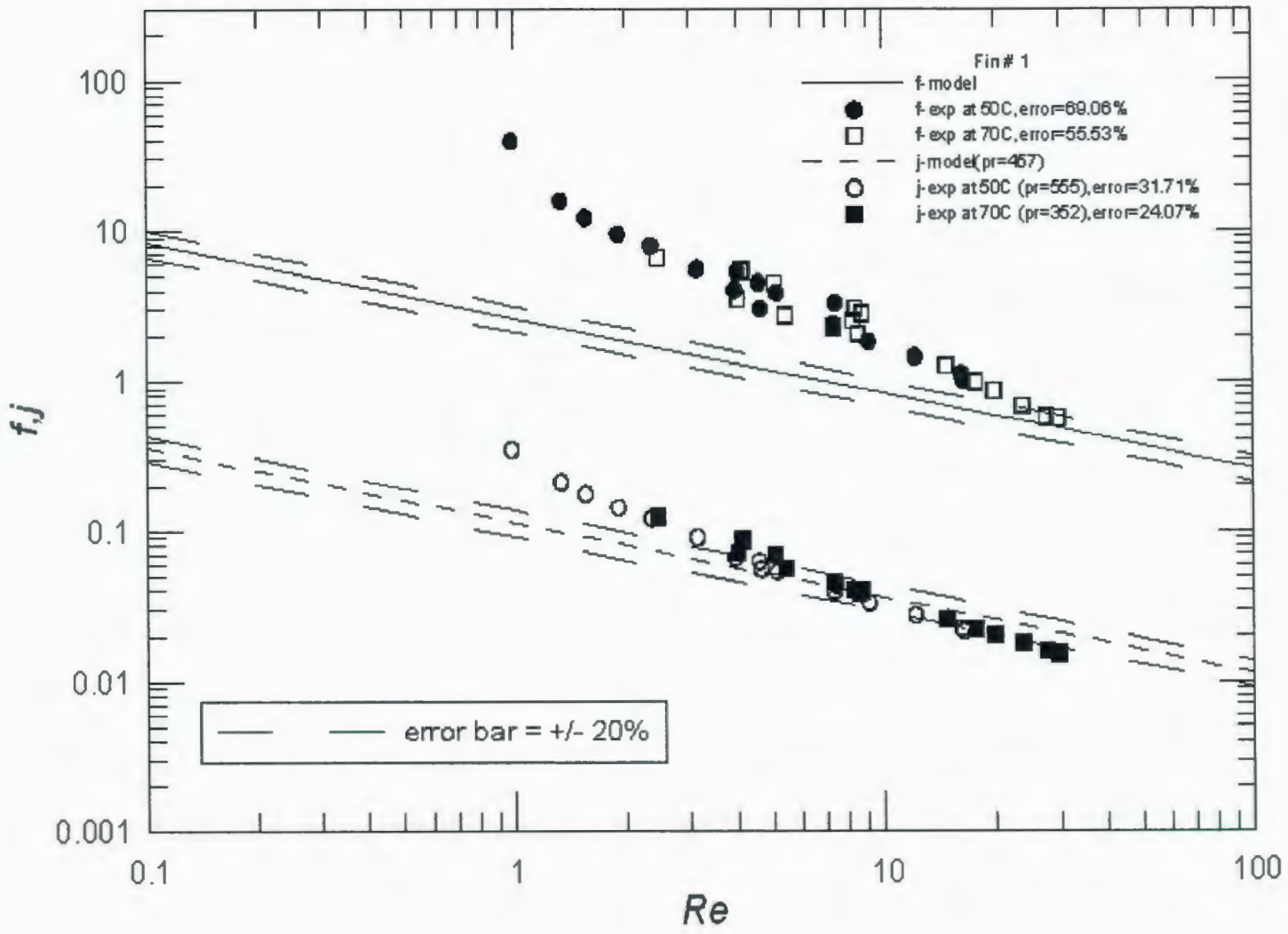

Fig. 5.3 – Comparison of Fin # 1 data with LBL Asymptote

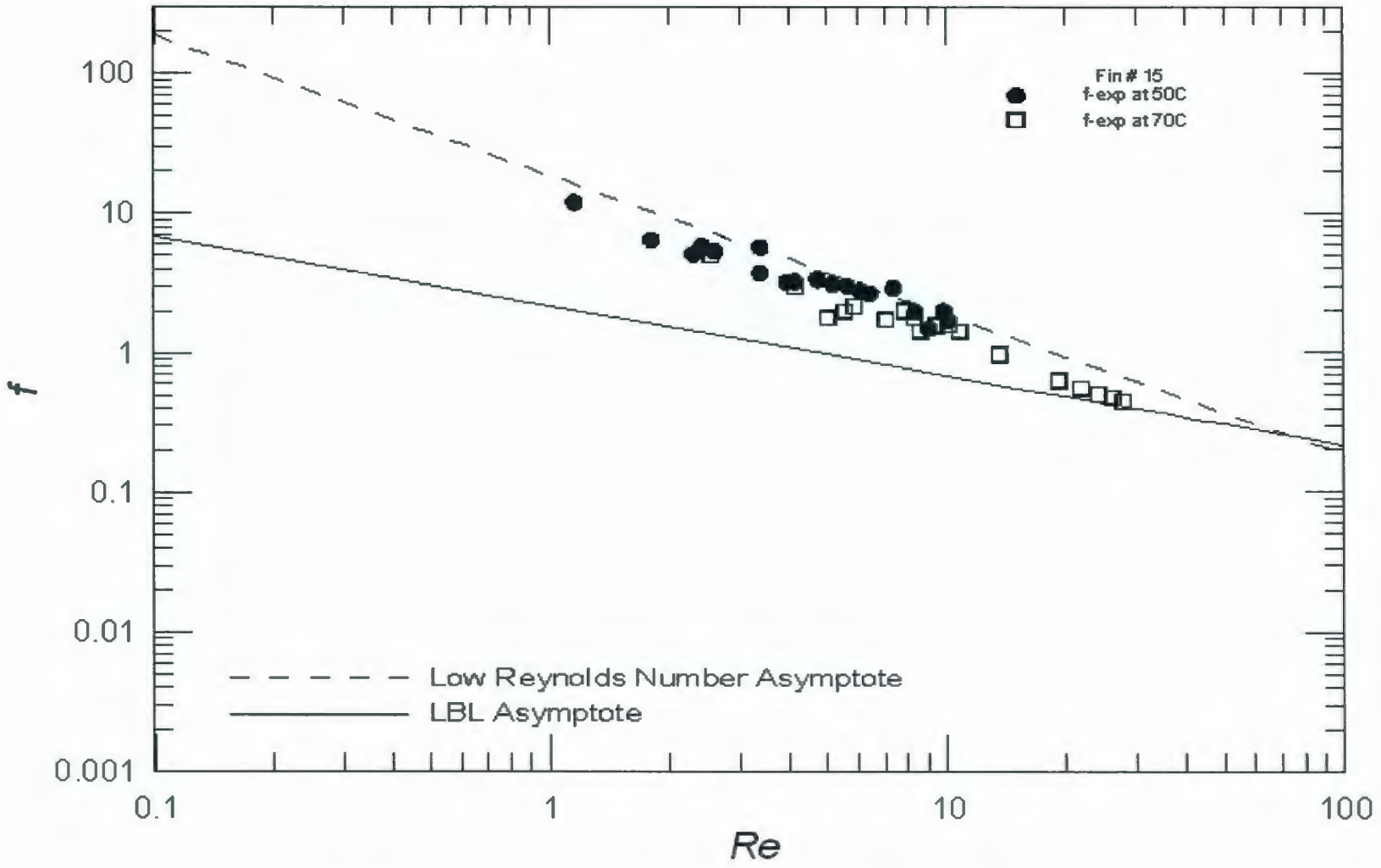

Fig. 5.4 – Comparison of Asymptotic solutions with data of fin # 15

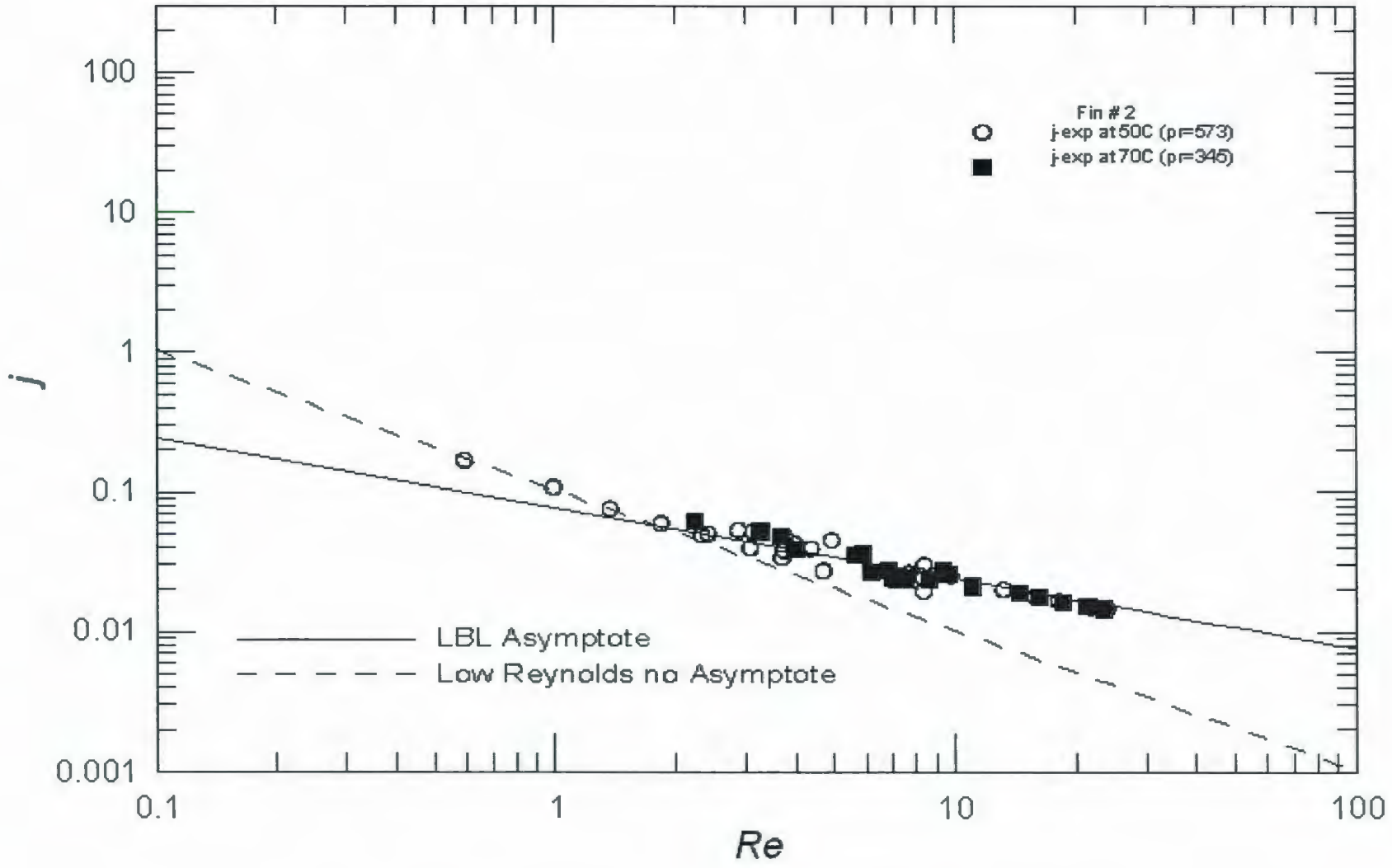

Fig. 5.5 – Comparison of Asymptotic solutions with data of fin # 2

5.5 Combination of Asymptotic Models

A general asymptotic model is developed by combining the model for low Reynolds number flow and the model for laminar boundary layer flow for both the friction factor and Colburn factor using the Churchill and Usage (1972) correlated method. It may predict the friction factor and Colburn factor over the entire range of Reynolds number for wavy fin geometry.

The combined asymptotic model of the frictional performance of the wavy fins is:

$$f = \left[\left(f_{wavy} \right)^2 + \left(f_{app} \right)^2 \right]^{1/2} \tag{5.17}$$

where f_{wavy} and f_{app} are determined from the eq. 5.10 and eq. 5.13 respectively. The asymptotic model of the heat transfer performance of the wavy fins at the uniform wall temperature boundary condition is

$$j = \left[\left(j_{wavy,T} \right)^5 + \left(j_{LBL} \right)^5 \right]^{1/5} \tag{5.18}$$

where j_{LBL} is defined by the eq. 5.16 and $j_{wavy,T}$ is expressed by the eq. bellow.

$$j_{wavy,T} = \frac{7.541}{\mathrm{Re}\ \mathrm{Pr}^{1/3}} (1 - 2.610\alpha + 4.970\alpha^2 - 5.119\alpha^3 + 2.702\alpha^4 - 0.548\alpha^5) \tag{5.19}$$

Thus, from the discussion in section 5.1, a very good approximation for high Prandtl number liquids as follows:

$$j_{liquid} = \frac{j}{AER} \tag{5.20}$$

By using the definition of Area enhancement ratio (AER) from 3.7,

$$j_{liquid} = j \cdot \left[\left(\frac{L_e}{\lambda} \right) \left(\frac{H}{W} \right) (1+\alpha) N_{ch} \right]^{-1} \tag{5.21}$$

5.6 Comparison of Models with data

The proposed models are compared with fifteen sets of experimental data. Good agreement between the proposed model and the wavy fin data is achieved for all except four data sets. Table 5.1 presents percents of root mean square errors for all experimental

data with models at both temperature levels. The errors were found higher for high temperature level and high Reynolds number for most of the fins data. Table 5.2 presents the total percentage of RMS errors for each fin. The global percentage of RMS was found 32.1 and 22.8 for friction factor and Colburn factor respectively. Most sets of data were predicted within approximately ± 25%. The data for fin-5, fin-6, fin-7, and fin -15 do not agree very well with the models. The models either under predicted or over predicted with the data which increased the global error. Only the comparison for fin # 1 has shown in this chapter. The rests would be provided in appendix-D.

Table 5.1

Comparison of Experimental Data with Models

at both temperature levels

Fin no	% RMS of f at 50°C	% RMS of f at 70°C	% RMS of j at 50°C	% RMS of j at 70°C
1	21.2	26.5	29	23.2
2	26.2	31.2	14.8	14.5
3	14.5	16.3	22	13.1
4	14.6	32.4	32.6	27
5	78.4	108.8	12.9	21.1
6	31.9	49.4	30.1	27.7
7	43.1	59.1	46.8	47.1
8	17.1	15.7	24.2	17.9
9	18.7	16.4	15.9	16.3
10	21.1	12.7	14.4	11.5
11	19.9	24.6	22.3	23.8
12	13.8	40.3	16.8	22.3
13	12.5	24.1	15.2	29.6
14	16.4	28.2	17.7	28.8
15	34.9	61.9	21.1	33.5

Table 5.2

Comparison of Experimental Data with Models

Fin no	Pr	Re	% RMS of f	% RMS of j
1	352-555	0.1-100	23.918	26.408
2	345-573	0.1-100	33.207	13.298
3	331-562	0.1-100	15.431	18.07
4	363-547	0.1-100	25.14	29.932
5	337-532	0.1-100	94.4	17.362
6	324-538	0.1-100	41.806	28.894
7	343-534	0.1-100	52.163	46.96
8	335-538	0.1-100	16.361	21.004
9	339-540	0.1-100	17.588	16.088
10	318-516	0.1-100	17.709	13.172
11	336-534	0.1-100	22.51	23.121
12	331-529	0.1-100	29.81	19.63
13	327-526	0.1-100	19.498	23.876
14	331-520	0.1-100	22.73	23.611
15	327-514	0.1-100	49.892	27.798
Global	-	-	*32.1*	*22.8*

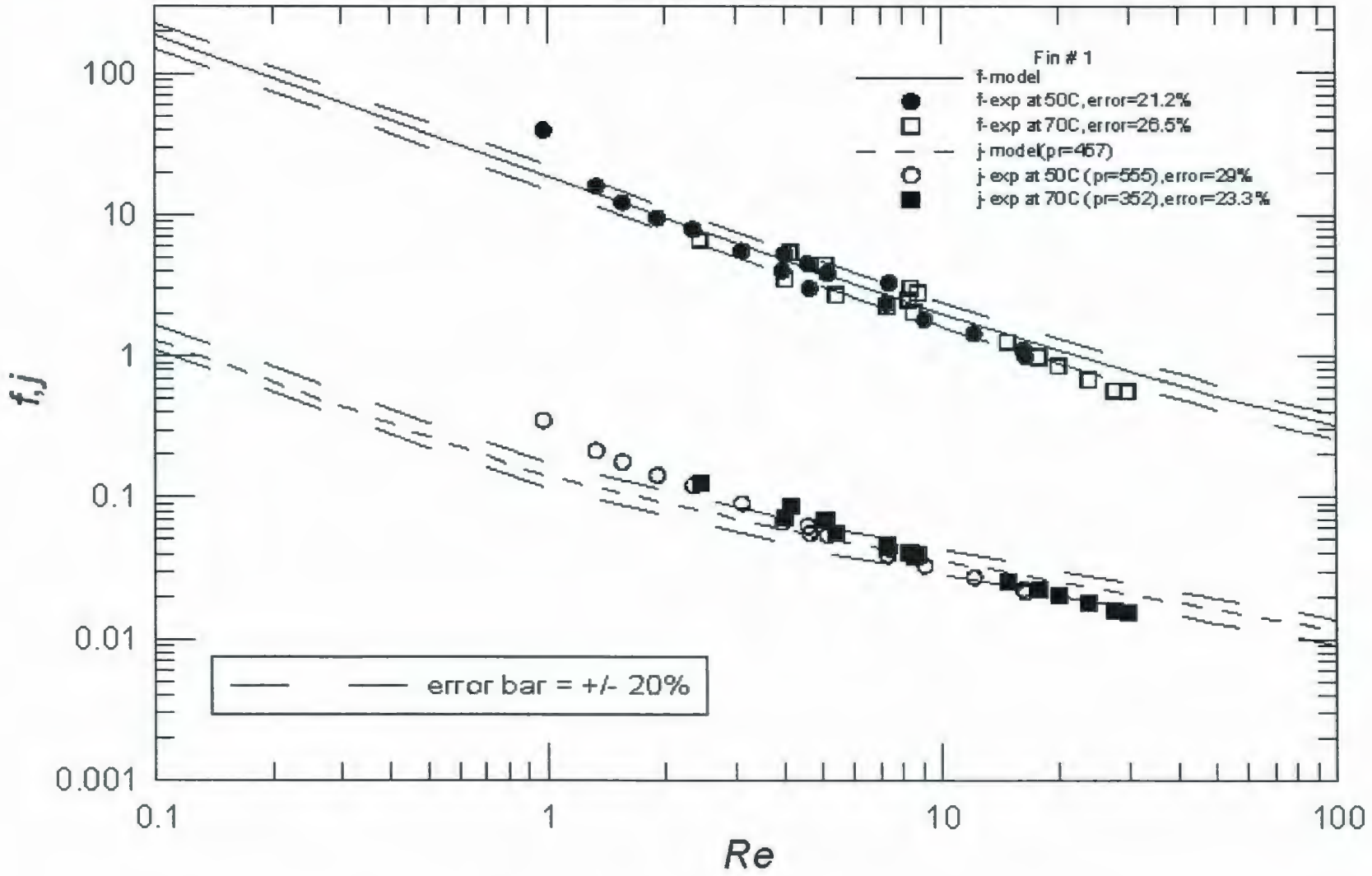

Fig. 5.5 – Comparison of Fin # 1 data with models

5.7 Summary

Models were developed for very high Prandtl number liquid (Pr = 318 to 573) which can predict the friction f factor and Colburn j factor data of wavy geometry within ± 25 %. Analytical expressions for both low Reynolds number flow regimes and laminar boundary layer regimes were combined using the asymptotic correlation method proposed by Churchill and Usagi (1972) which can cover a wide range of Reynolds number. Experimental data for fifteen different fin geometries were used to validate this asymptotic model.

Chapter 6

Summary and Conclusions

6.1 Summary of Present Work

The heat transfer and pressure drop characteristics for wavy fin heat exchangers were examined in this thesis. The experimental results presented in this work provided a detailed understanding of forced convection behaviour in wavy plate-fin channels with fifteen different geometric combinations of the following parameters: $0.07 < \alpha < 0.67$, $0.1 < \gamma < 0.18$, and $0.4 < \varepsilon < 1.23$. The experiments were conducted for larger Prandtl number ($318 < Pr < 573$) and very low Reynolds number ($0.1 < Re < 100$) using 5W30 oil as a test fluid.

The experimental ($f - Re$) and ($j - Re$) results suggest two flow regimes, namely, the low Reynolds number regime and the laminar boundary layer regime. At low Reynolds number, the flow behaviour is the same as that in rectangular ducts. The heat transfer coefficient and friction losses are increased due to the larger effective area of wavy surfaces at those regimes. The higher heat transfer performance and pressure drop penalty are observed at LBL flow regimes due to induced vortices in the wall waviness valley region with the increase of Reynolds number.

A robust model which includes geometric variables (fin height, fin spacing and fin amplitude), Reynolds numbers (Re) and Prandtl number (Pr) model is developed using fundamental theory of heat transfer and fluid mechanics to predict the thermal-hydraulic characteristics over a entire range of Reynolds number in wavy fin heat exchangers. This model is the combination of the simple asymptotic solutions for the low Reynolds number and laminar boundary layer regions using a simple correlation method proposed by Churchill and Usagi (1972). This new models predicts most of the present

experimental data sets within ± 25% for both the Fanning friction factor, f and Colburn j factor.

6.2 Recommendations for Future Work

The following work is recommended for future study:

The current experiment was conducted using two rubber silicon surface heaters at both sides of the test cells instead of using the coolant. The flow rate was also determined from the input power supplied to the heaters due to lack of an accurate flow meter. To test the wavy channels of present experiments using coolant and an efficient flow meter may provide more accurate results of heat transfers and frictional losses.

Flow visualization experiment was not performed in this work. It is very important to measure the pressure drop, velocity distribution, and flow pattern of high viscous liquid flowing through the wavy fin passages.

The asymptotic models for the wavy fin channel have been developed over a wide range of Reynolds numbers. But the data has only been obtained from the present experiment for a narrow range of Reynolds number ($0.1 < Re < 100$) to validate the model. It is necessary to validate the proposed model with wider range of Reynolds number.

References

Ali, M. M., and Ramadhyani, S., (1992) Experiments on Convective Heat Transfer in Corrugated Channels, *Experimental Heat Transfer*, 5 (3), pp. 175-193.

Amano, R. S., (1985) A Numerical Study of Laminar and Turbulent Heat Transfer in a Periodically Corrugated Wall Channel, *ASME Journal of Heat Transfer*, 107 (3), pp. 564-569.

Amano, R. S., Bagherlee, A., Smith, R. J., and Niess, T. G., (1987) Turbulent Heat Transfer in Corrugated Wall Channels with and without Fins, *ASME Journal of Heat Transfer*, 109 (1), pp.62-67.

Asako, Y., Nakamura, H., and Faghri, M., (1988) Heat Transfer and Pressure Drop Characteristics in a Corrugated Duct with Rounded Corners, *International Journal of Heat and Mass Transfer*, 31 (6), pp. 1237-1245.

Asako, Y., and Faghri, M., (1987) Finite-Volume Solutions for Laminar Flow and Heat Transfer in a Corrugated Duct, *ASME Journal of Heat Transfer*, 109 (3), pp. 627-634.

Bergles, A. E., (1998), Techniques to enhance heat transfer, Handbook of heat transfer (W. M. Rohsenow, J.p. Hartnett, and Y.I. Cho, Eds), 3rd ed., McGraw-Hill, Newwork, Ch. 11.

Churchill, S. W. and Usagi, R., A general *Expression for the Correlation of Rates of Transfer and Other Phenomena*, American Institute of Chemical Engineers, Vol.18, 1972, pp. 1121-1128.

Goldstein, L., and Sparrow, E. M., (1977) Heat/Mass Transfer Characteristics for Flow in a Corrugated Wall Channel, *ASME Journal of Heat Transfer*, 99 (2), pp. 187-195.

Gschwind, P., and Kottke, V., (1999) Heat and Mass Transfer of Free-Flow Arrangements with Corresponding Pressure Drop, In R. K. Shah, Editor, *Compact Heat Exchangers and Enhancement Technology for the Process Industries*, New York: Begell House.

Gupta, J. P., (1990) *Working with Heat Exchangers*, Hemisphere Publishing Corporation.

Holman, J. P., (Seventh Edition) *Experimental Methods for Engineers*, Mc Graw-Hill.

Junqi, D., Jiangping, C., Zhijiu, C., Yimin, Z., and Wenfeng, Z., (2007) Heat Transfer and Pressure Drop Correlations for the Wavy Fin and Flat Tube Heat Exchangers, *Applied Thermal Engineering*, 27 (11-12), pp. 2066-2073.

Kakak, S., and Liu, H., (1998) *Heat Exchanger Selection, Ratings, and Thermal Design*, CRC Press LLC.

Kays, W. M. and London, A. L., (1984) *Compact Heat Exchangers*, Kreiger Publishing.

Kuppon, T., (2000) *Heat exchanger Design Handbook*, Marcel Dekker.

Lin, Y.-T., Hwang, Y.-M., and Wang, C.-C., (2002) Performance of the Herringbone Wavy Fin under Dehumidifying Conditions, *International Journal of Heat and Mass Transfer*, 45 (25), pp. 5035-5044.

Lemczyk, T.F., and Molloy, D., (1996), Fluid Properties Research Report: Advanced Engineering NP-329, Long Manufacturing.

Manglik, R. M., Zhang, J., and Muley, A., (2005) Low Reynolds Number Forced Convection in Three-Dimensional Wavy-Plate-Fin Compact Channels: Fin Density Effects," *International Journal of Heat and Mass Transfer*, 48 (8), pp. 1439-1449.

Metwally, H. M., and Manglik, R. M., (2000) A Computational Study of Enhanced Heat Transfer in Laminar Flows of Non-Newtonian Fluids in Corrugated-Plate Channels, *Advances in Enhanced Heat Transfer* (Manglik, R. M. et al., Eds.), HTD-vol. 365/PID-vol.4, pp.41-48.

Metwally, H. M., (2002), A computational Study of Enhanced Laminar Forced Convection Heat Transfer to Newtonian and Non-Newtonian Fliud Flows in Sinusoidal Corrugated-Plate Channels, Ph.D. Thesis, University of Cincinnati.

Moffat, R. J., (1988) Describing Uncertainties in Experimental Results, *Experimental Thermal Fluid Science*, 1 (1), pp. 3-17.

Mulay, A., Borghese, J., Manglik, R. M., Kundu, J., (2002) Experimental and Numerical Investigation of Thermal-Hydraulic Characteristics of Wavy-Channel Compact Heat Exchanger, *Proc. of the 12th International Heat Transfer Conference*, France, vol. 4, pp. 417-422.

Muley, A., Borghese, J. B., White, S. L., and Manglik, R. M., (2006) Enhanced Thermal-Hydraulic Performance of a Wavy-Plate-Fin Compact Heat Exchanger: Effect of Corrugation Severity, *Proceedings of 2006 ASME International Mechanical Engineering Congress and Exposition (IMECE2006)*, Chicago, IL, USA, IMECE2006-14755.

Muzychka, Y. S., (1999) *Analytical and Experimental Study of Fluid Friction and Heat Transfer in Low Reynolds Number Flow Heat Exchangers*, Ph.D. Thesis, University of Waterloo.

Muzychka, Y.S. and Kenway, G., (2009) A Model for the Thermal Hydraulic Characteristics of the Offset Strip Fin Array for Large Prandtl Number Liquids, *Journal of Enhanced Heat Transfer*, 16 (1), pp. 73-92.

O'Brien, J. E. and Sparrow, E. M., (1982) Corrugated Duct Heat Transfer, Pressure Drop, and Flow Visualization, *ASME Journal of Heat Transfer*, 104 (3), pp. 410-416.

Rush, T. A., Newell, T. A., and Jacobi, A. M., (1999) An Experimental Study of Flow and Heat Transfer in Sinusoidal Wavy Passages, *International Journal of Heat and Mass Transfer*, 42 (9), pp. 1541-1553.

Shah, R. K. and London, A. L., (1978) *Advances in Heat Transfer, Suppl. 1, Laminar Forced Flow Convection in Ducts*, Academic Press, New York.

Shah, R. K. and Sekulic, D., (2003), *Fundamentals of Heat Exchanger Design*, Wiley.

Shapiro, A. H., Siegel, R., and Kline, S. J., (1954) Friction Factor in the Laminar Entry Region of a Smooth Tube, *Proceedings of the 2nd U.S. National Congress of Applied Mechanics*, pp. 733-741.

Sparrow, E. M., and Comb, J. W., (1983) Effect of Interwall Spacing and Fluid Flow Inlet Conditions on a Corrugated-Wall Heat Exchanger, *International Journal of Heat and Mass Transfer*, 26 (7), pp. 993-1005.

Sparrow, E. M., and Hossfeld, L. M., (1984) Effect of Rounding of Protruding Edges on Heat Transfer and Pressure Drop in a Duct, *International Journal of Heat and Mass Transfer*, 27 (10), pp. 1715-1723.

Tao, Y. B., He, Y. L., Wu, Z. G., and Tao, W. Q., (2007) Numerical Design of an Efficient Wavy Fin Surface Based on the Local Heat Transfer Coefficient Study, *Journal of Enhanced Heat Transfer*, 14 (4), pp. 315-322.

Webb, R and Kim, N-H, (2005) *Principles of Enhanced Heat Transfer*, Taylor and Francis.

Vyas, S., Zhang, J., and Manglik, R. M., (2004) Steady Recirculation and Laminar Forced Convection in a Sinusoidal Wavy Channel, *ASME Journal of Heat Transfer*, 126 (4), pp. 500.

Zhang, J., (2005) *Numerical Simulations of Steady Low-Reynolds-Number Flows and Enhanced Heat Transfer in Wavy Plate-Fin Passages*, Ph. D. thesis, University of Cincinnati.

Zhang, J., Kundu, J., and Manglik, R. M., (2004) Effect of Fin Waviness and Spacing on the Lateral Vortex Structure and Laminar Heat Transfer in Wavy-Plate-Fin Cores, *International Journal of Heat and Mass Transfer*, 47 (8-9), pp. 1719-1730.

Zhang, J., Muley, A., Borghese, J. B., and Manglik, R. M., (2003) Computational and Experimental Study of Enhanced Laminar Flow Heat Transfer in Three-Dimensional Sinusoidal Wavy-Plate-Fin Channels, *Proceedings of the ASME Summer Heat Transfer Conference*, vol. 1, pp. 665-672.

Appendix A

Test core Specifications

Five test plates have machined in different heights to test the different fin specimens. One common cover plate with two inlet/exit manifolds at the edges have also used in test section. Fig A.1 to A.3 shows the details specifications of the components of the test core.

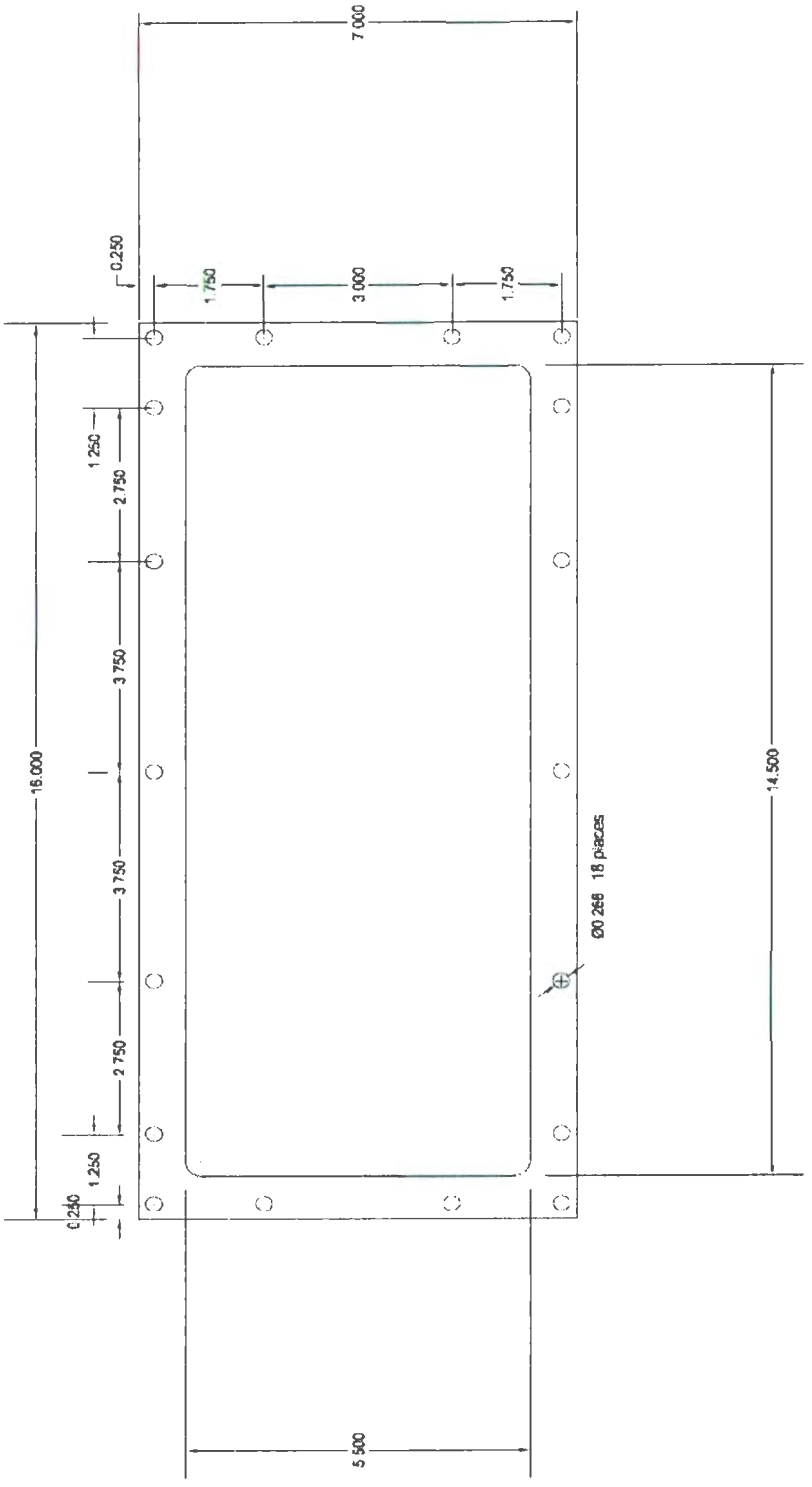

Fig. A.1 - Test Channel

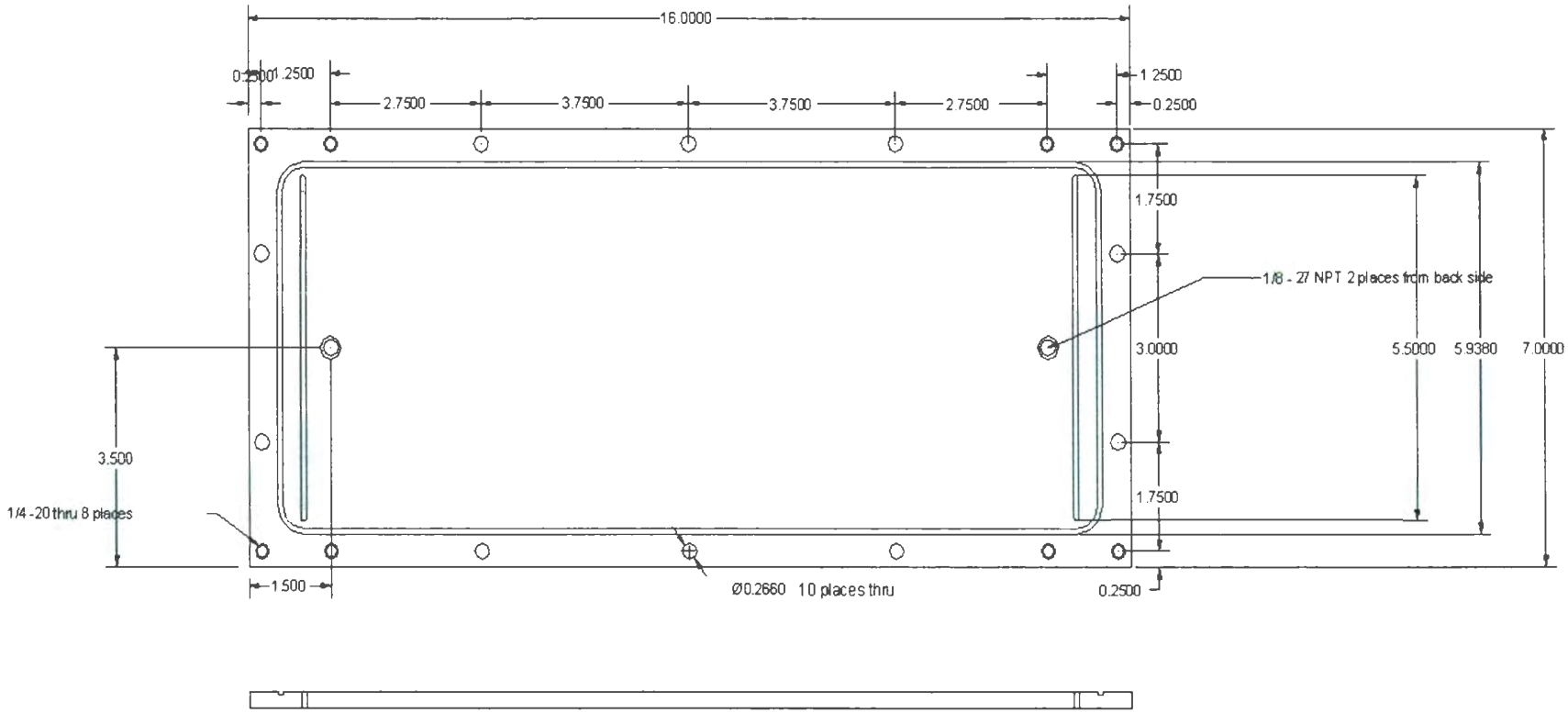

Fig. A.2 - Cover Plate

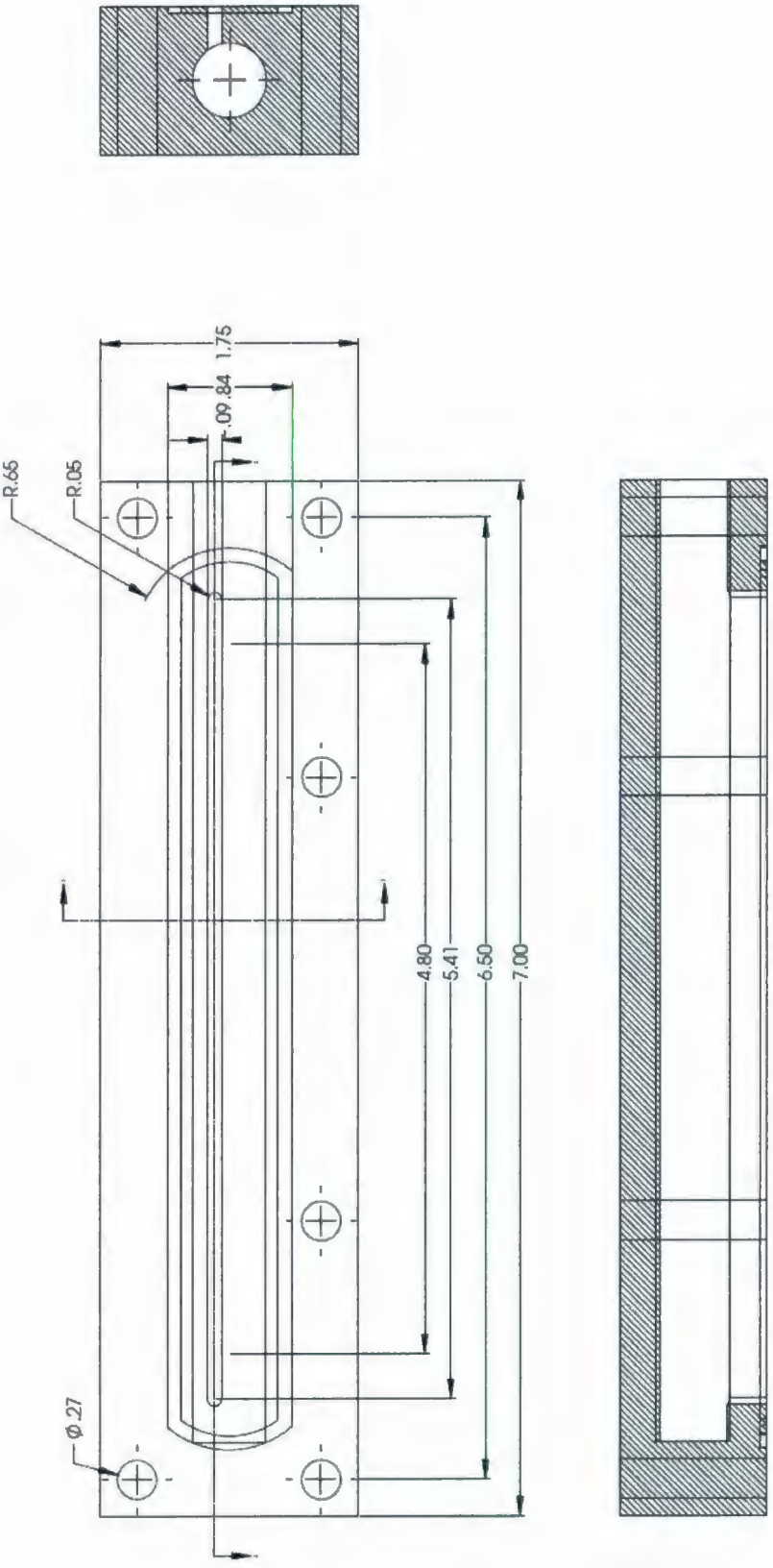

Fig. A.3 – Inlet/Exit Manifold

Appendix B

Uncertainty Analysis

B.1 Introduction

The uncertainty in the present experimental measurements was determined using the root sum square method, (Holman (1984), Moffat (1988)). Two different data samples having maximum (ΔT=4.5°C) and minimum (ΔT=1.5°C) possible temperature differences within the experiment (Fin #10) were considered. The same data samples are considered to determine the uncertainty in Log Mean Temperature Difference. The uncertainty for Reynolds number and friction factor were sensitive at different ΔT as Colburn factor and Nusselt number due to cause of determining the flow rate from the supplied heat as well as power input.

B.2 Uncertainty Analysis

The uncertainty according to the root sum square method can be estimated in the calculated result on the basis of the uncertainties in the primary measurements. If the result R is a given function of the independent variables $x_1, x_2, x_3, \ldots, x_n$, then

$$R = R(x_1, x_2, x_3, \ldots, x_n) \qquad \text{B.1}$$

where x_i are independent measure quantity. If w_R be the uncertainty in the result and w_1, w_2, w_3,…,w_n be the uncertainties in the independent variables, and then the uncertainty w_R in the Result R is given by

$$w_R = \left[\left(\frac{\partial R}{\partial x_1} w_1\right)^2 + \left(\frac{\partial R}{\partial x_2} w_2\right)^2 + \ldots \left(\frac{\partial R}{\partial x_n} w_n\right)^2\right]^{\frac{1}{2}} \qquad \text{B.2}$$

where w_i are the uncertainties in the independent variable x_i.(Holman (1984))

B.3 Uncertainty in Different Experimental Parameters

Uncertainty due to measurement error and fluid properties have already discussed in Chapter -3. The uncertainty in mass flow rate measurements are determined from

$$\frac{\delta \dot{m}}{\dot{m}} = \left\{ \left(\frac{\delta Q}{Q} \right)^2 + \left(\frac{\delta C_p}{C_p} \right)^2 + \left(\frac{\delta \Delta T}{\Delta T} \right)^2 \right\}^{\frac{1}{2}} \qquad \text{B.3}$$

where

$$\frac{\delta \Delta T}{\Delta T} = \left\{ \left(\frac{\delta T_i}{T_o} \right)^2 + \left(\frac{\delta T_o}{T_o} \right)^2 \right\}^{\frac{1}{2}} \qquad \text{B.4}$$

The overall uncertainty in Reynolds number may be determined from

$$\frac{\delta Re}{Re} = \left\{ \left(\frac{\delta \dot{m}}{\dot{m}} \right)^2 + \left(\frac{\delta D_h}{D_h} \right)^2 + \left(\frac{\delta A}{A} \right)^2 + \left(\frac{\delta \mu}{\mu} \right)^2 \right\}^{\frac{1}{2}} \qquad \text{B.5}$$

The uncertainty in overall heat transfer coefficient may be determined from

$$\frac{\delta UA}{UA} = \left\{ \left(\frac{\delta Q}{Q} \right)^2 + \left(\frac{\delta \Delta T_{LMTD}}{\Delta T_{LMTD}} \right)^2 \right\}^{\frac{1}{2}} \qquad \text{B.6}$$

The overall uncertainty in Prandtl number may be determined from

$$\frac{\delta Pr}{Pr} = \left\{ \left(\frac{\delta \mu}{\mu} \right)^2 + \left(\frac{\delta C_p}{C_p} \right)^2 + \left(\frac{\delta k}{k} \right)^2 \right\}^{\frac{1}{2}} \qquad \text{B.7}$$

The overall uncertainty in Nusselt number may be determined from

$$\frac{\delta Nu}{Nu} = \left\{ \left(\frac{\delta h}{h} \right)^2 + \left(\frac{\delta D_h}{D_h} \right)^2 + \left(\frac{\delta k}{k} \right)^2 \right\}^{\frac{1}{2}} \qquad \text{B.8}$$

Where

$$\frac{\delta h}{h} = \left\{ \left(\frac{\delta UA}{UA} \right)^2 + \left(\frac{\delta \eta_o}{\eta_o} \right)^2 + \left(\frac{\delta A}{A} \right)^2 \right\}^{\frac{1}{2}} \qquad \text{B.9}$$

Finally the uncertainty in heat transfer and frictional loss calculation are determined from the following equations using the uncertainty in the above parameters

$$\frac{\delta j}{j} = \left\{ \left(\frac{\delta Nu}{Nu} \right)^2 + \left(\frac{\delta Re}{Re} \right)^2 + \left(\frac{1}{3} \frac{\delta Pr}{Pr} \right)^2 \right\}^{\frac{1}{2}} \quad \text{B.10}$$

$$\frac{\delta f}{f} = \left\{ \left(\frac{\delta \Delta P}{\Delta P} \right)^2 + \left(\frac{\delta D_h}{D_h} \right)^2 + \left(\frac{\delta L}{L} \right)^2 + \left(\frac{\delta \rho}{\rho} \right)^2 + \left(2 \frac{\delta u_m}{u_m} \right) \right\}^{\frac{1}{2}} \quad \text{B.11}$$

Where

$$\frac{\delta u_m}{u_m} = \left\{ \left(\frac{\delta \rho}{\rho} \right)^2 + \left(\frac{\delta \dot{m}}{\dot{m}} \right)^2 + \left(\frac{\delta A}{A} \right)^2 \right\}^{\frac{1}{2}} \quad \text{B.12}$$

Using the above expression the results of uncertainties in most of the parameters related to the present experiment are presented in Table B.1.The analysis has done for two different sample data having maximum and minimum possible temperature differences.

Table B.1

Uncertainty in experimental parameters

Parameters	Uncertainty at ΔT = 1.5	Uncertainty at ΔT = 4.5
f	9.81 %	4.14 %
j	5.05 %	2.24 %
Nu	1.31 %	2.54 %
Re	4.87 %	1.99 %
Pr	0.87 %	0.87 %
$\dot{m}$	4.85 %	1.92 %
UA	1.21 %	2.49 %

Appendix C

Data Reduction Code

Maple V10 Symbolic Programming Language Code

```
> restart;
> Digits:=12:
>Parameters:=[dh=0.0029882,H=0.00635,t=0.000154,twall=0.0254*0.25, ERR=0.89943,
AER=4.4685, FAR=0.77621, FL=0.0041520, L=11.8*0.0254, W=5.5*0.0254, kfin=200,
kwall=200, epsilon=0.30768, X=1.0664, Leff=0.0050787]:
```

Data Input

```
> Data:=readdata(`c:/wavyfindata/DataFin1All.txt`,12):
> array(Data);
> N:=nops(Data);
```

Fluid Property Calculations

```
>mu:=10^(9274-2437.83*Tm^.5+256.145*Tm-13.4449*Tm^1.5+.352491*Tm^2-
0.369285e-2*Tm^2.5);
> k:=0.183482-0.00123141*Tm^.5-0.0000613542*Tm;
> ρ:=1021.18+4.2243*Tm^.5-0.703867*Tm;
> cp:=1286.63-71.4665*Tm^.5+6.20997*Tm;
> Tms:=[seq((Data[i,4]+Data[i,11])/2+273.15,i=1..N)];
>Tsurface:=[seq((Data[i][5]+Data[i][6]+Data[i][7]+Data[i][8]+Data[i][9]+Data[i][10])/6,
i=1..N)];
> mus:=evalf([seq(μ,Tm=Tms)]);
> ks:=evalf([seq(k,Tm=Tms)]);
> rhos:=evalf([seq(ρ,Tm=Tms)]);
> cps:=evalf([seq(cp,Tm=Tms)]);
> Prs:=[seq(mus[i]*Cps[i]/ks[i], i=1..N)];
> rhoCp:=[seq(rhos[i]*Cps[i]/1000/60, i=1..N)];
> Prmean:=add(Prs[i], i=1..N)/N;
```

Energy Balance Calculations

```
> DeltaT:=[seq((Data[i][4]-Data[i][11]), i=1..N)];
```

```
>Qout:=[seq([Data[i][3],rhos[i]*Cps[i]*Data[i][3]/60/1000*(Data[i][4]Data[i][11])],
i=1..N)];
> Qin:=[seq([Data[i][3], Data[i][1]], i=1..N)];
> Qavg:=[seq([Data[i][3], (Qout[i][2]+Qin[i][2])/2], i=1..N)];
> Flow:=[seq(Data[i][1]/rhos[i]/Cps[i]/DeltaT[i]*60*1000, i=1..N)];
> Qbalance:=[seq((Qin[i][2]-Qout[i][2])/Qin[i][2]*100, i=1..N)];
> rms:=sqrt(add(Qbalance[i]^2, i=9..N-6)/(N-14));
> plot({Qin, Qout}, axes=boxed, view=[0..12, 0..400]);
```

Calculation of Velocity and Reynolds Number

```
Vs:=[seq(subs(parameters,Flow[i]/(W*H*ERR)/60/1000),i=1..N)];
REs:=[seq(subs(parameters,rhos[i]*Vs[i]/mus[i]*dh),i=1..N)];
```

Calculation of Friction Factor – f

```
> f1:=[seq(subs(parameters,(Data[i][2])*1000/L*dh/4/(0.5*rhos[i]*Vs[i]^2)),i=1..N)];
>fdata:=plots[loglogplot](fplot,style=point,axes=boxed,view=[0.1..100,0.01..100],color=
red):
> plots[display](fdata);
```

Calculation of LMTD Using Mean Surface Temperature and Using Local Inlet/Outlet surface Temperature

```
> LMTDMean:=[seq(((Tsurface[i]-Data[i][11])-(Tsurface[i]-Data[i][4]))/ln((Tsurface[i]-
Data[i][11])/(Tsurface[i]-Data[i][4])),i=1..N)];
>LMTDLocal:=[seq(((Data[i][5]-Data[i][11])-(Data[i][10]-Data[i][4]))/ln((Data[i][5]-
Data[i][11])/(Data[i][10]-Data[i][4])),i=1..N)];
> [seq(LMTDMean[i]/LMTDLocal[i],i=1..N)];
```

Calculation of Heat Transfer Coefficient and Colburn j Factor

```
> eta:=1-FAR*(1-tanh(sqrt(2*h/kfin/t)*FL)/(sqrt(2*h/kfin/t)*FL));
> eq := UA[i] = h*(2*W*L*AER)*eta;
>  UA:=[seq(subs(parameters,Data[i][1]/LMTDMean[i]),i=1..N)];
> hs:=[seq(fsolve(subs(parameters,eq),h),i=1..N)];
> NU:=[seq(subs(parameters,hs[i]*dh/ks[i]),i=1..N)];
> j1:=[seq(subs(parameters,NU[i]/REs[i]/Prs[i]^(1/3)),i=1..N)];
> jplot:=[seq([REs[i],j1[i]],i=1..N)];
>jdata:=plots[loglogplot](jplot,style=point,axes=boxed,view=[0.1..100,0.001..10],color=
blue):
> plots[display](jdata);
```

Models

```
> f:=((3.44/sqrt(Leff/RE/dh)/RE)^n+(X*C1/RE)^n)^(1/n);
> f:=subs(n=2,f);
```

```
>C1:=24*(1-1.3553*epsilon+1.9467*epsilon^2-1.7012*epsilon^3+.9564*epsilon^4-
0.2537*epsilon^5);
> j:=((0.664/sqrt(RE)*sqrt(dh/Leff))^m+(C2/RE/Pr^(1/3))^m)^(1/m);
> j:=evalf(subs(m=5,j));
>C2:=7.541*(1-2.61*epsilon+5.97*epsilon^2-5.119*epsilon^3+2.702*epsilon^4-
.548*epsilon^5);
> models:=plots[loglogplot](subs(parameters,Pr=Prmean,{f,j/AER}),RE=0.1..100):
> plots[display]({fdata, models, jdata});
>jtheory:=[seq(subs(parameters,RE=REs[i],pr=prs[i],1/AER.(0.129074483790*(dh/Leff)
^(5/2)/RE^(5/2)+1/RE^5*pr^(5/3)*(7.541-19.68201*epsilon+45.01977*epsilon^2-
38.602379*epsilon^3+20.375782*epsilon^4-4.132468*epsilon^5)^5))^(1/5)),i=1..N)];
> errors:=[seq((1-jtheory[i]/j1[i]).100,i=1..N)];
> rms:=sqrt(add(errors[i]^2,i=1..N)/N);
>ftheory:=[seq(subs(parameters,RE=REs[i],pr=prs[i],(11.8336*dh/Leff*RE+1/RE^2(X^
2(24-32.5272*epailon+46.7208*epsilon^2-40.8288*epsilon^3+22.9536*epsilon^4-
6.0888*epsilon^5)^2))^(1/2)),i=1..N)];
> errors:=[seq((1-ftheory[i]/f1[i]).100,i=1..N)];
> rms:=sqrt(add(errors[i]^2,i=1..N)/N);
```

Appendix D

Experimental Plots

Fig. D.1 - D.14 show the experimental data for Fin # 2 to Fin # 15.

Fig. D.15 – D.19 show the comparison between different fins having same height.

Fig. D.20 – D.33 show the comparison of experimental data with low Reynolds number asymptote for Fin # 2 to Fin # 15.

Fig. D.20 – D.33 show the comparison of experimental data with LBL asymptote for Fin # 2 to Fin # 15.

Fig. D.20 – D.33 show the comparison of experimental data with combined asymptotic model for Fin # 2 to Fin # 15.

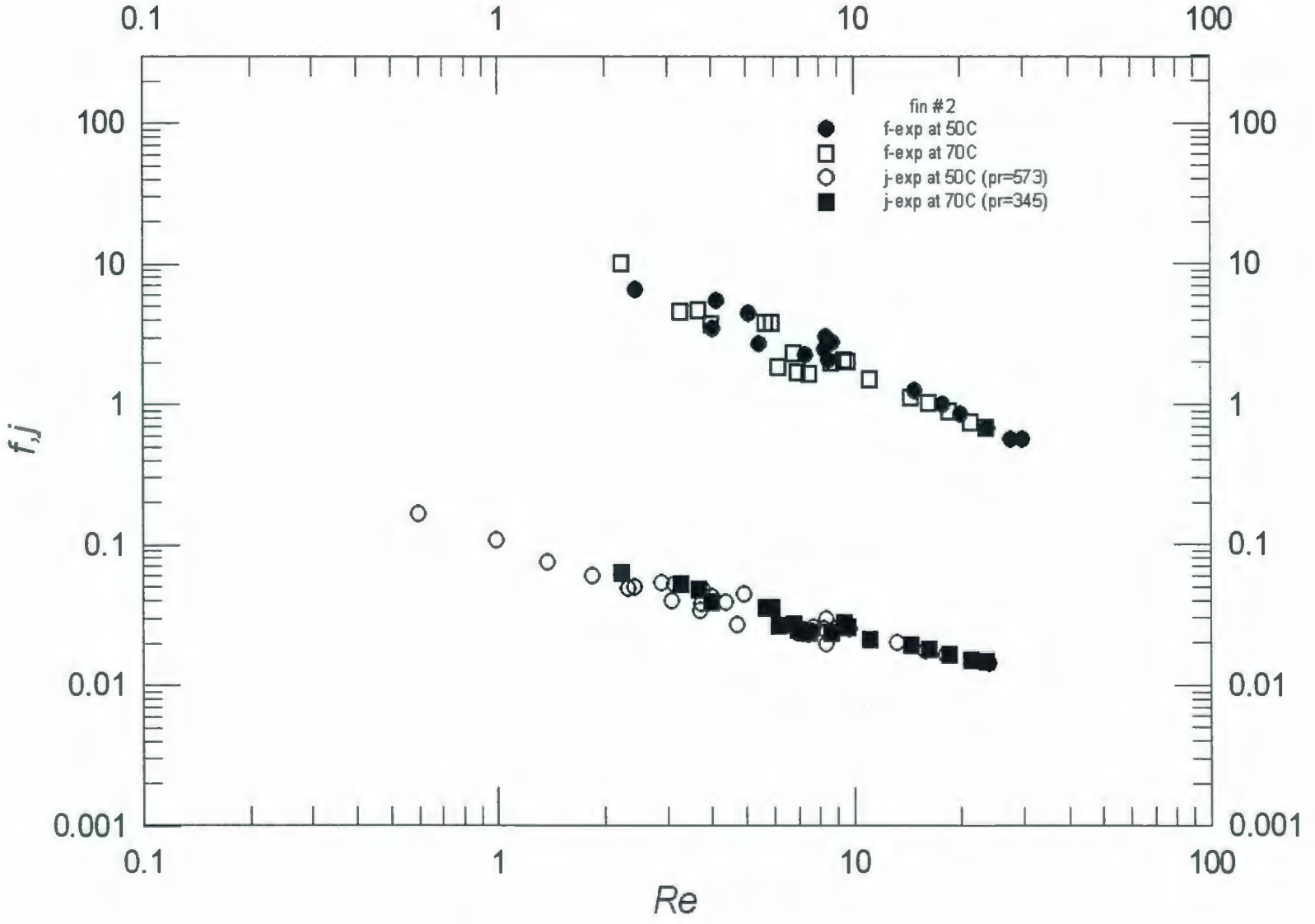

Fig. D.1- Fin # 2 Experimental Data

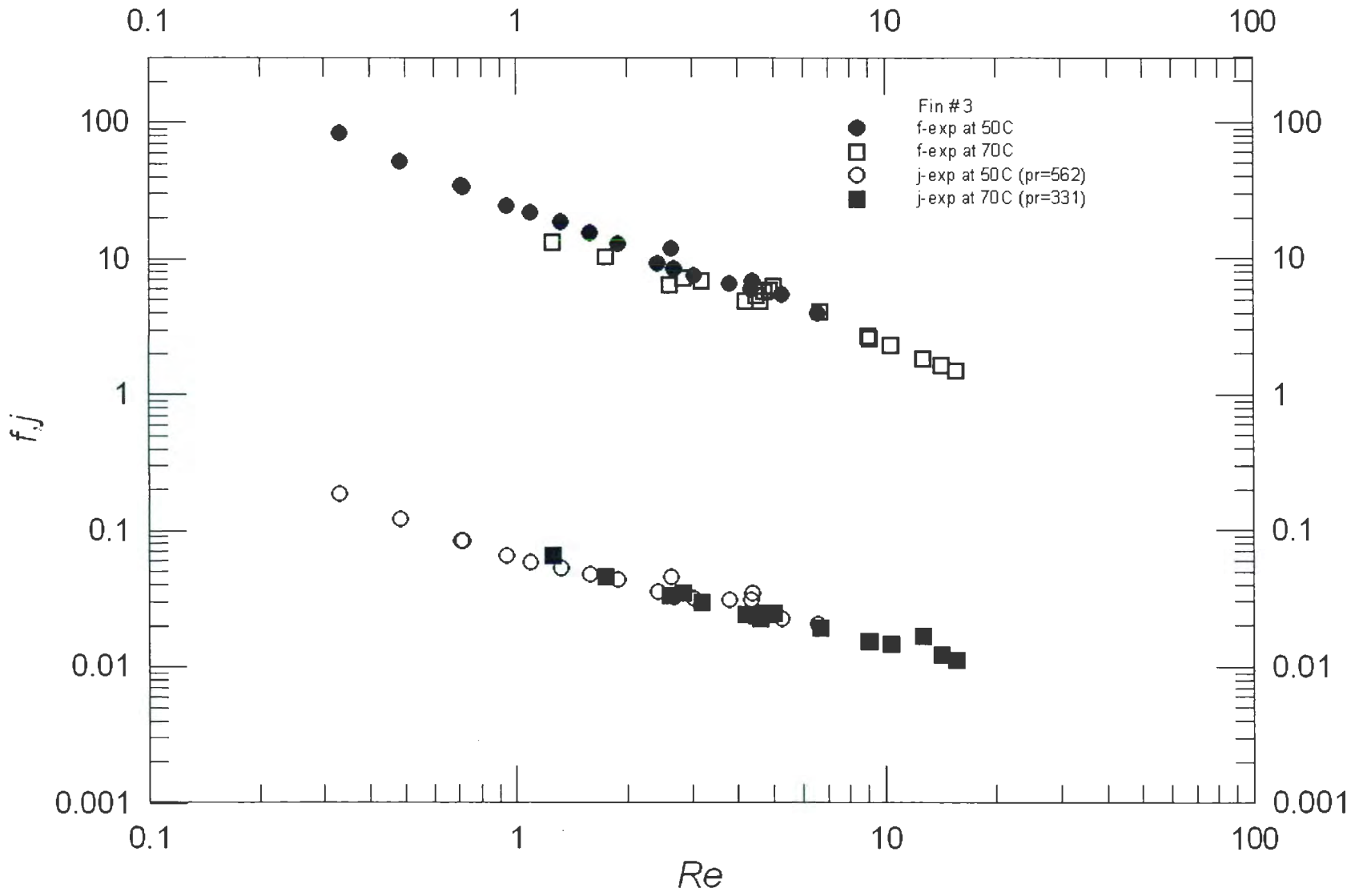

Fig. D.2- Fin # 3 Experimental Data

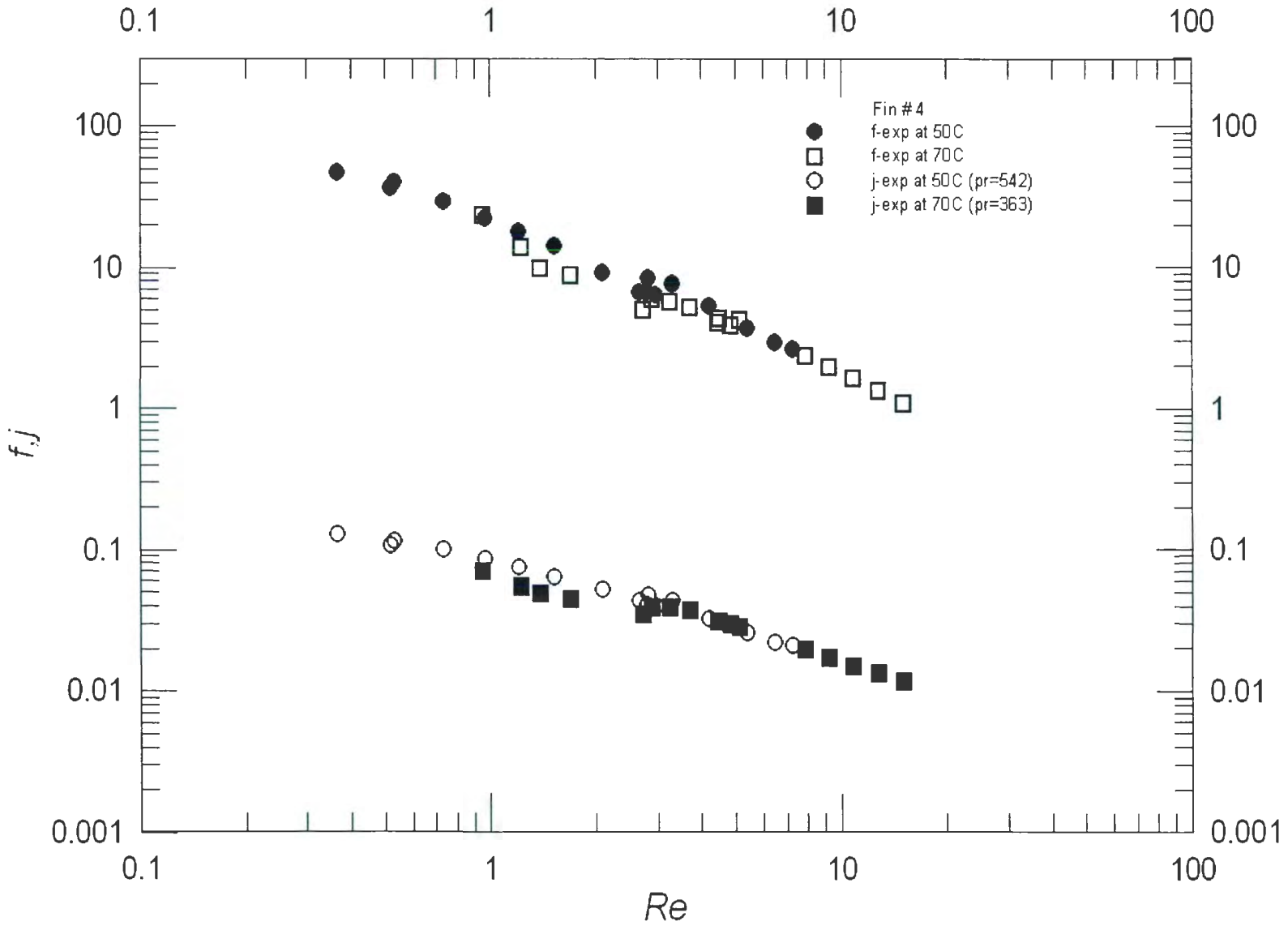

Fig. D.3- Fin # 4 Experimental Data

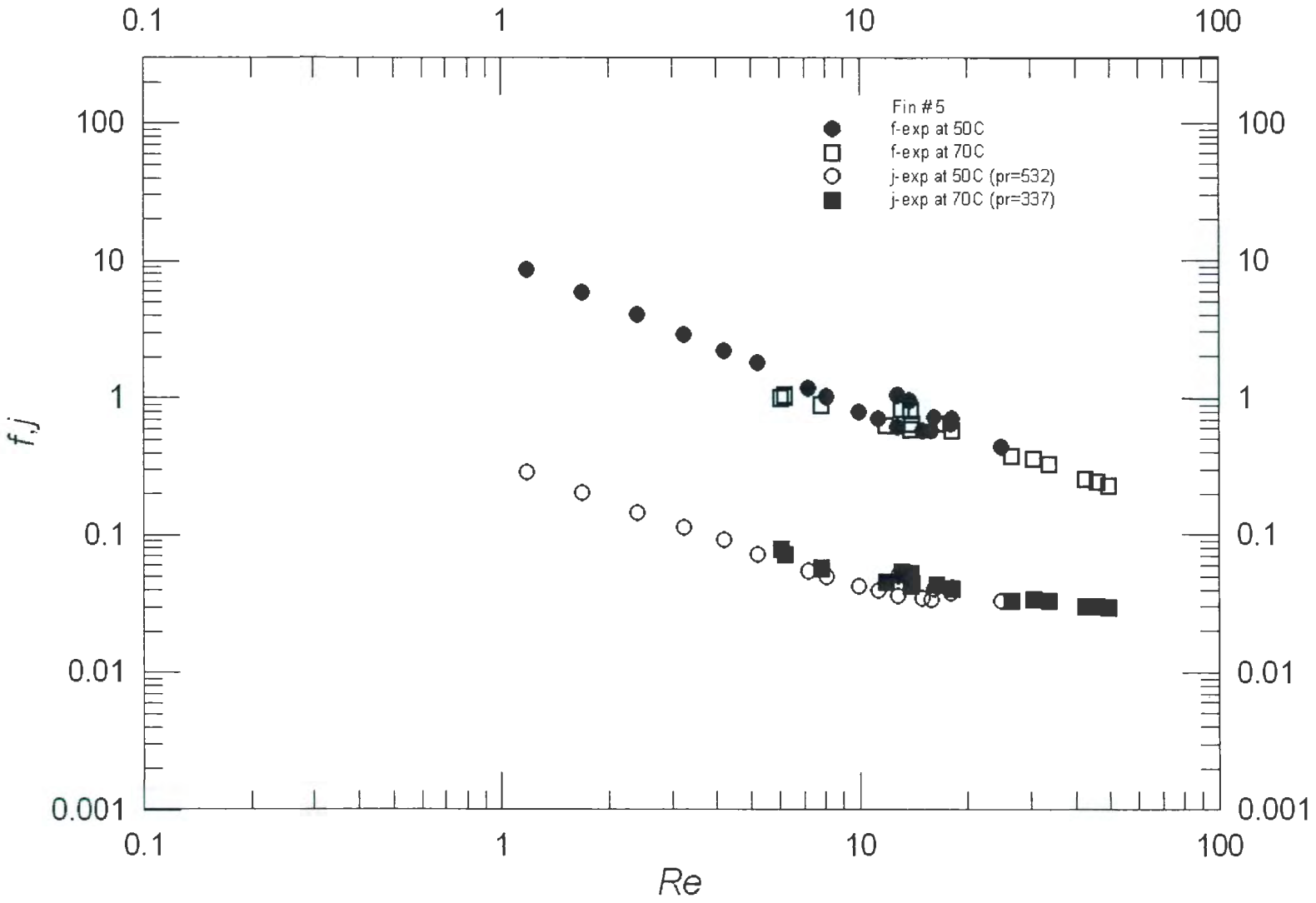

Fig. D.4- Fin # 5 Experimental Data

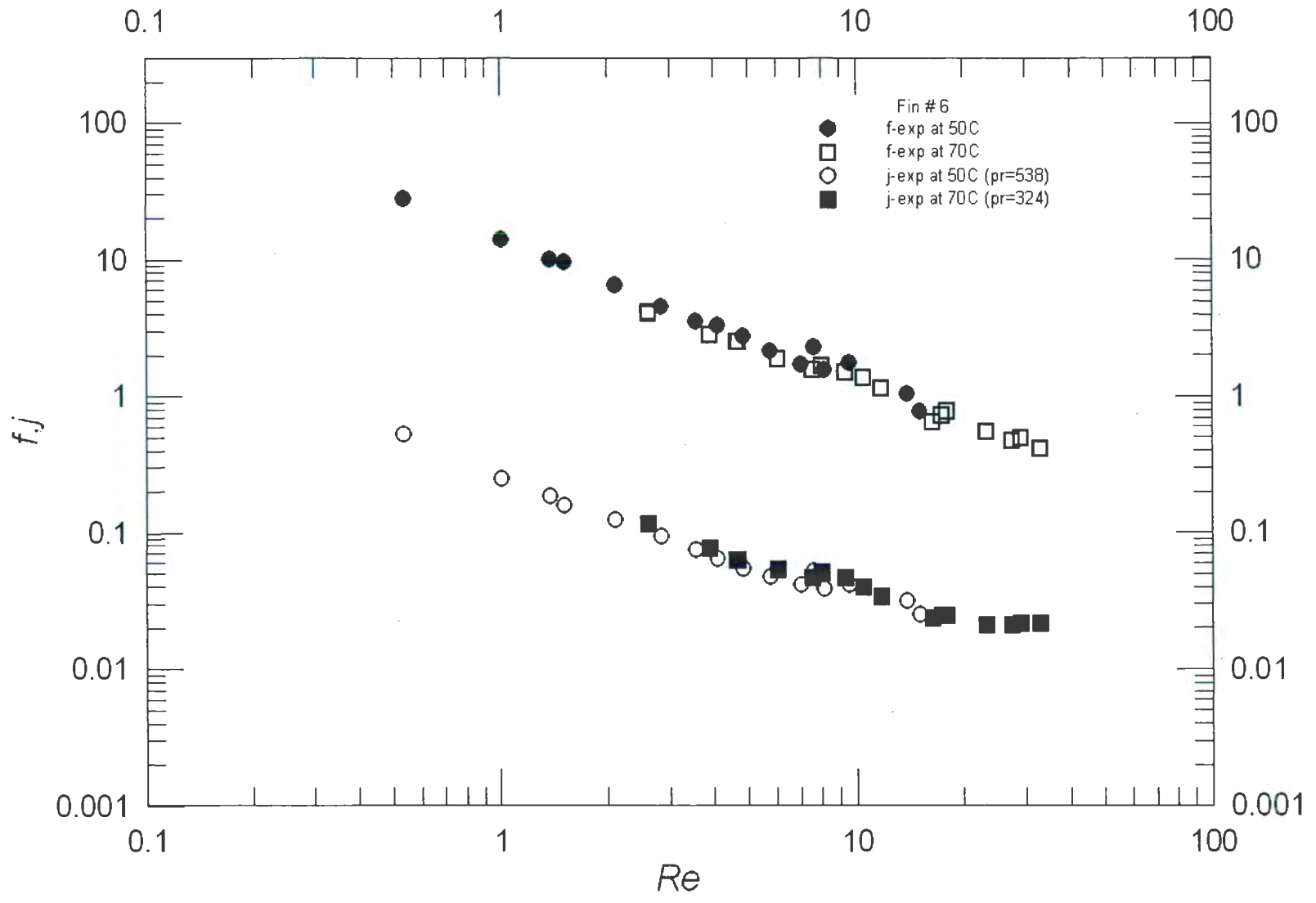

Fig. D.5- Fin # 6 Experimental Data

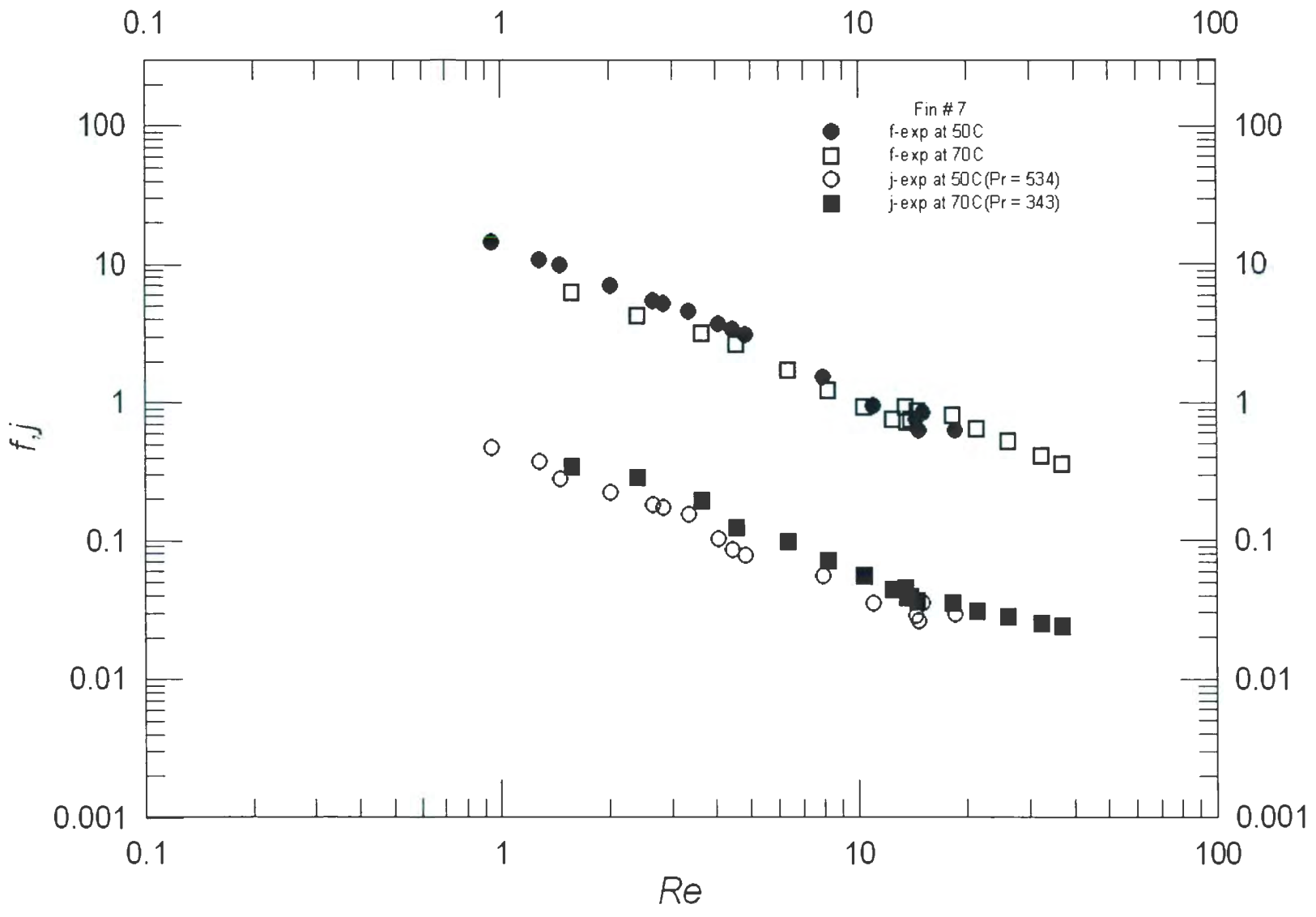

Fig. D.6- Fin # 7 Experimental Data

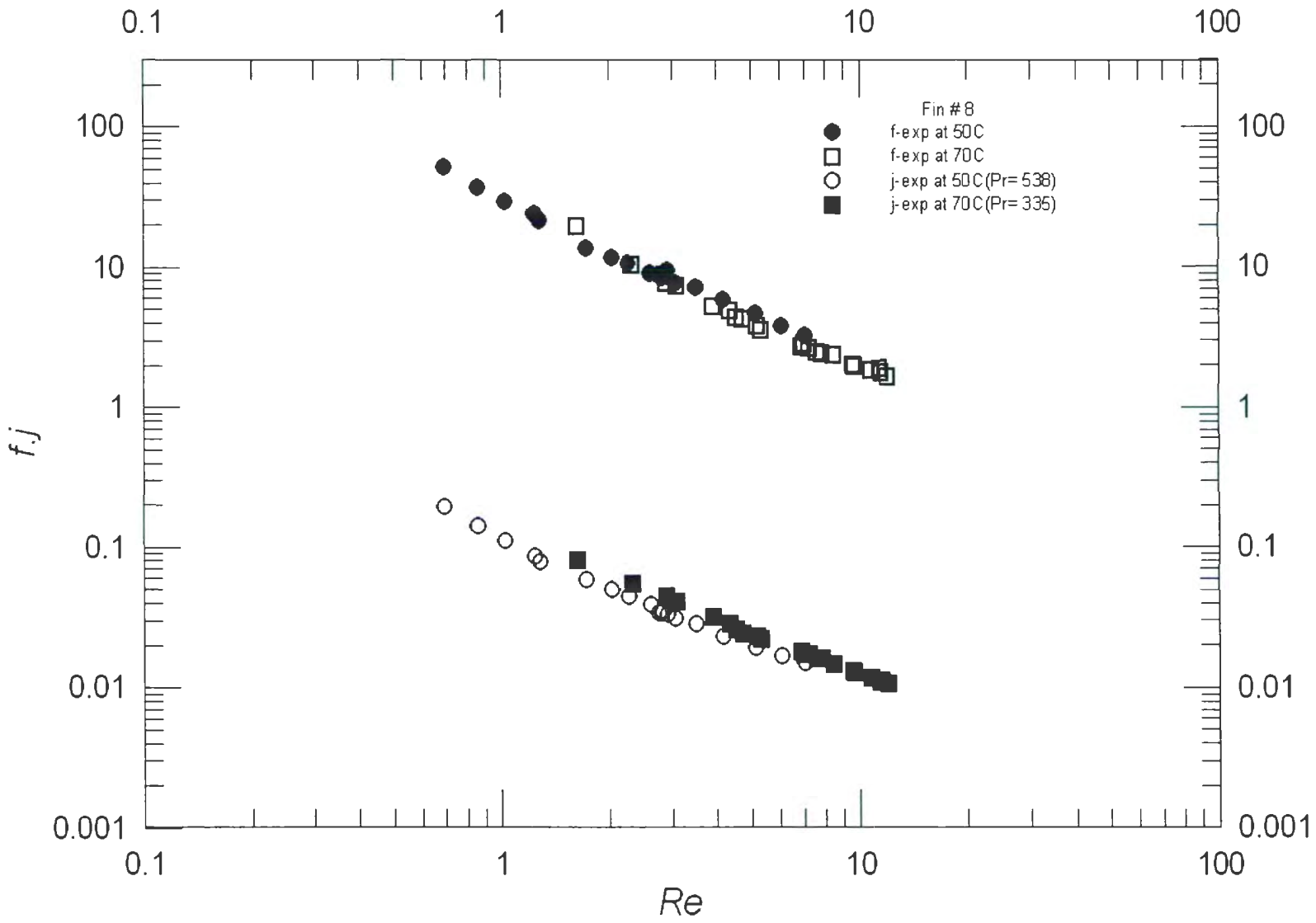

Fig. D.7- Fin # 8 Experimental Data

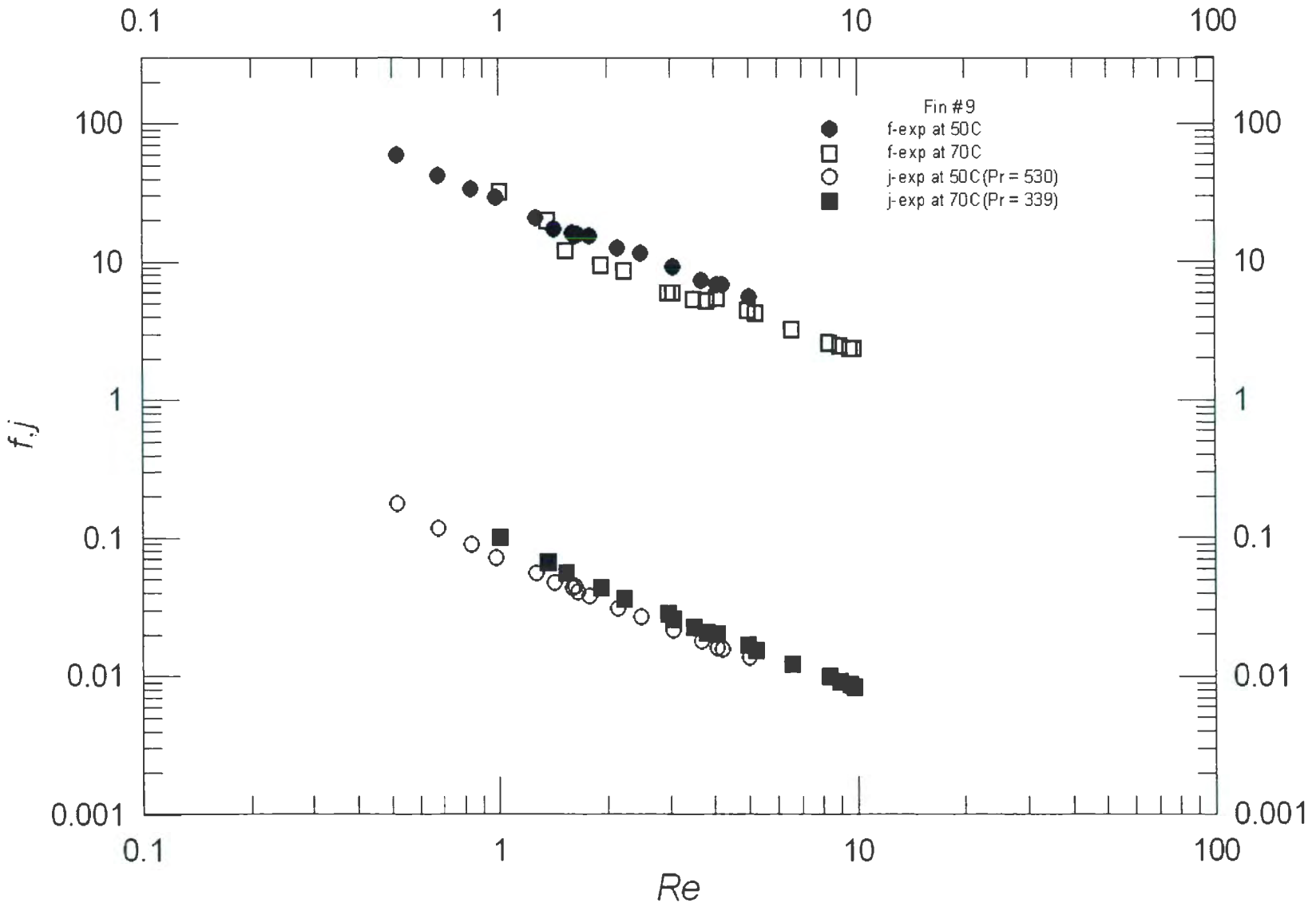

Fig. D.8- Fin # 9 Experimental Data

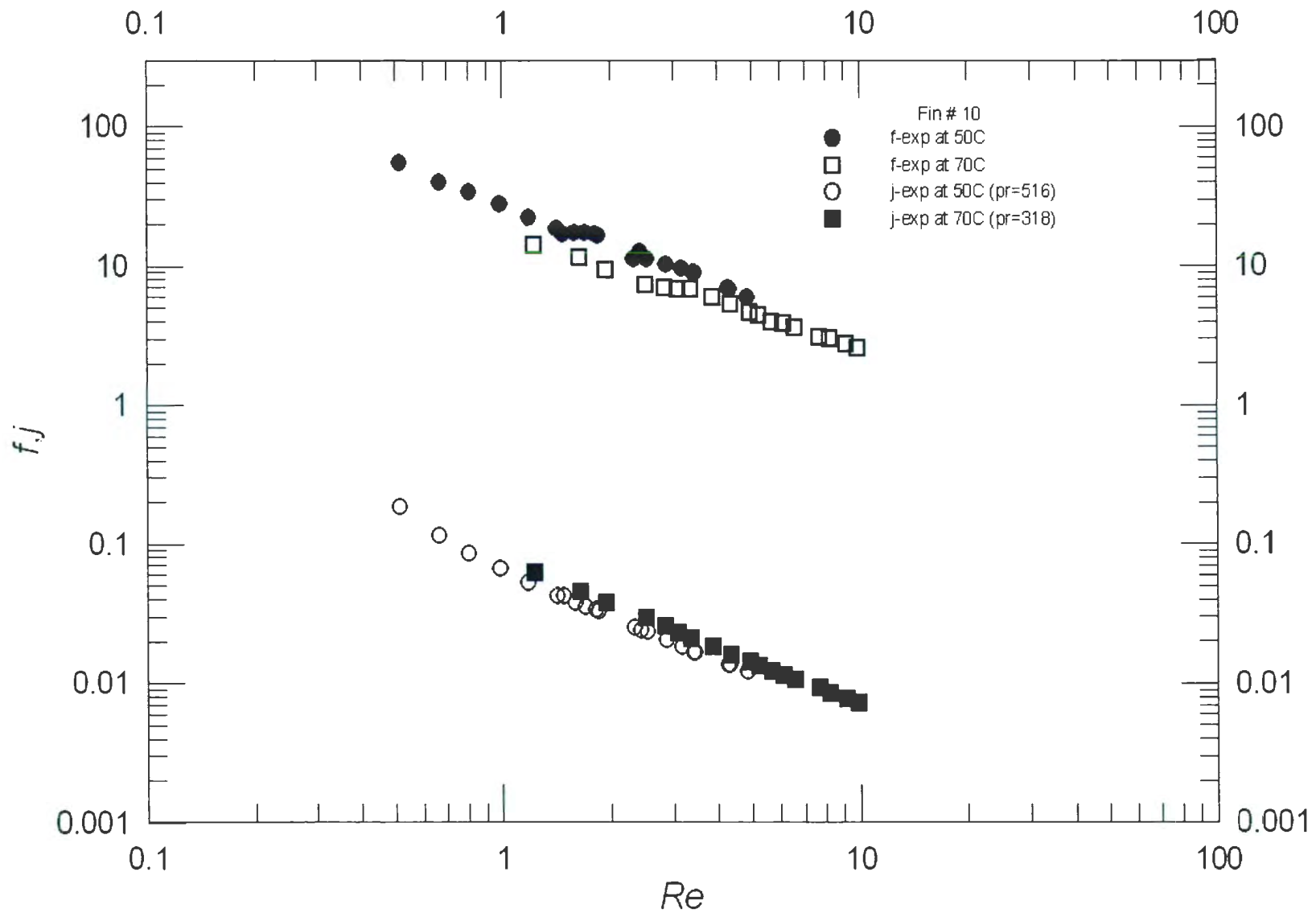

Fig. D.9- Fin # 10 Experimental Data

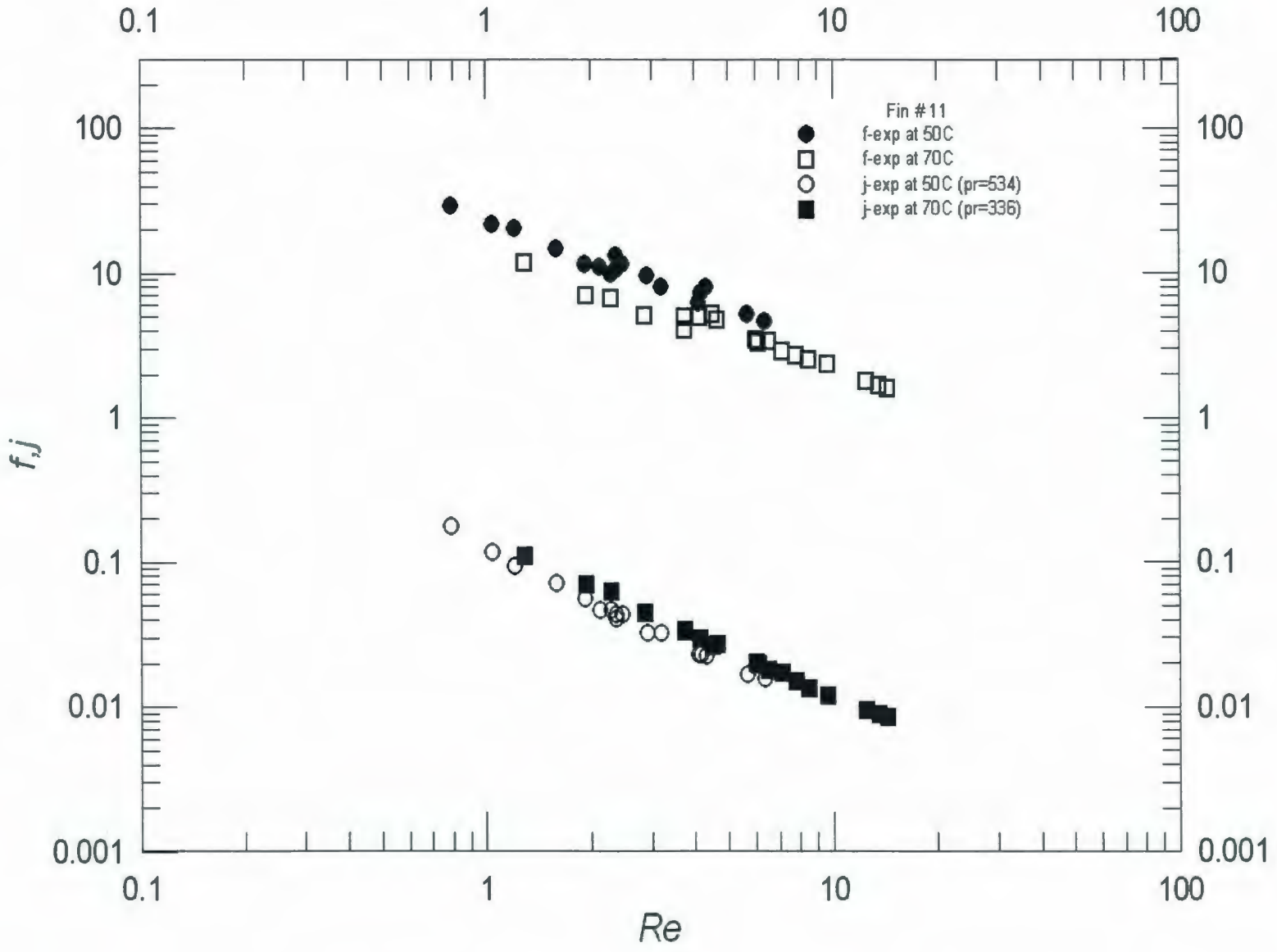

Fig. D.10- Fin # 11 Experimental Data

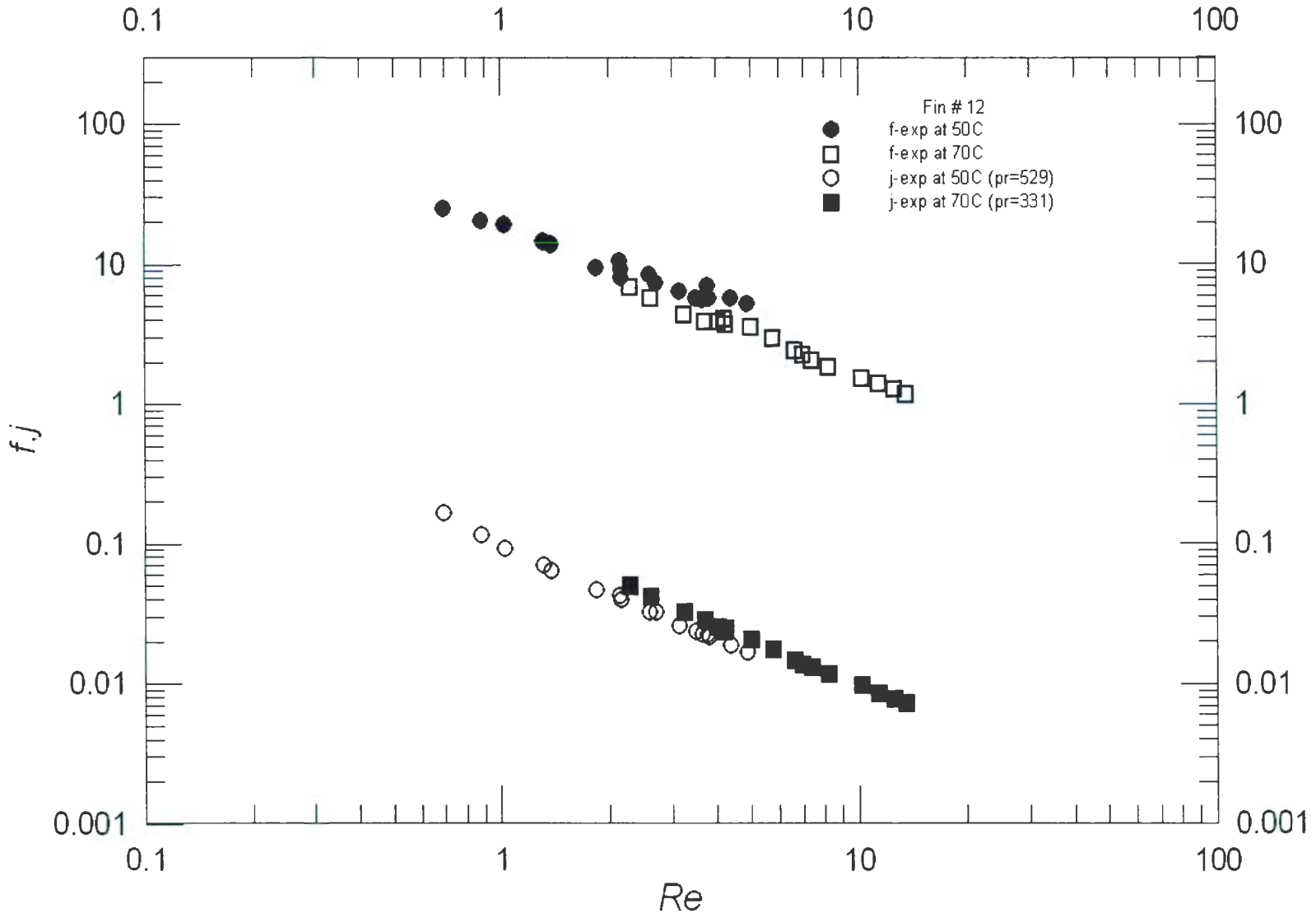

Fig. D.11- Fin # 12 Experimental Data

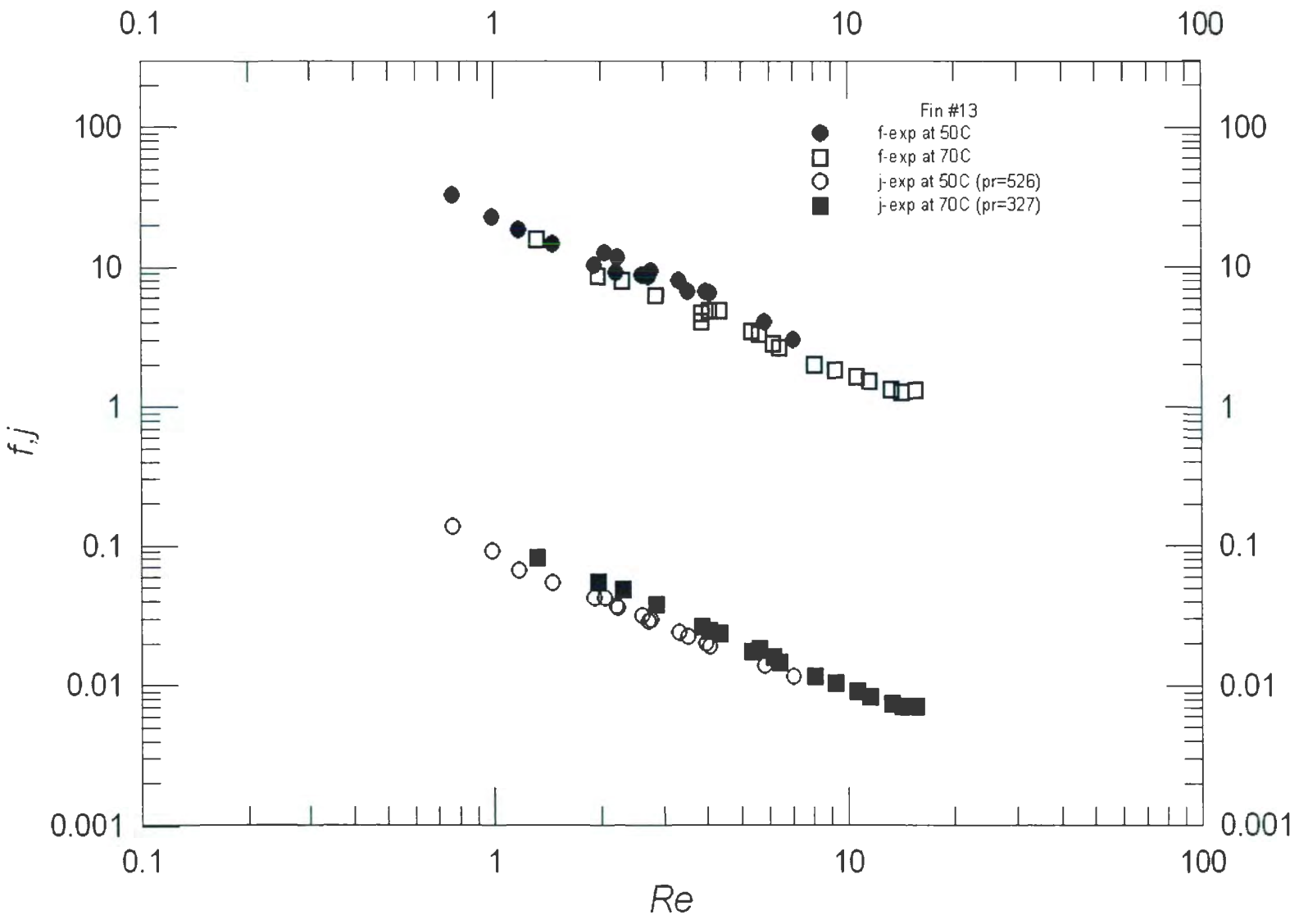

Fig. D.12- Fin # 13 Experimental Data

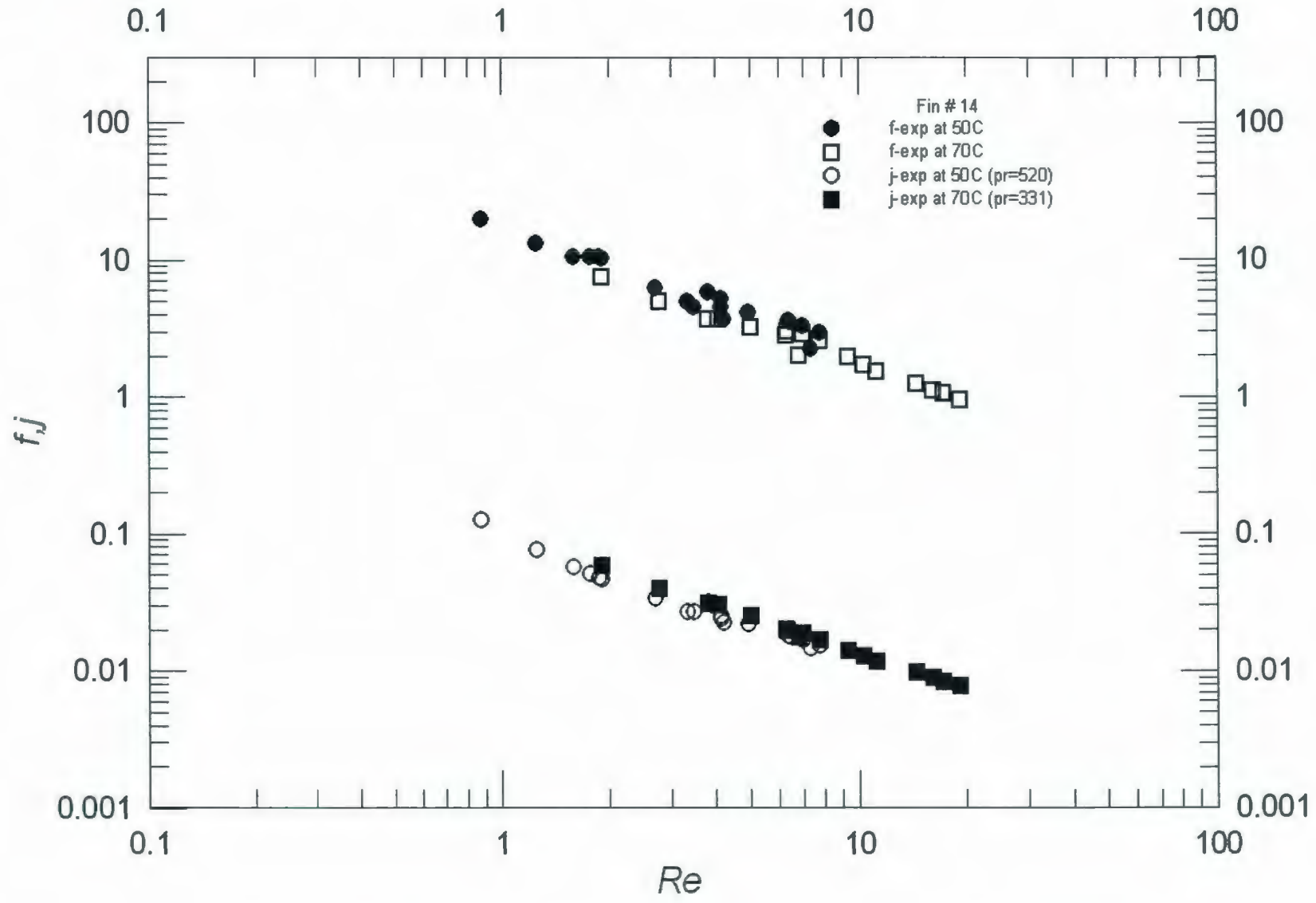

Fig. D.13- Fin # 14 Experimental Data

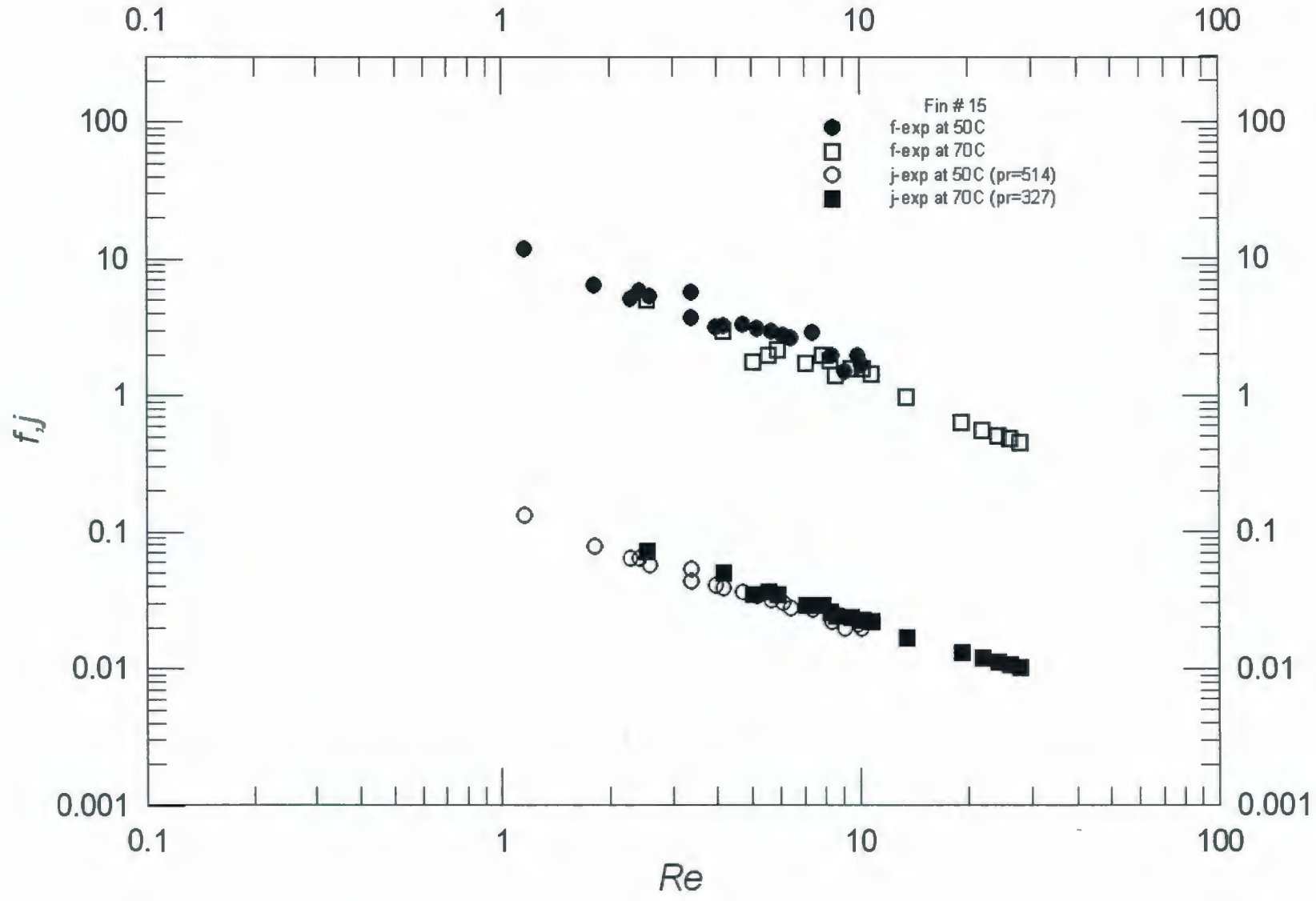

Fig. D.14- Fin # 15 Experimental Data

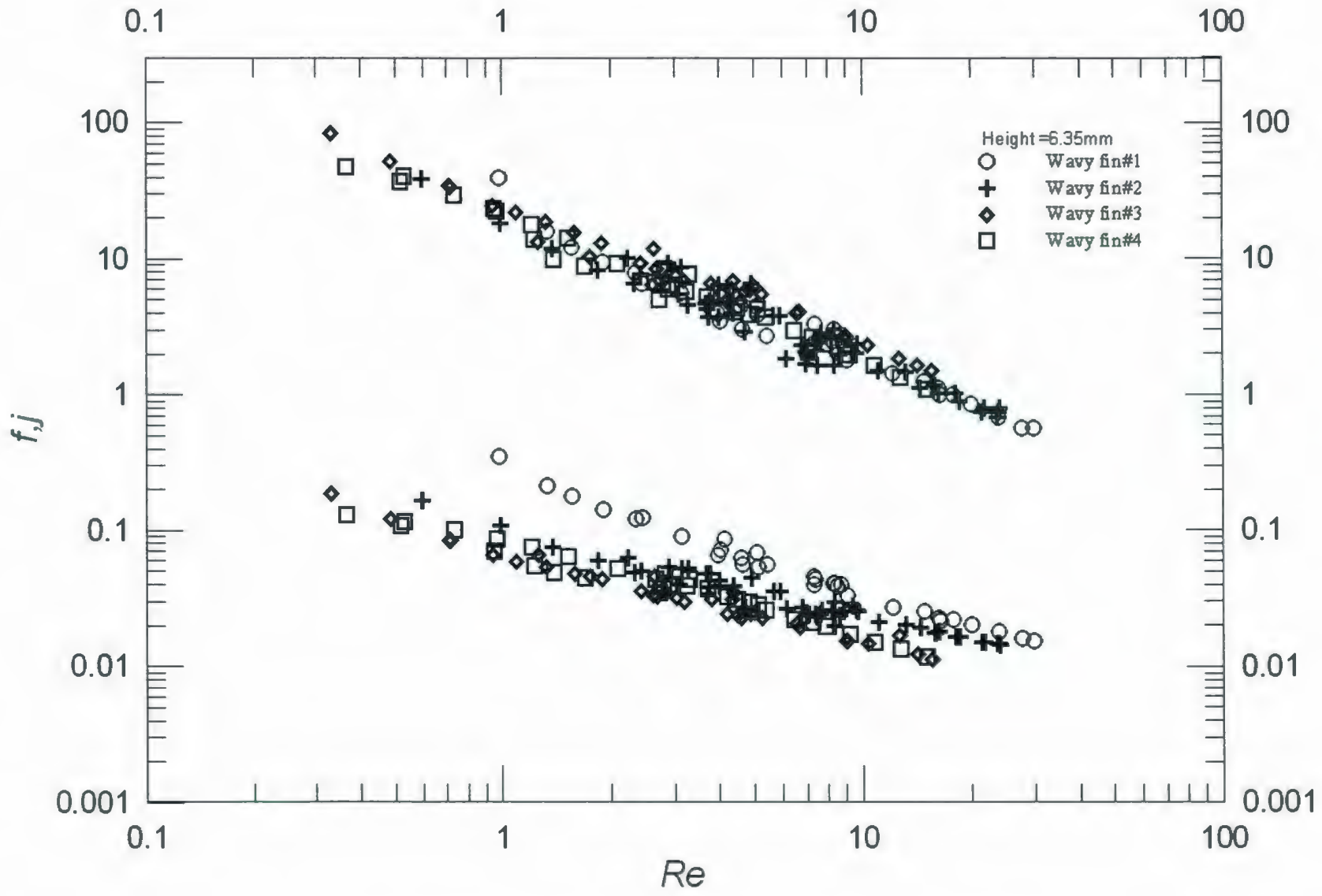

Fig. D.15- Comparison of all fins of 6.35 mm height

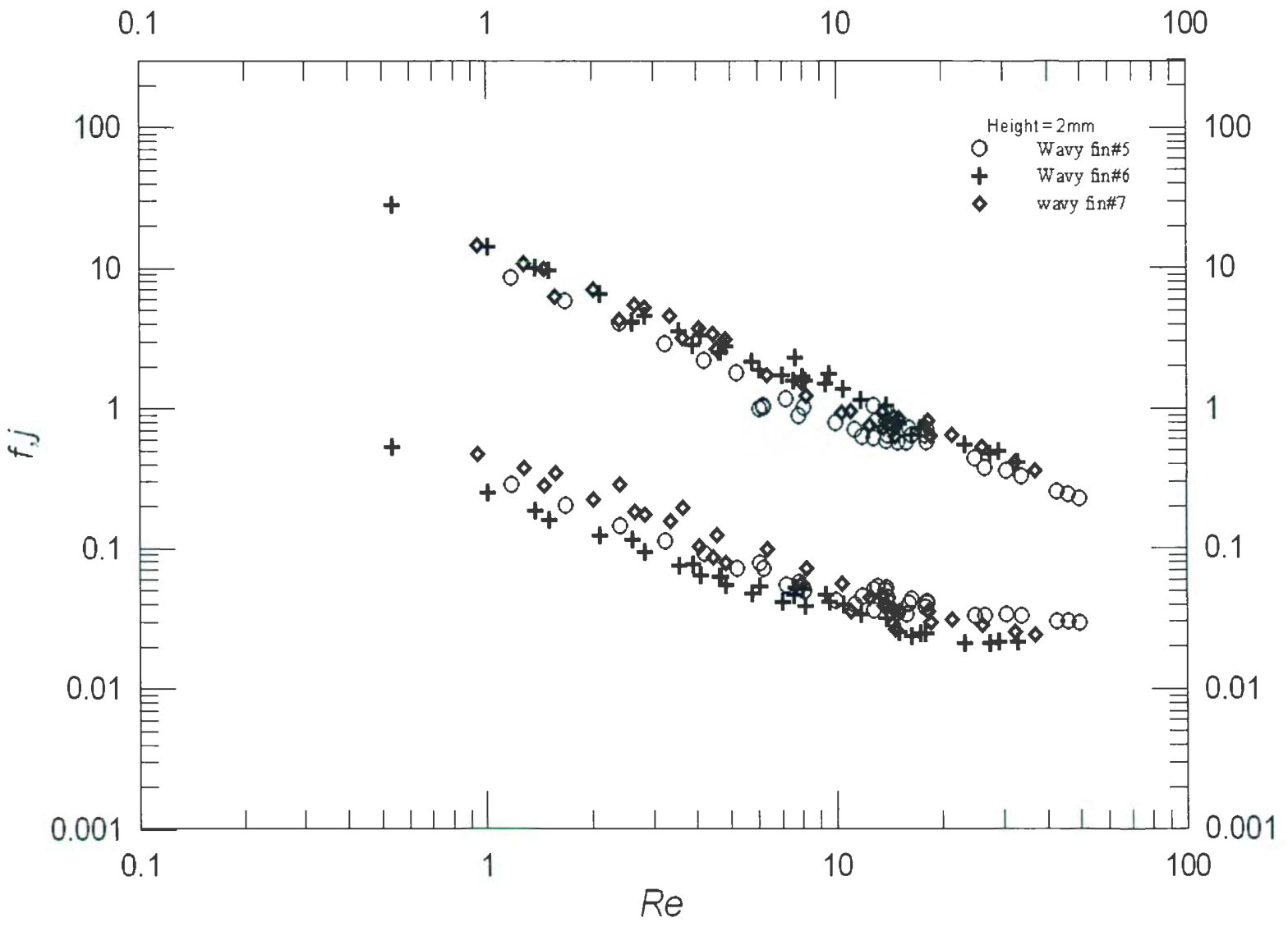

Fig. D.16- Comparison of all fins of 2 mm height

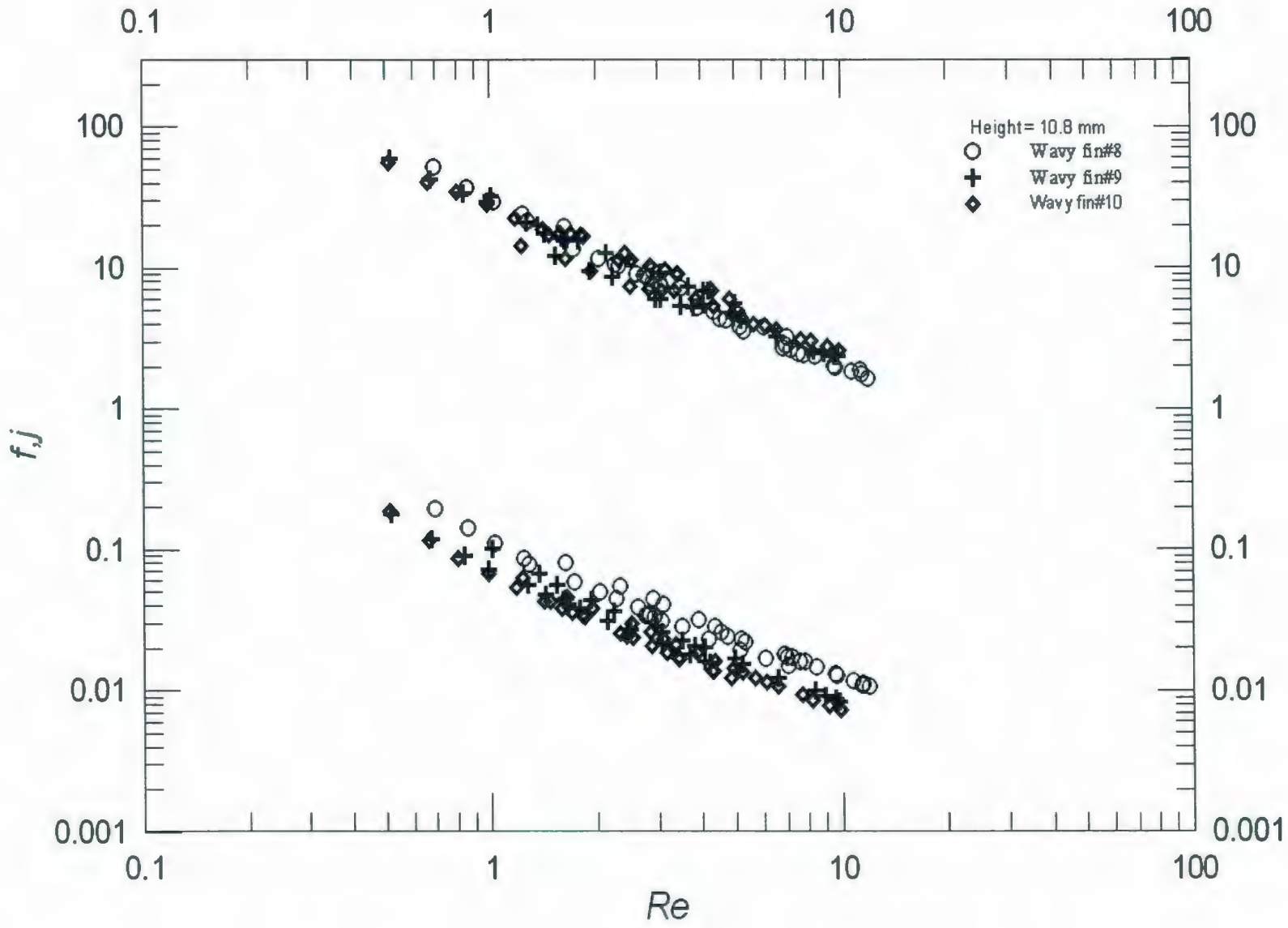

Fig. D.17- Comparison of all fins of 10.8 mm height

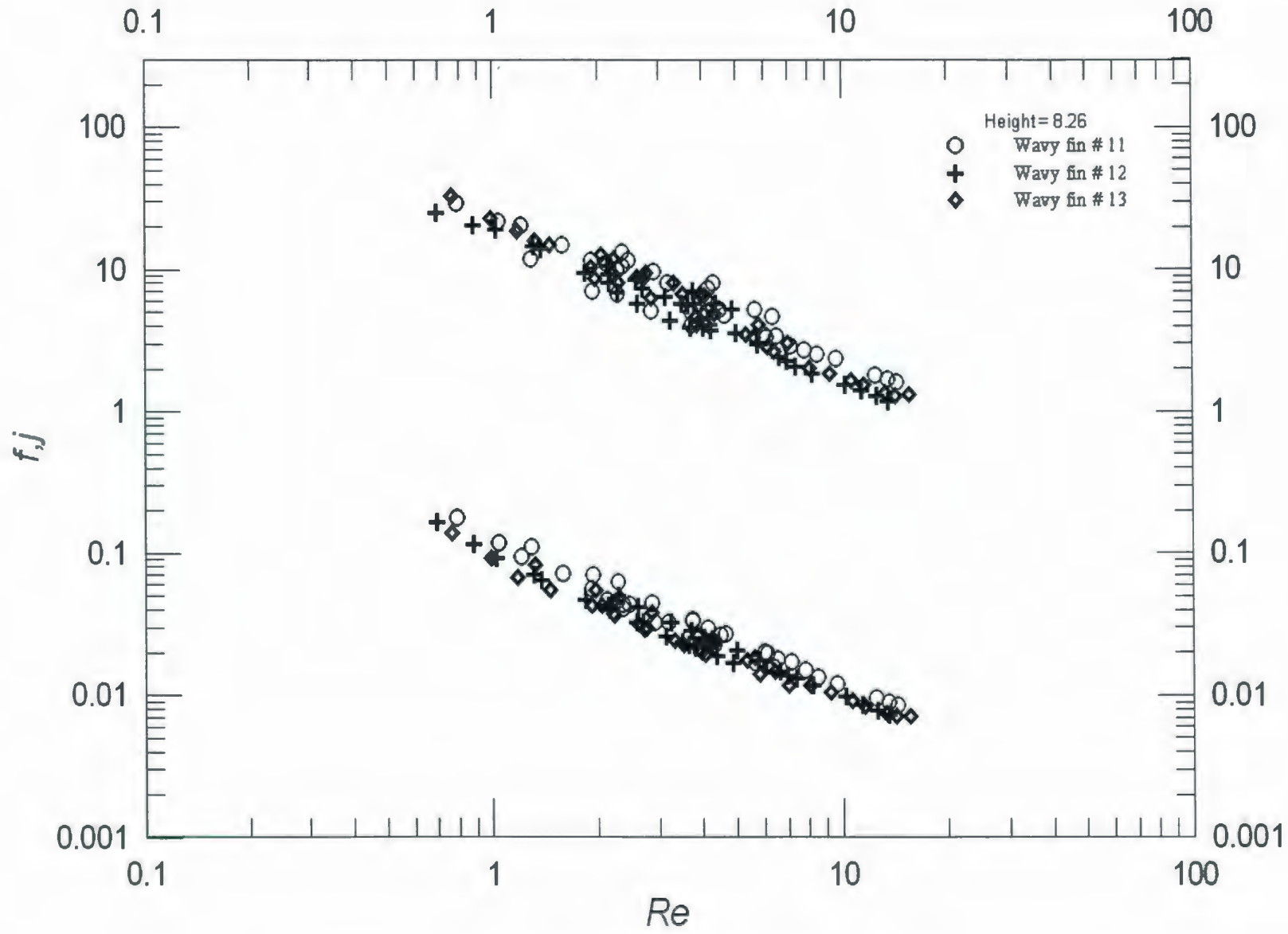

Fig. D.18- Comparison of all fins of 8.26 mm height

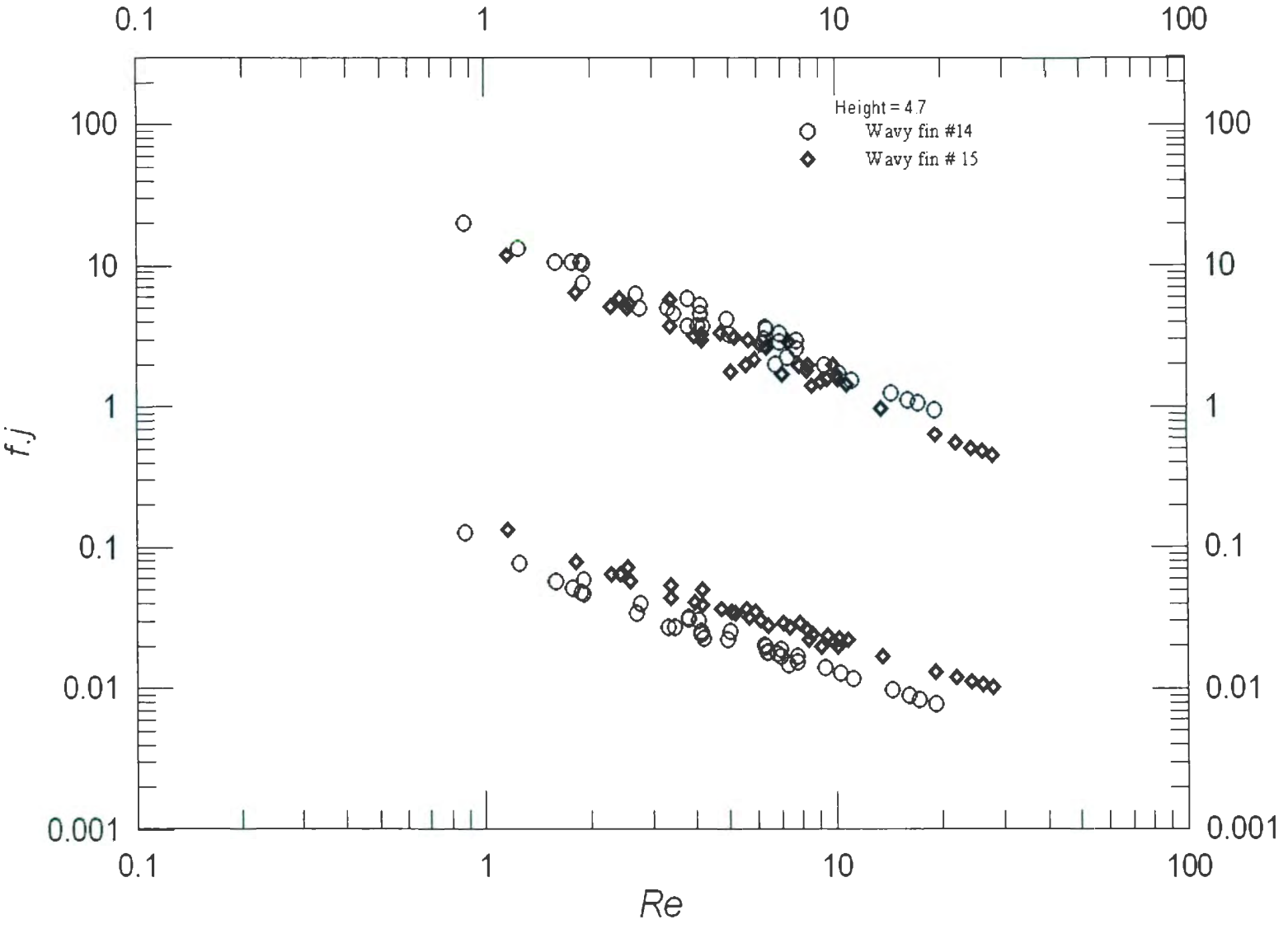

Fig. D.19- Comparison of all fins of 4.7 mm height

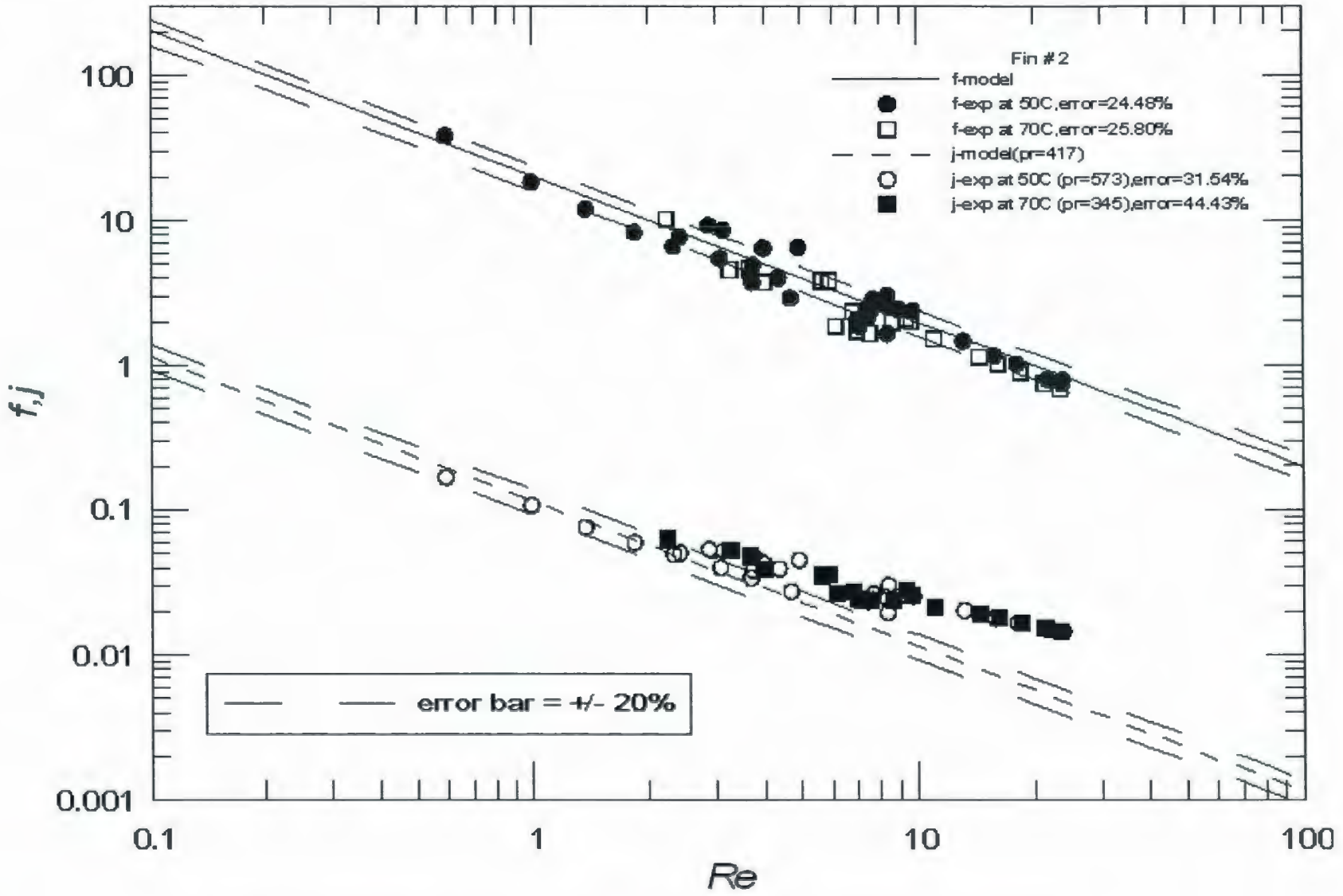

Fig. D.20 – Comparison of Fin # 2 data with low Reynolds number Asymptote

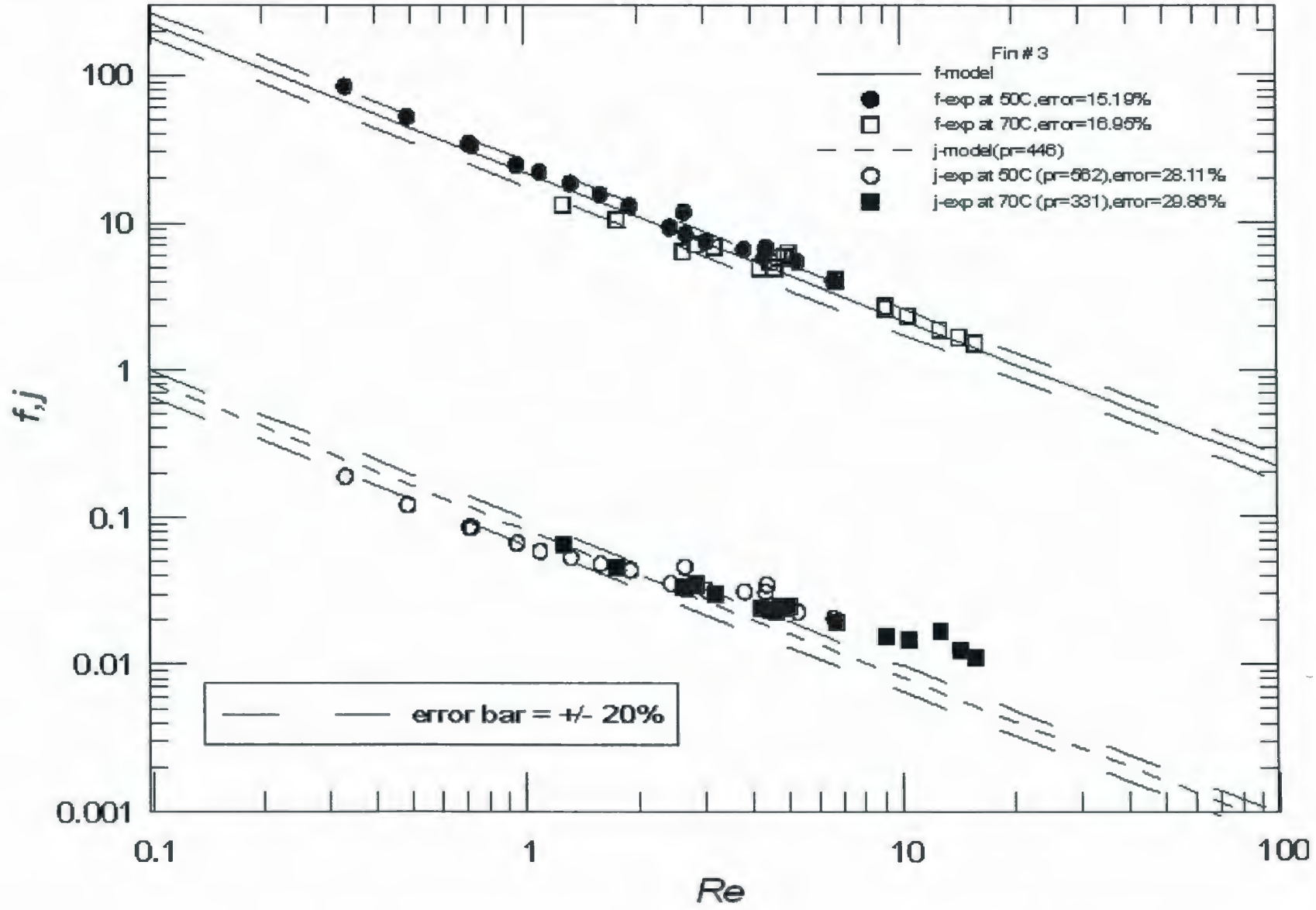

Fig. D.21– Comparison of Fin # 3 data with low Reynolds number Asymptote

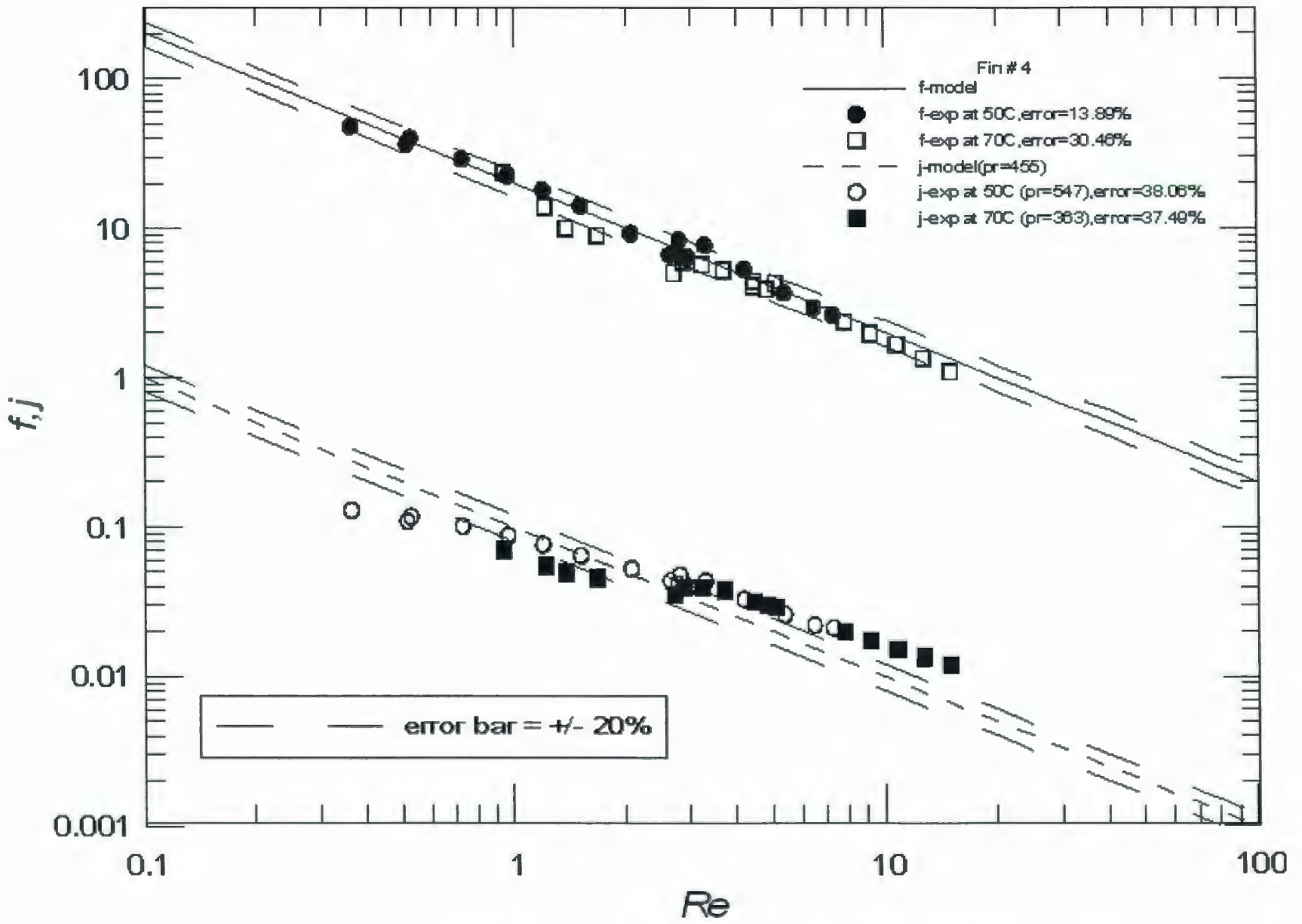

Fig. D.22 – Comparison of Fin # 4 data with low Reynolds number Asymptote

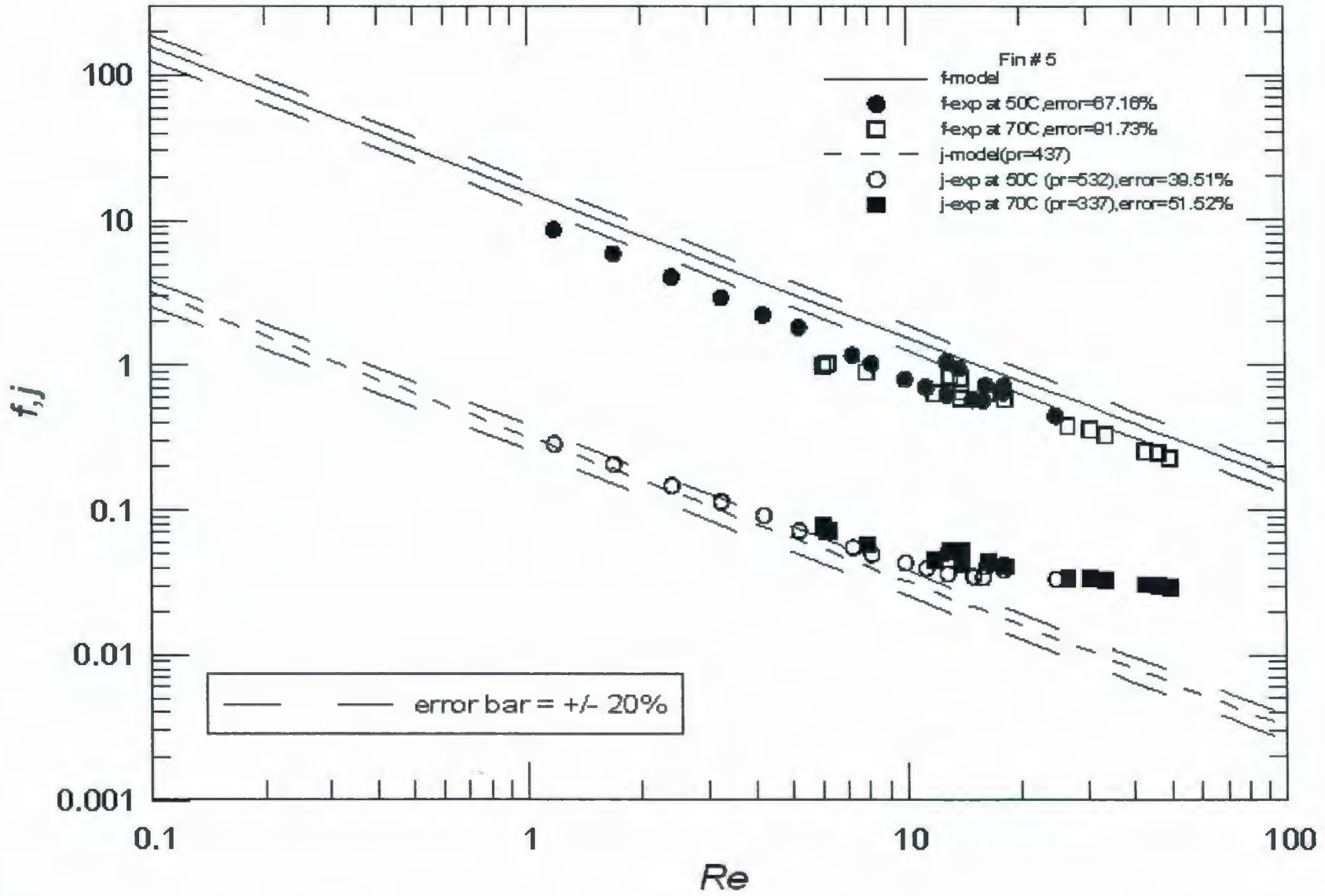

Fig. D.23 – Comparison of Fin # 5 data with low Reynolds number Asymptote

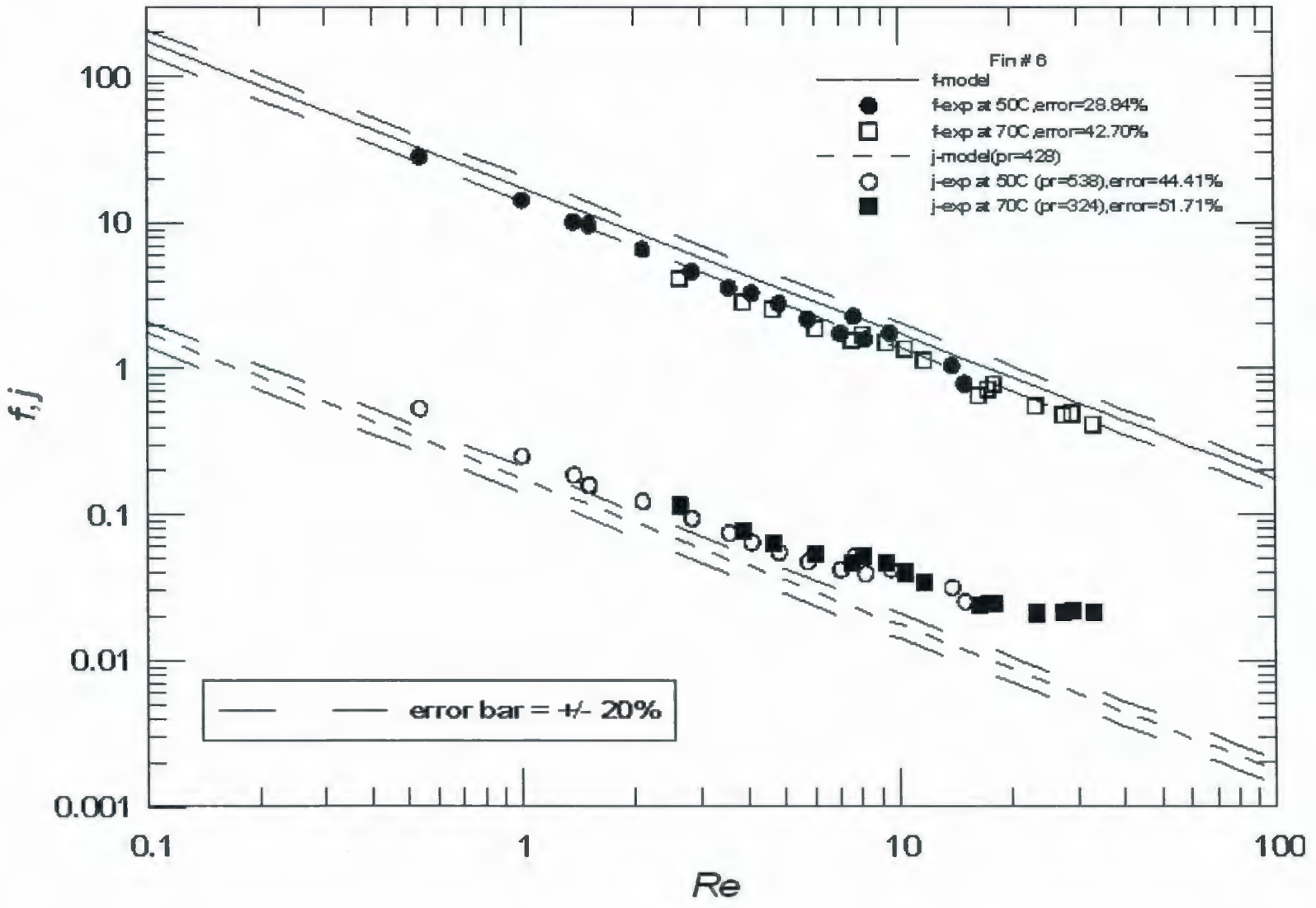

Fig. D.24 – Comparison of Fin # 6 data with low Reynolds number Asymptote

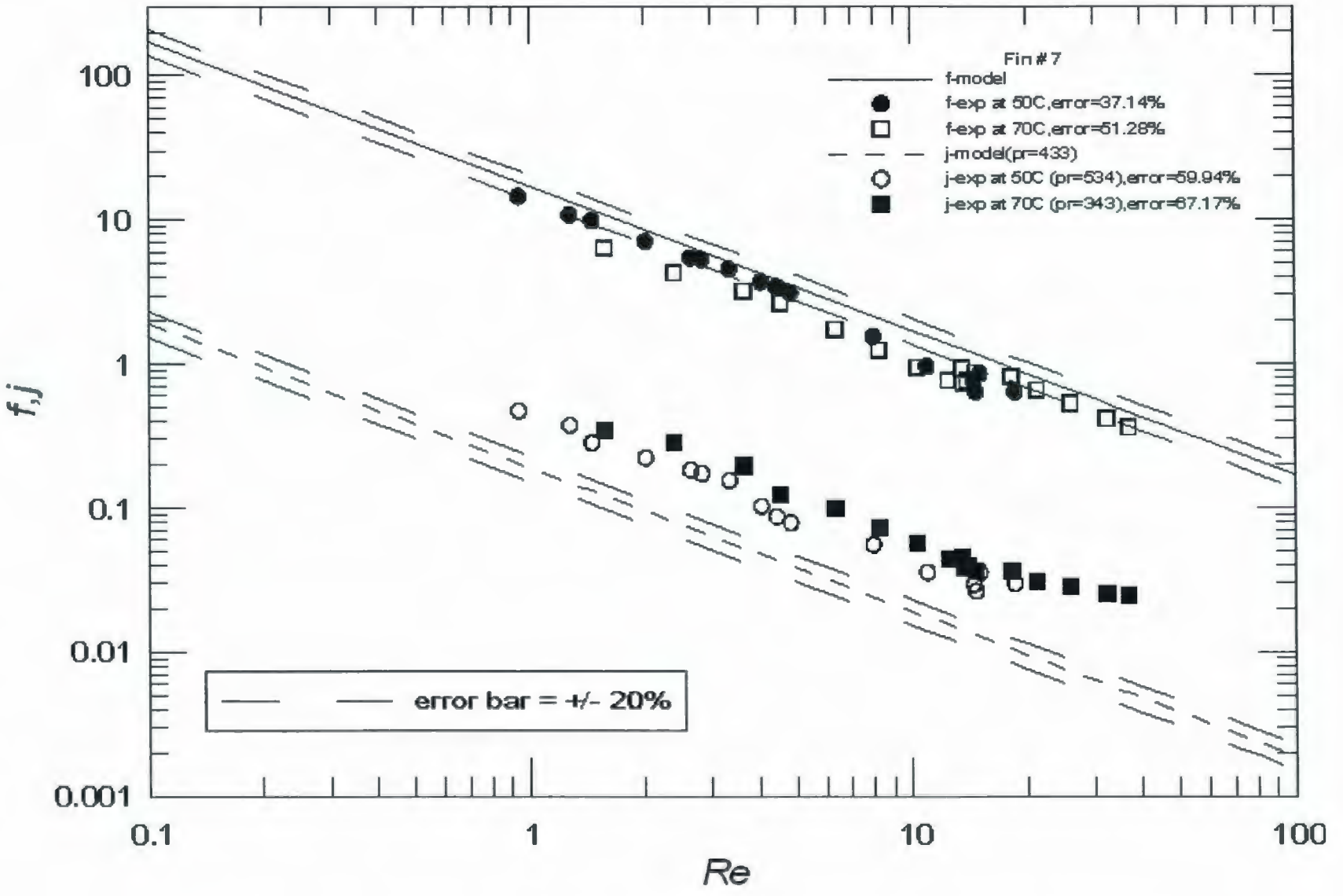

Fig. D.25 – Comparison of Fin # 7 data with low Reynolds number Asymptote

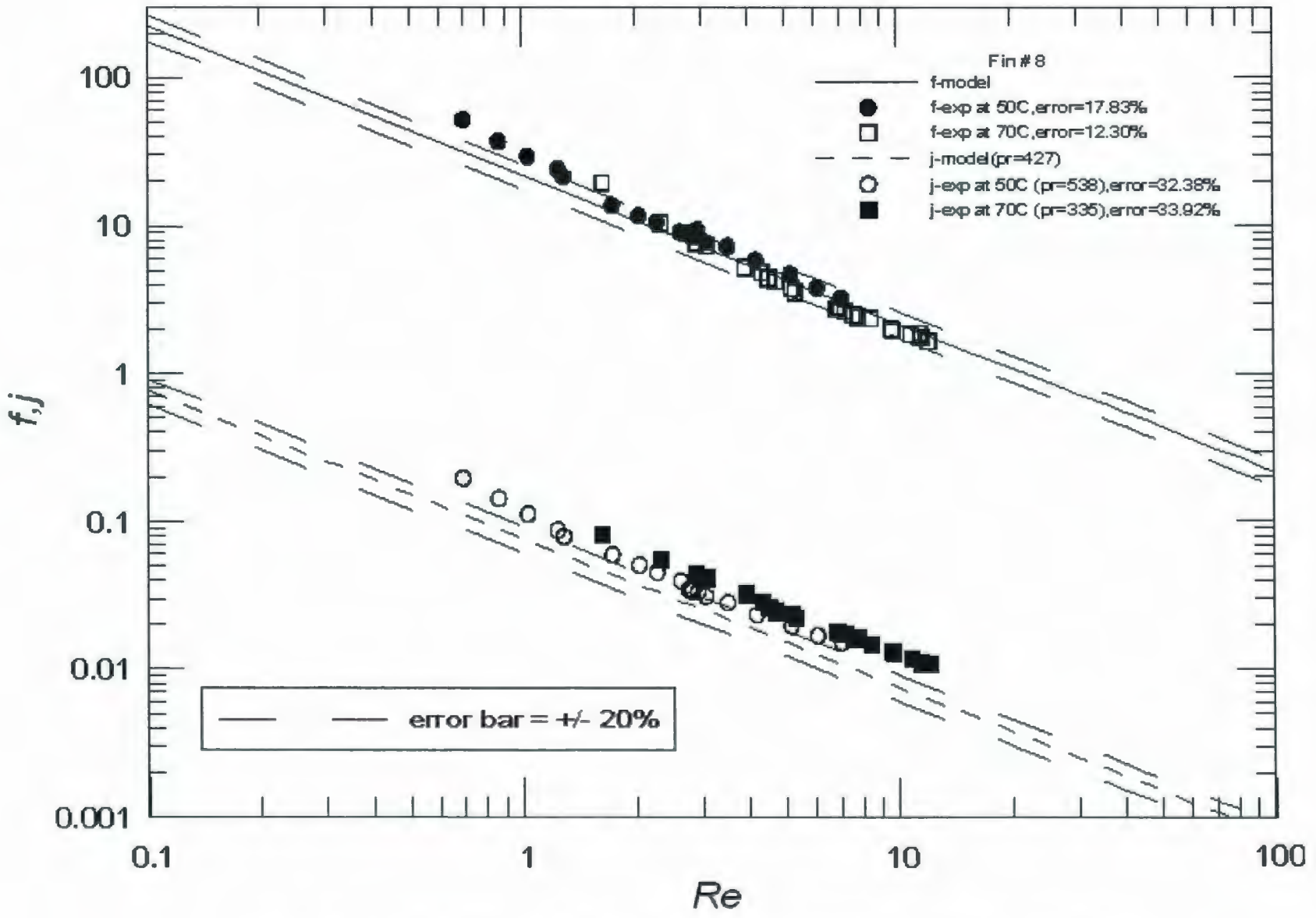

Fig. D.26 – Comparison of Fin # 8 data with low Reynolds number Asymptote

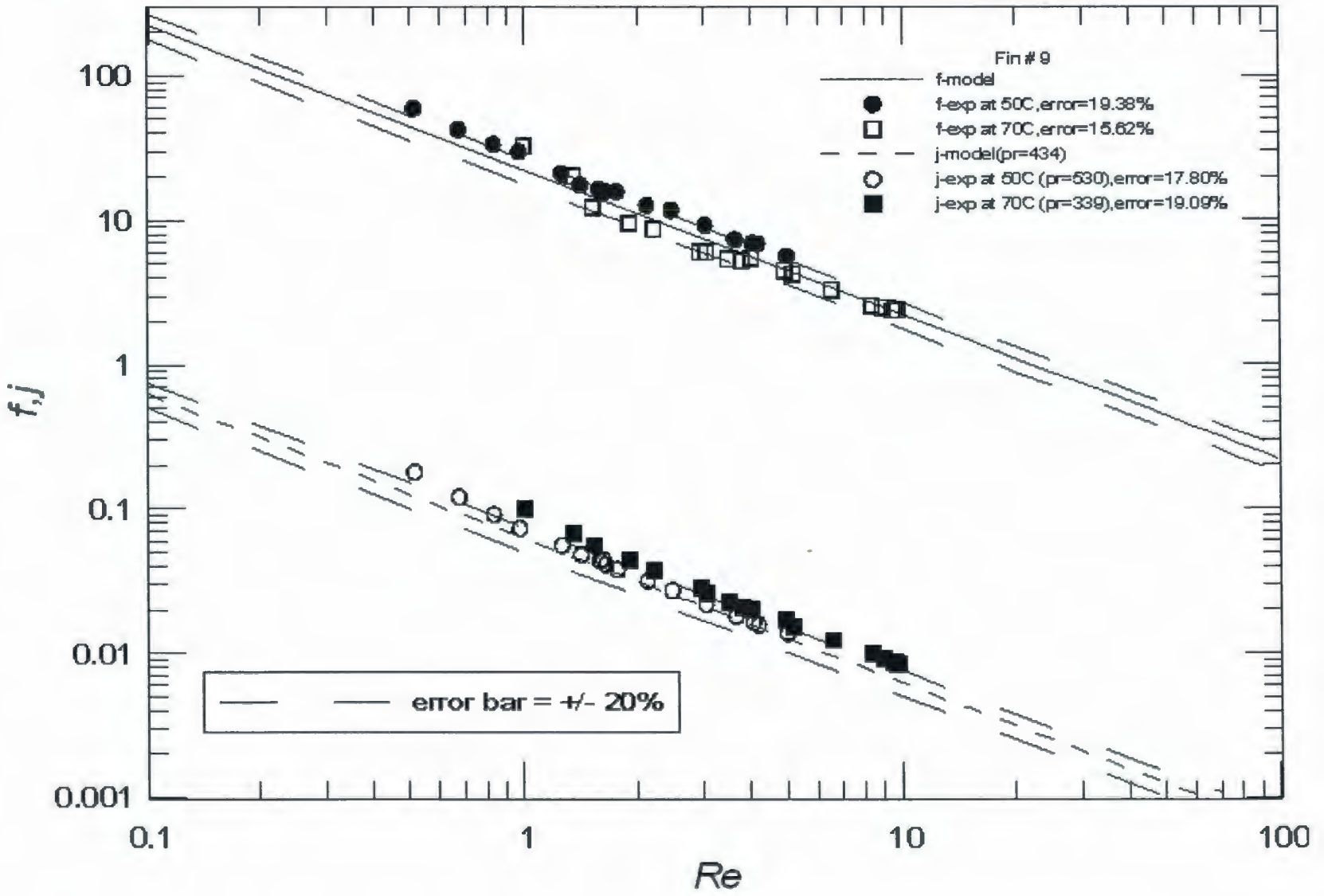

Fig. D.27 – Comparison of Fin # 9 data with low Reynolds number Asymptote

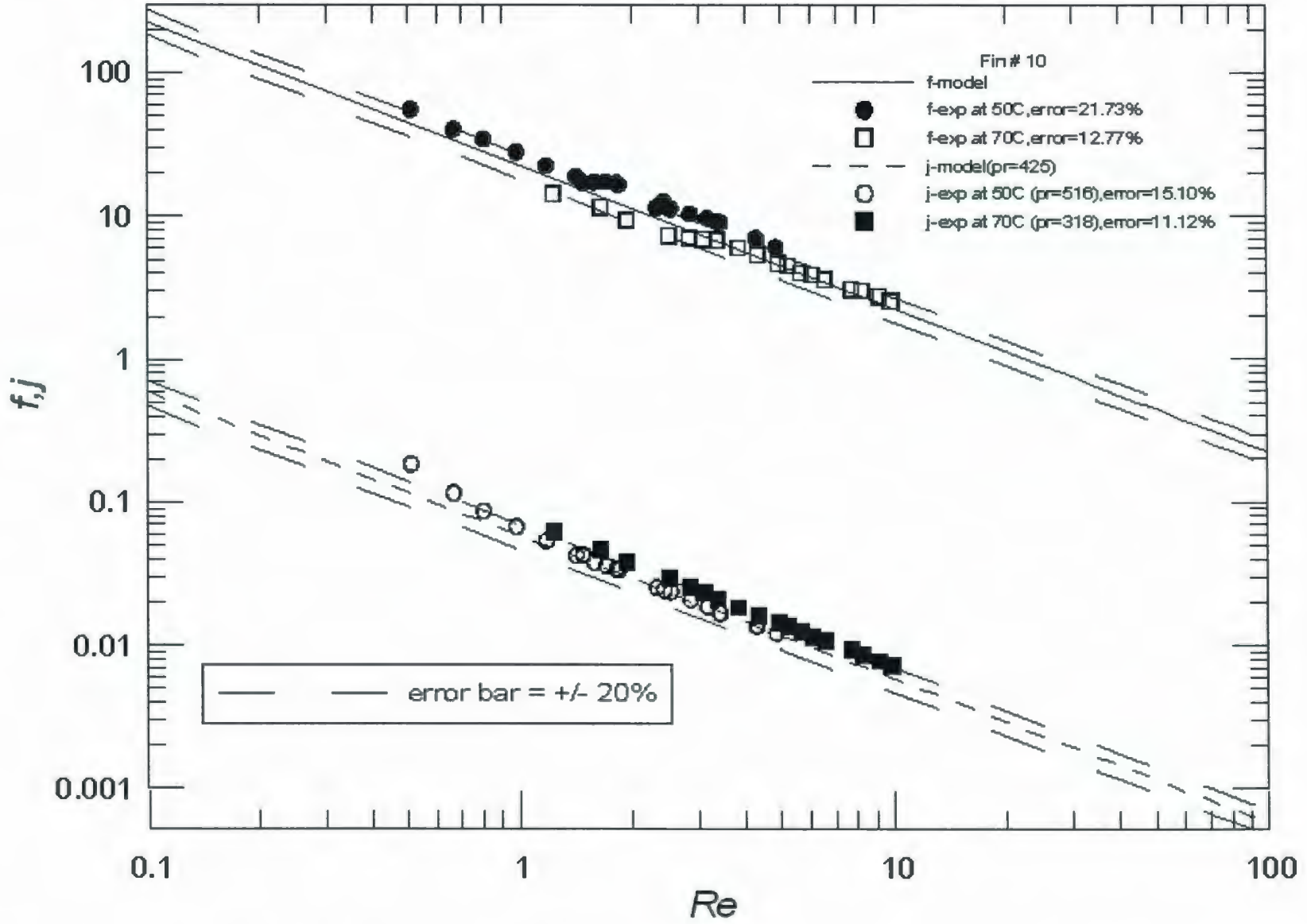

Fig. D.28 – Comparison of Fin # 10 data with low Reynolds number Asymptote

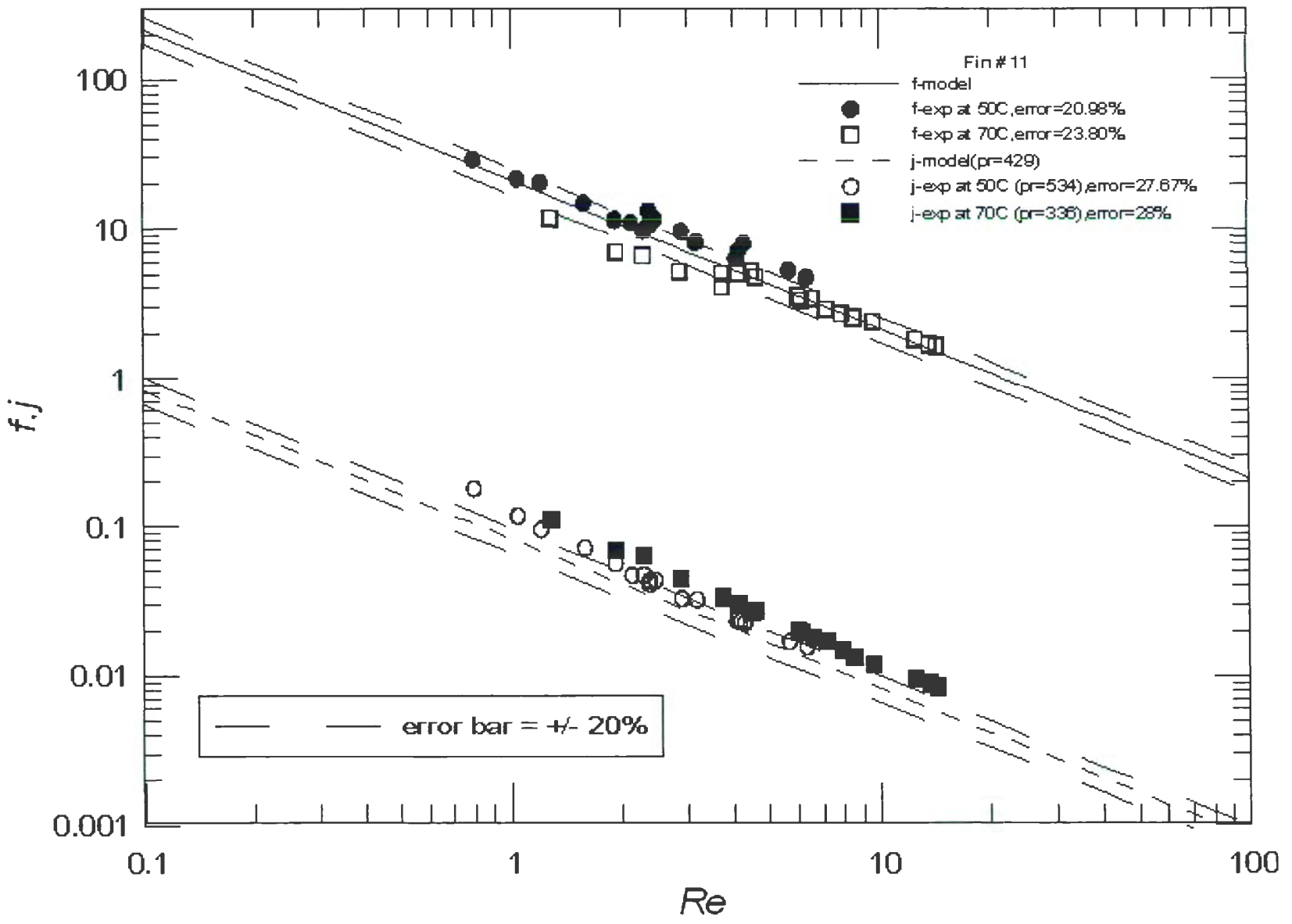

Fig. D.29 – Comparison of Fin # 11 data with low Reynolds number Asymptote

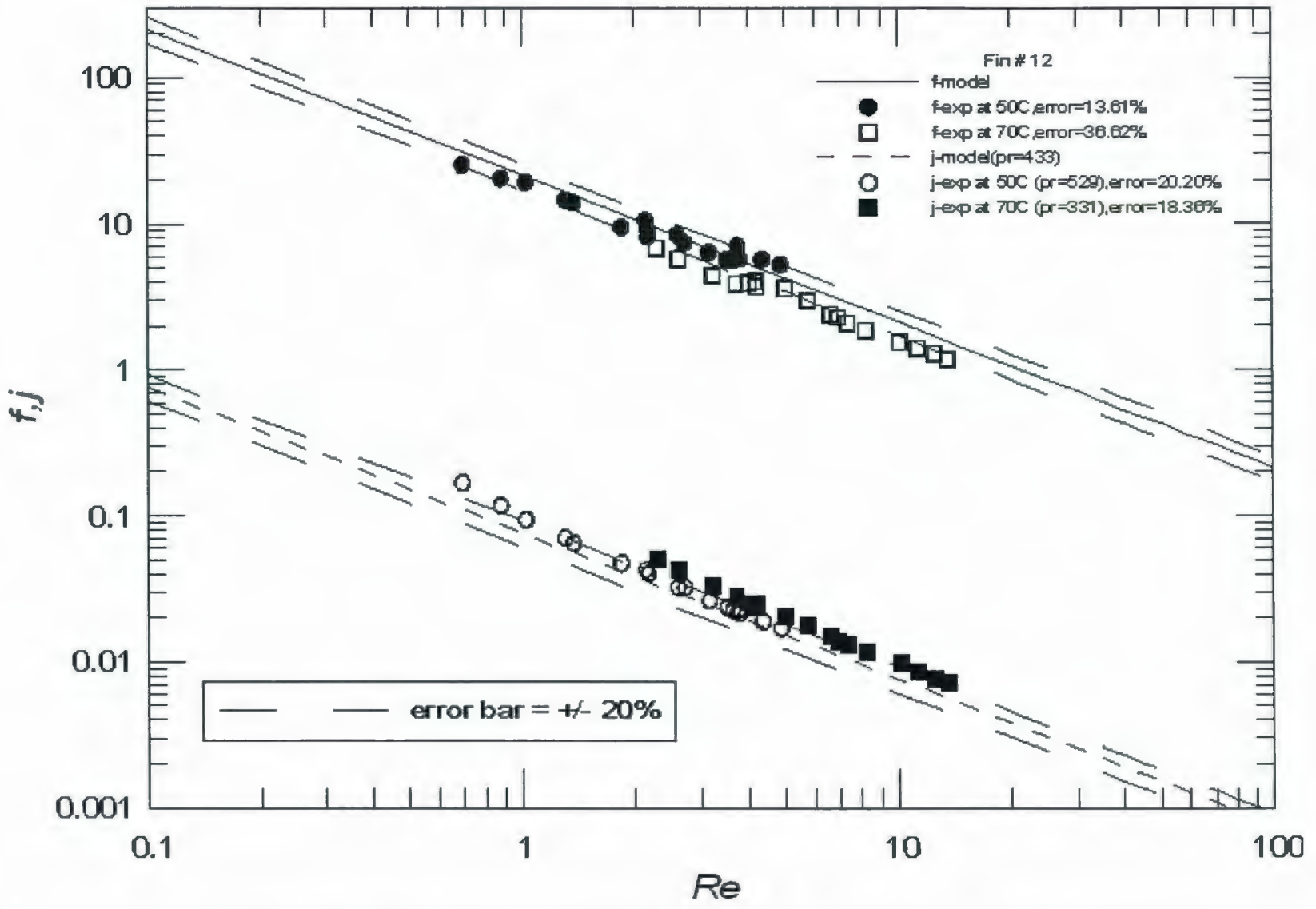

Fig. D.30 – Comparison of Fin # 12 data with low Reynolds number Asymptote

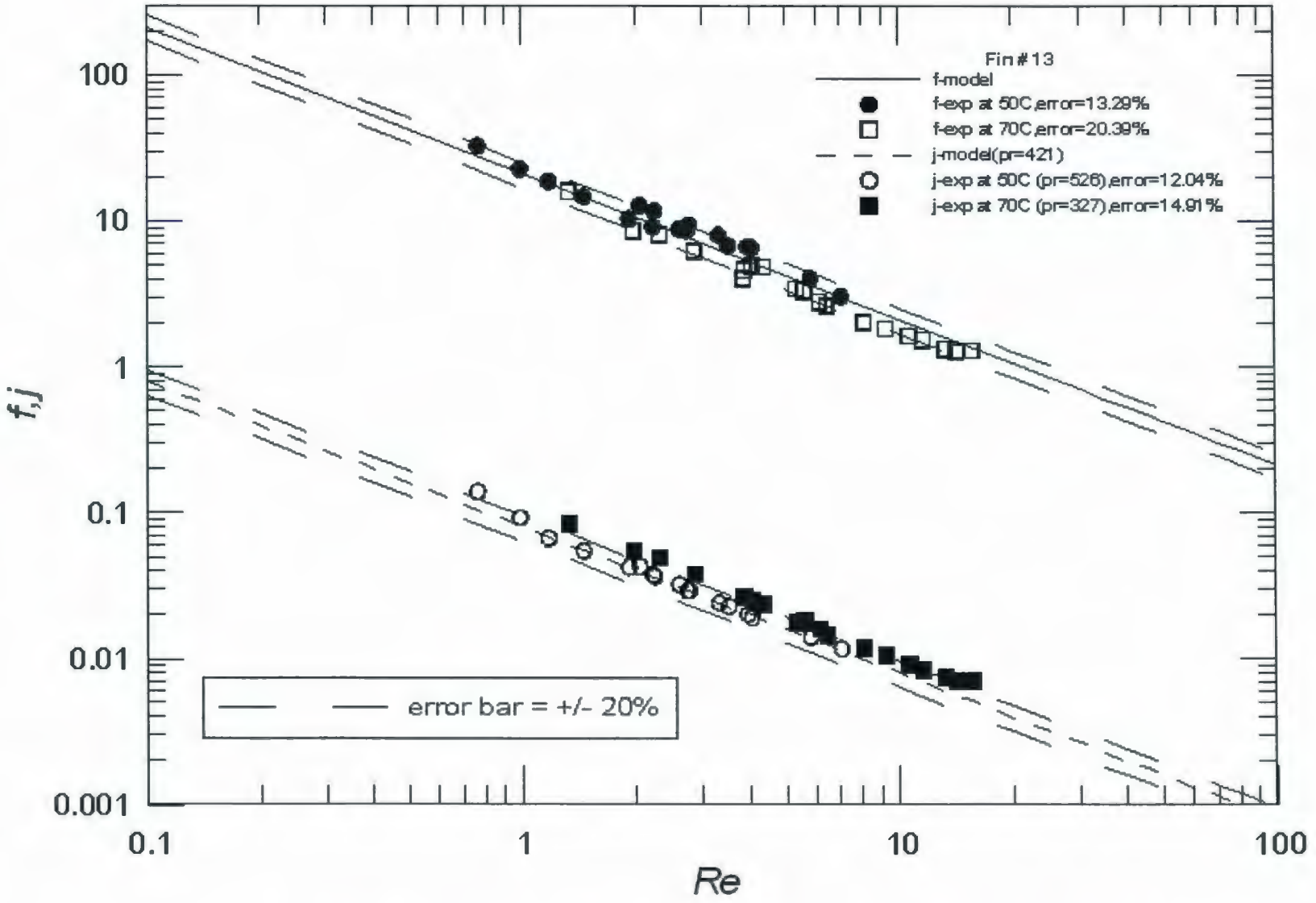

Fig. D.31 – Comparison of Fin # 13 data with low Reynolds number Asymptote

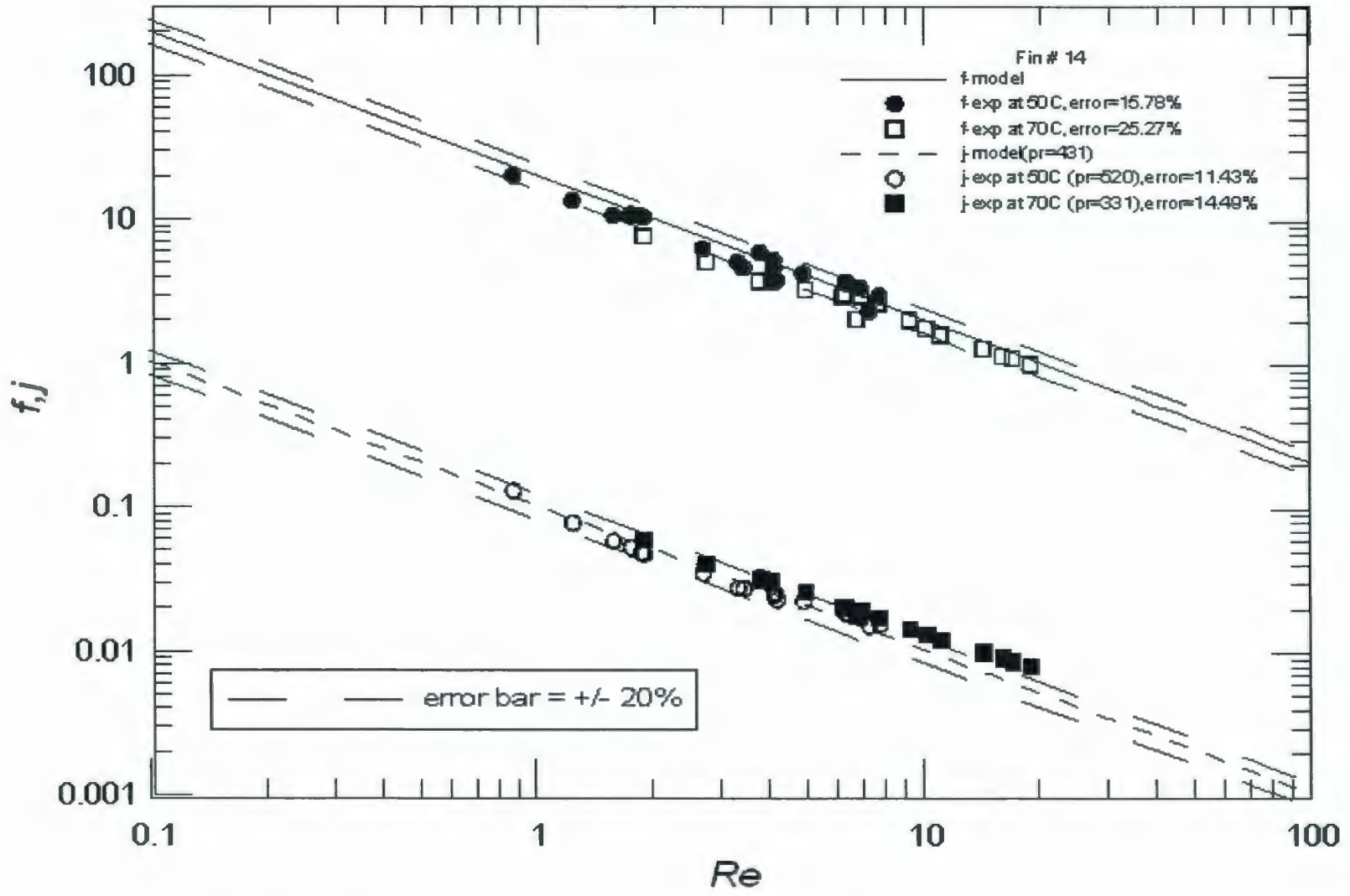

Fig. D.32 – Comparison of Fin # 14 data with low Reynolds number Asymptote

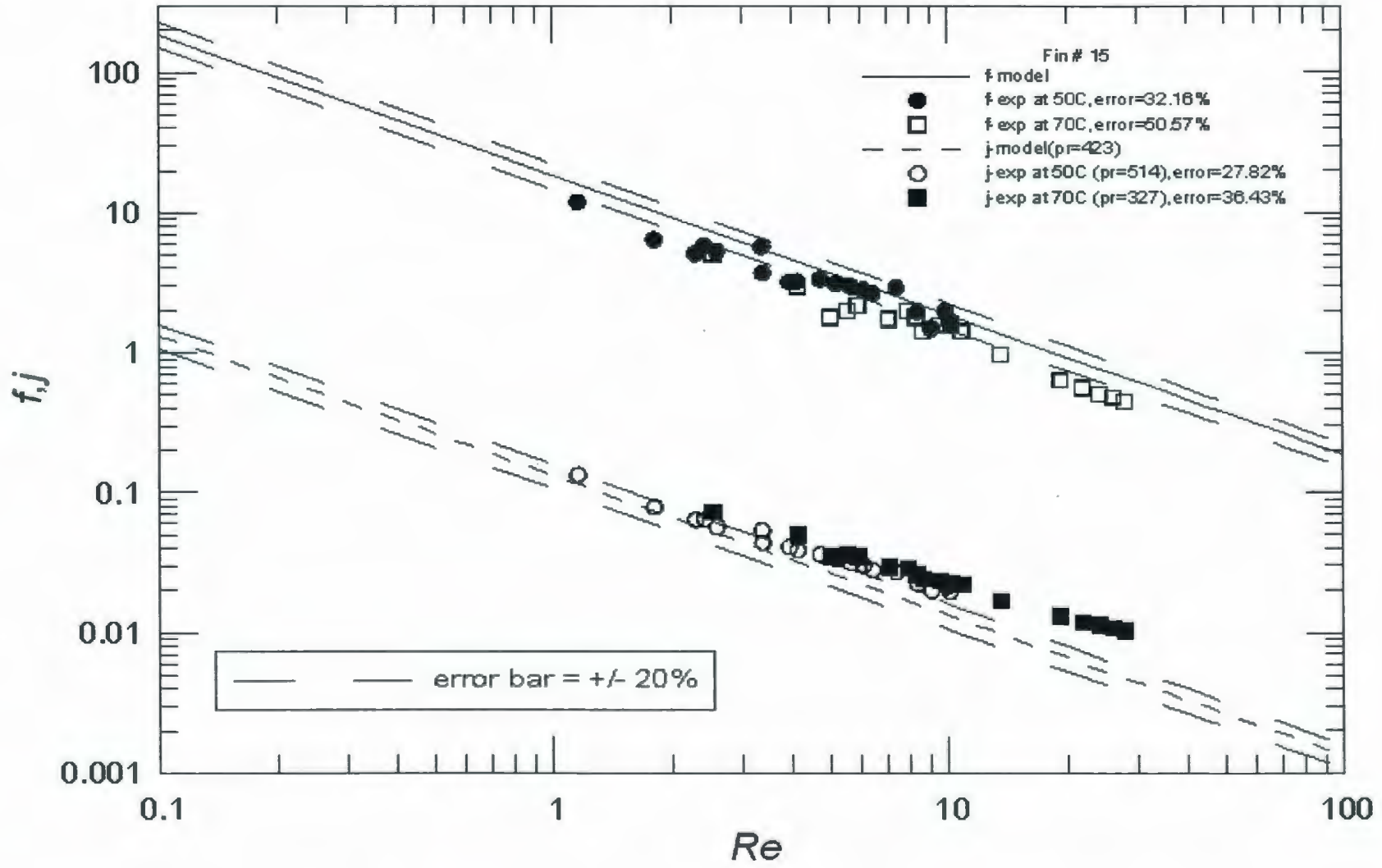

Fig. D.33 – Comparison of Fin # 15 data with low Reynolds number Asymptote

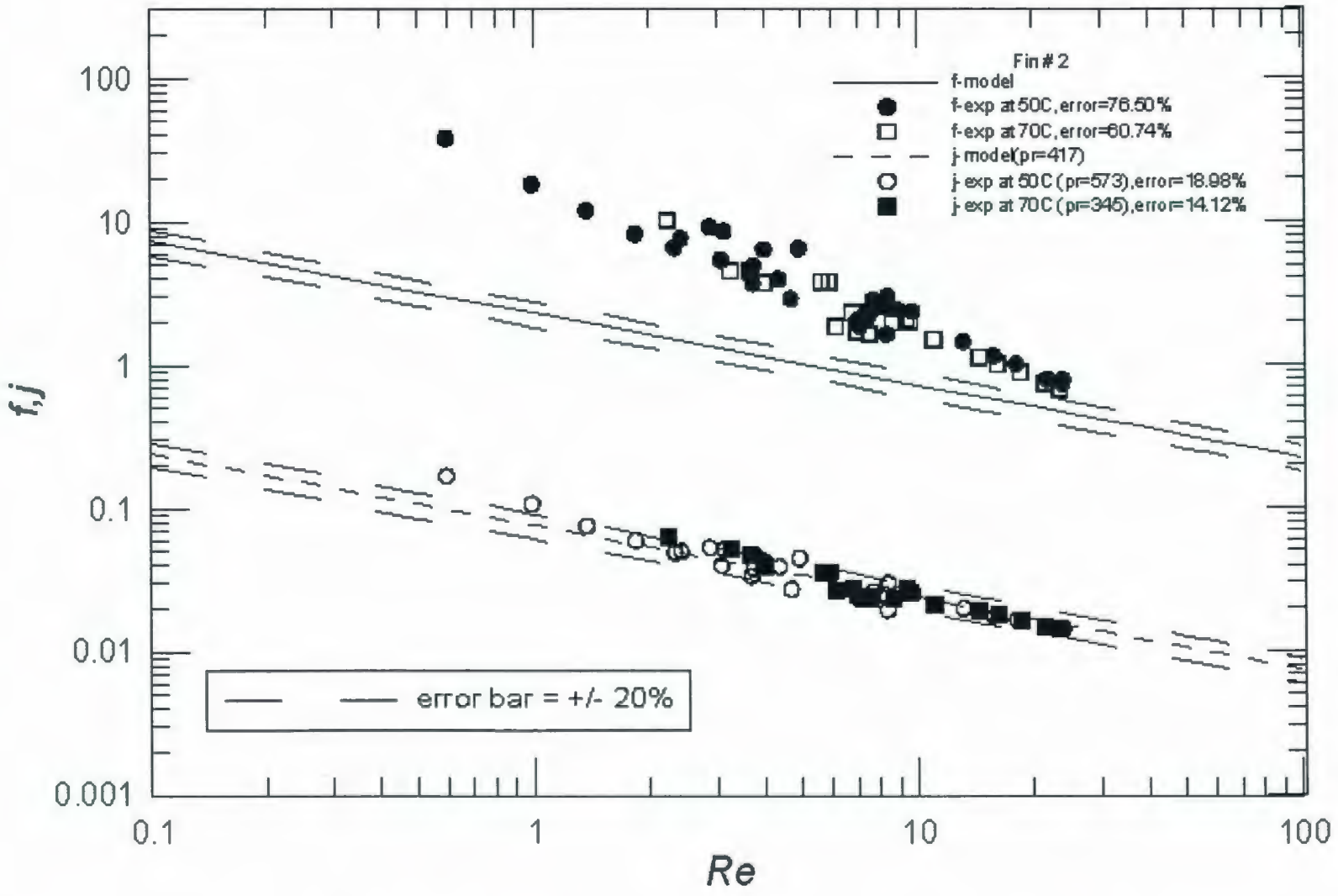

Fig. D.34– Comparison of Fin # 2 data with LBL Asymptote

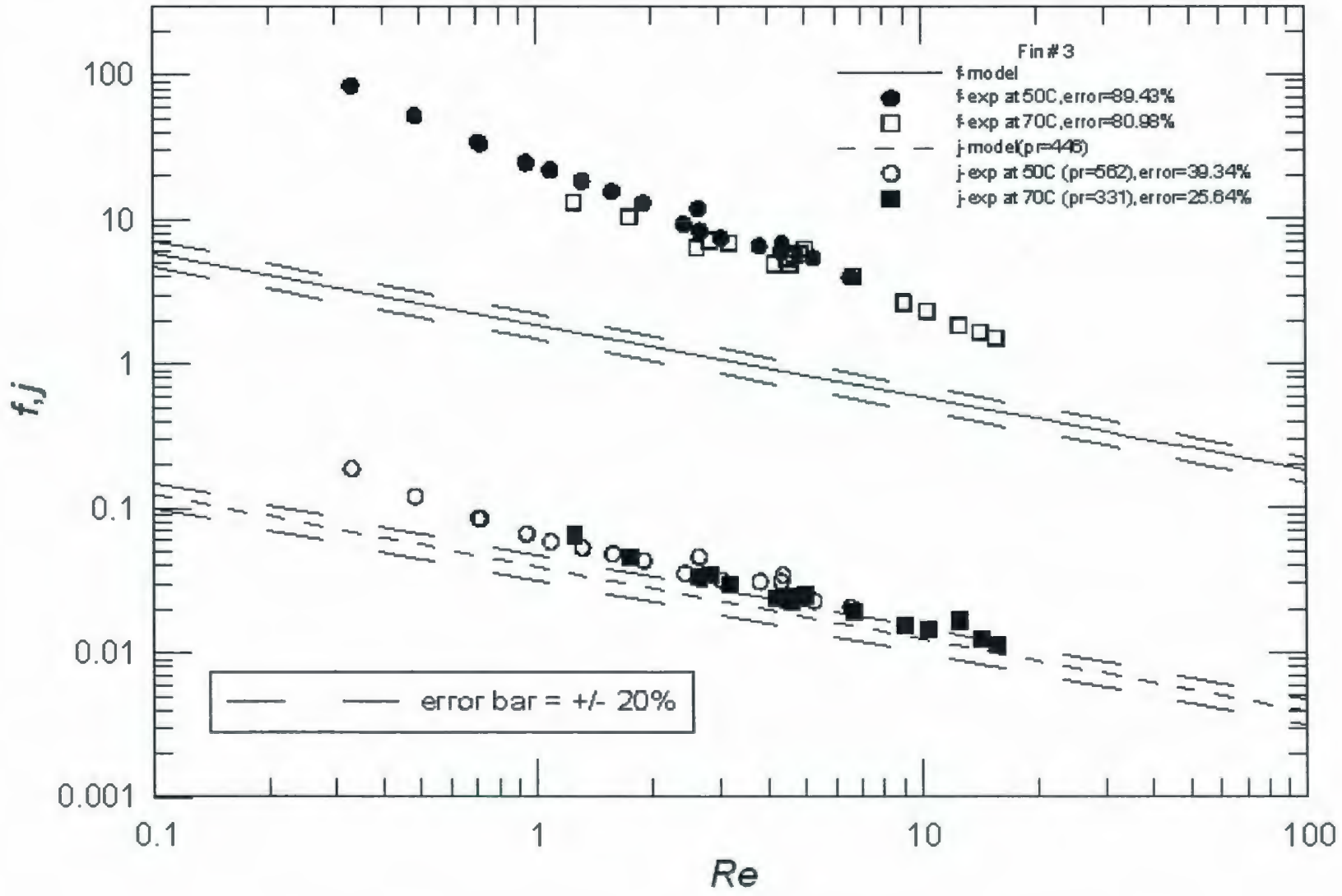

Fig. D.35 – Comparison of Fin # 3 data with LBL Asymptote

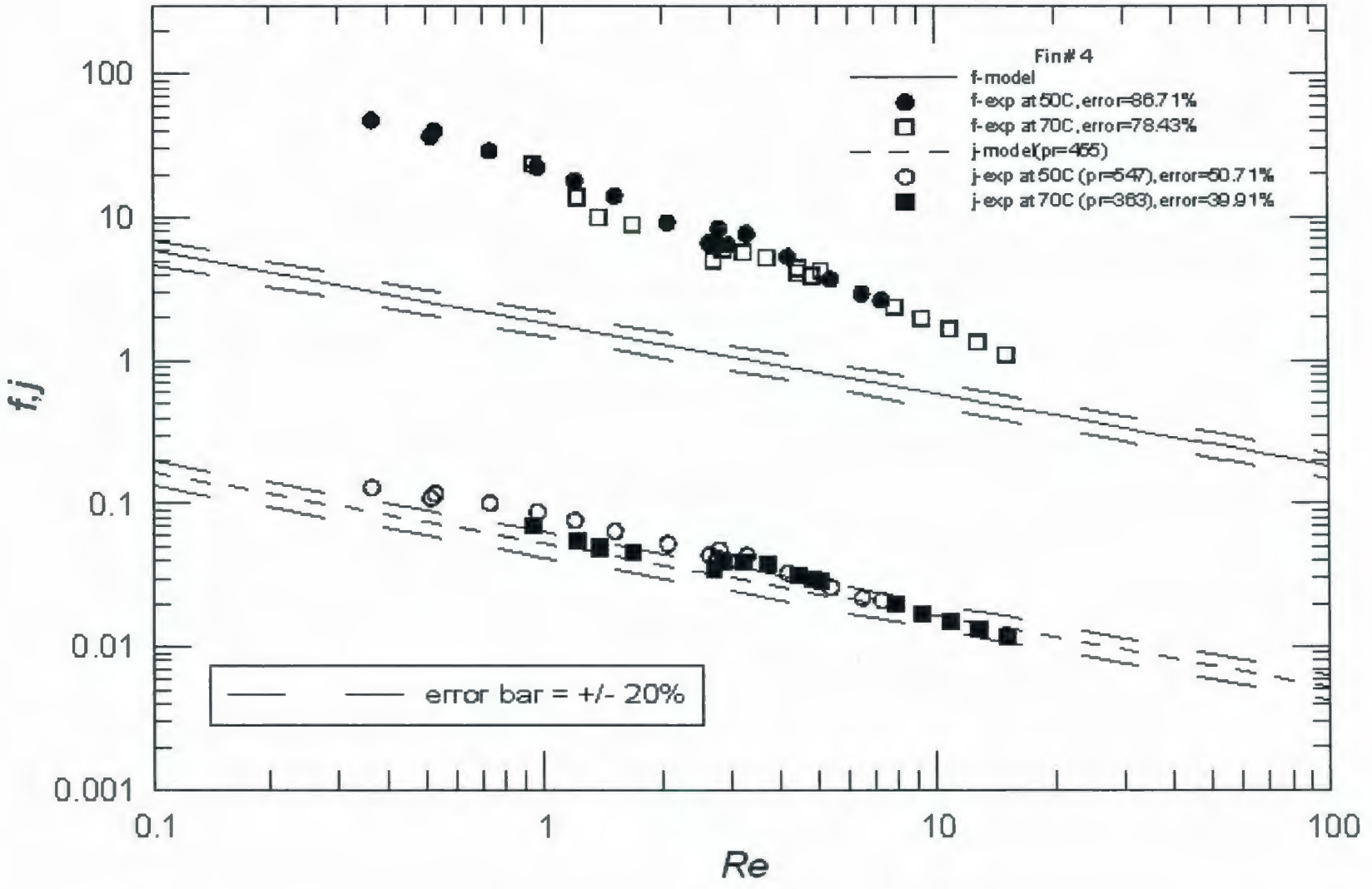

Fig. D.36 – Comparison of Fin # 4 data with LBL Asymptote

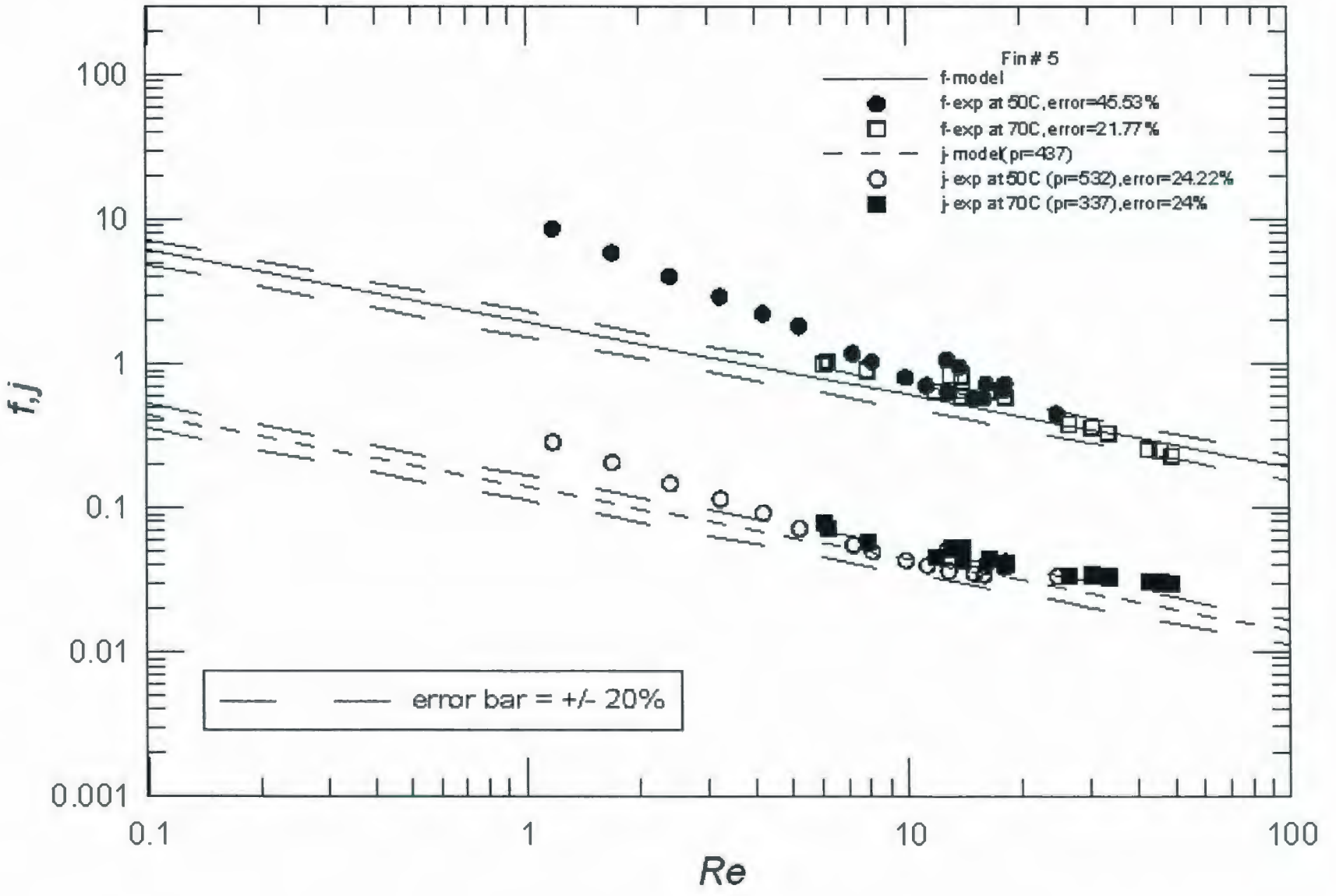

Fig. D.37 – Comparison of Fin # 5 data with LBL Asymptote

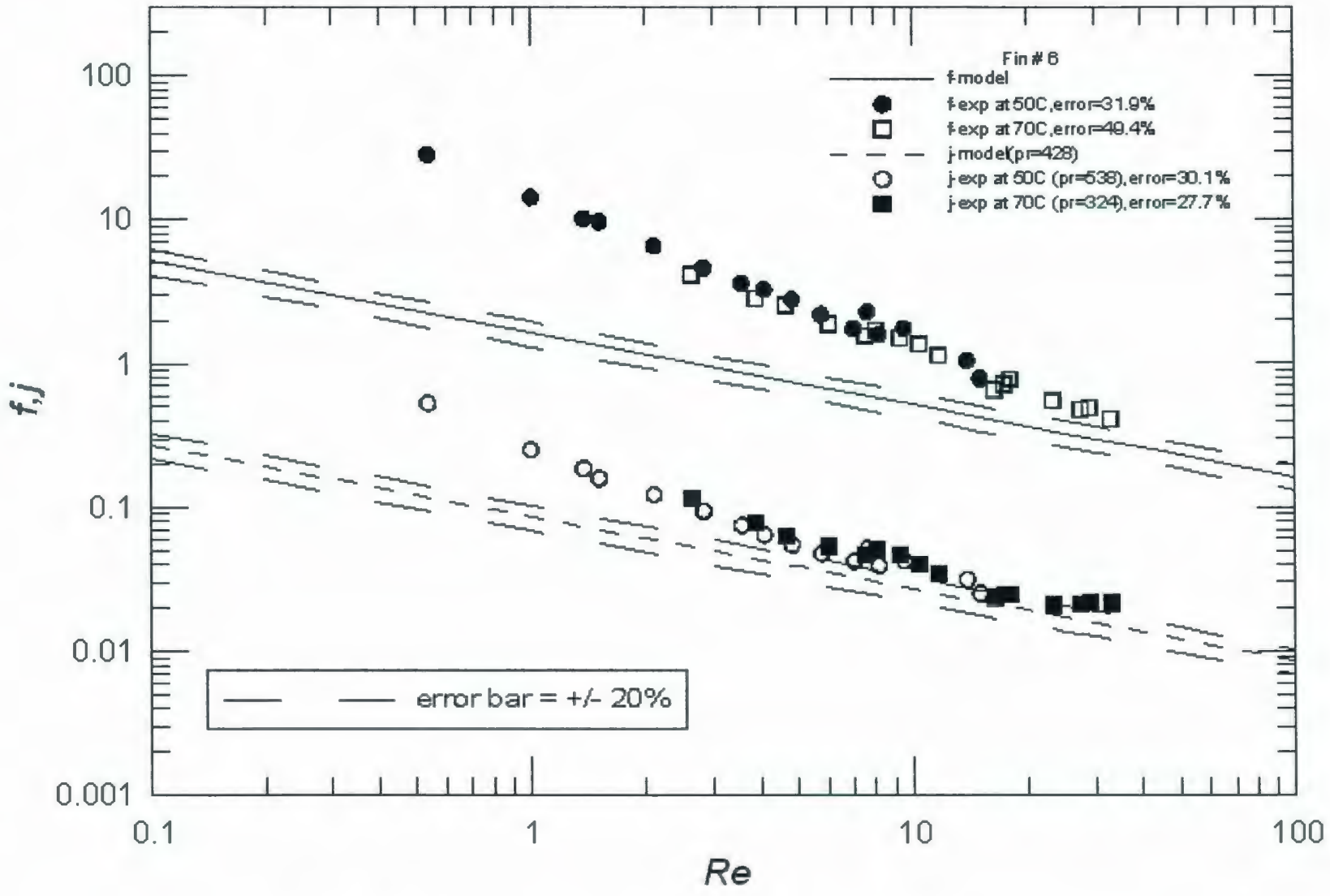

Fig. D.38 – Comparison of Fin # 6 data with LBL Asymptote

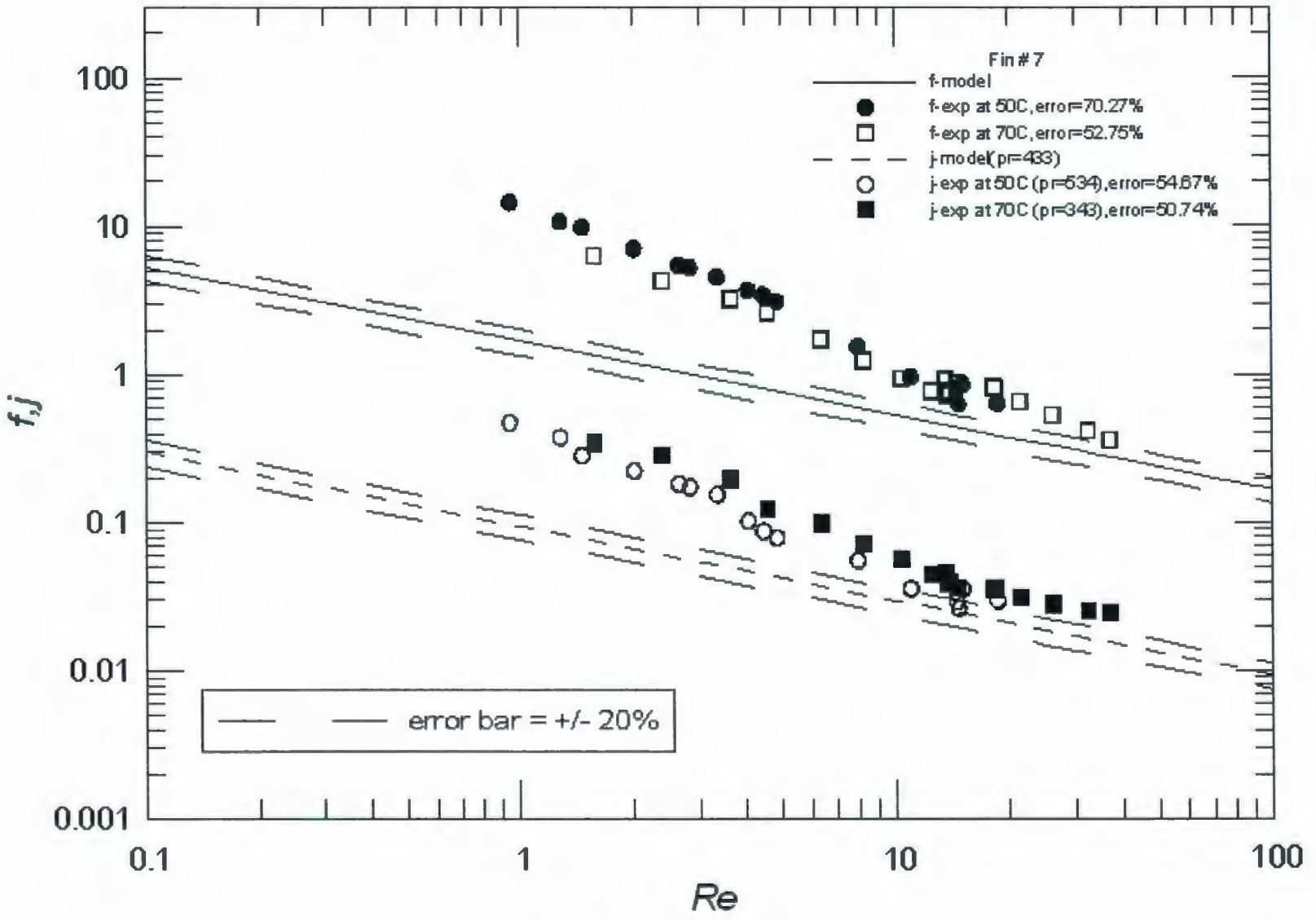

Fig. D.39 – Comparison of Fin # 7 data with LBL Asymptote

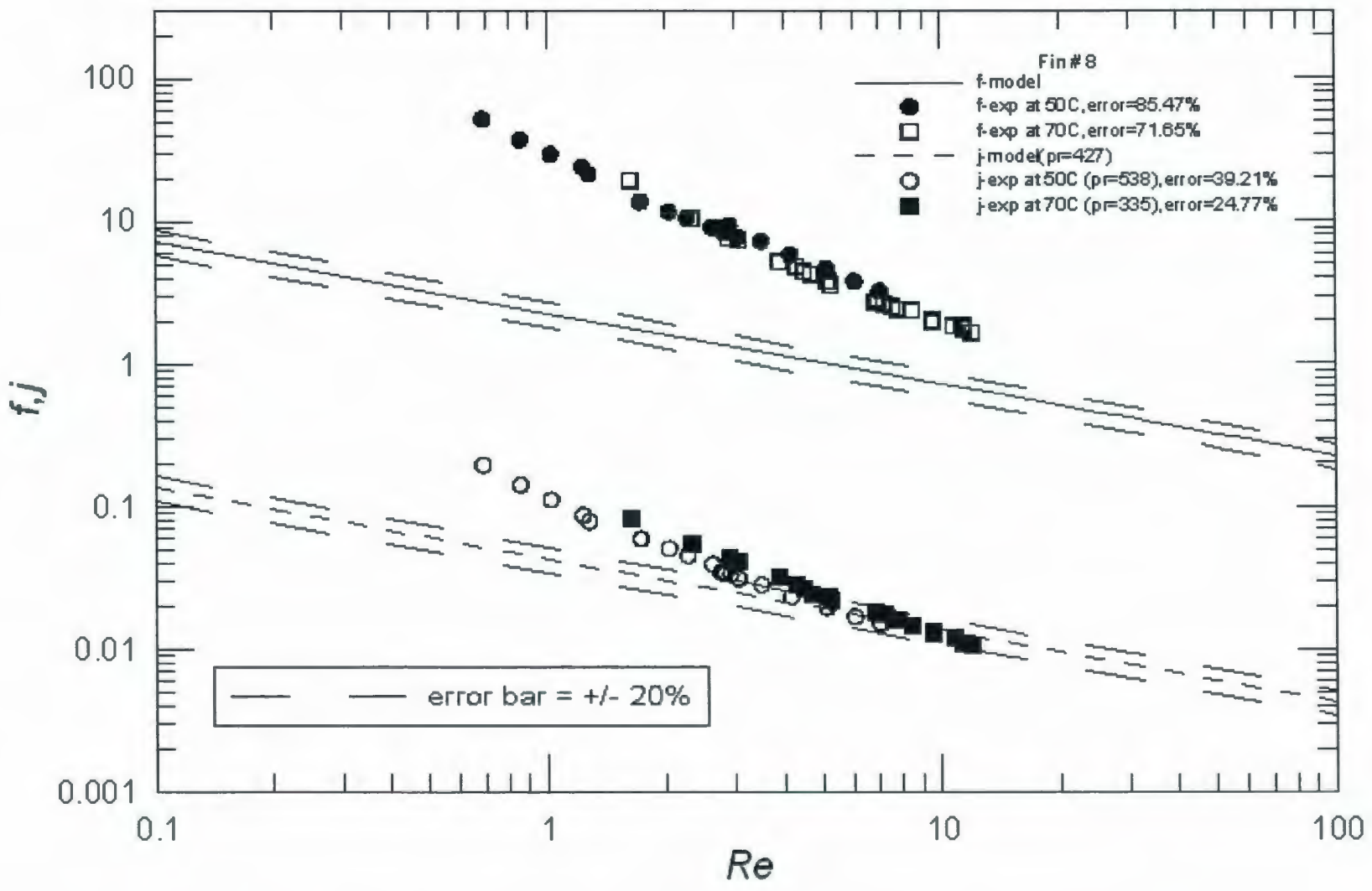

Fig. D.40 – Comparison of Fin # 8 data with LBL Asymptote

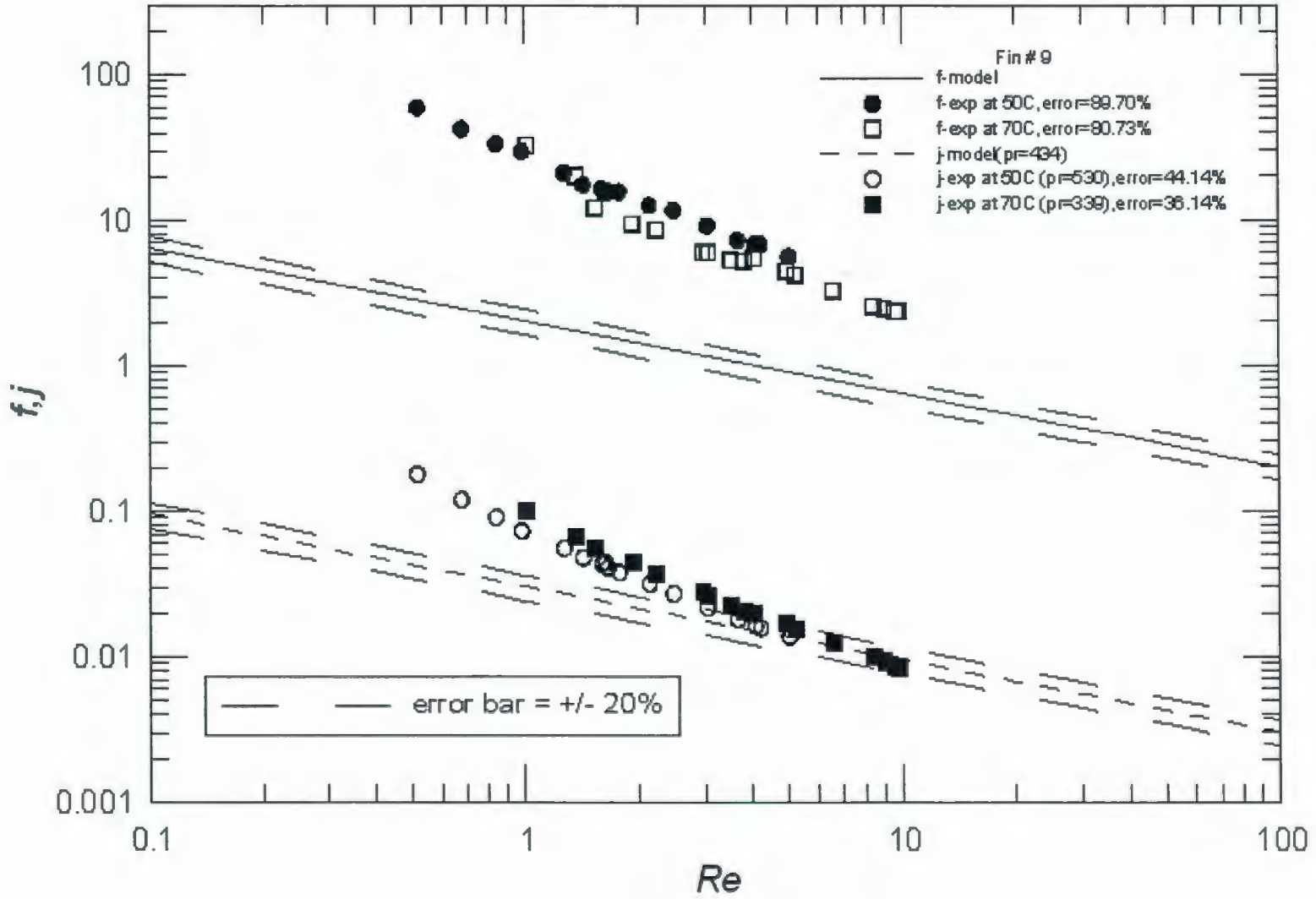

Fig. D.41 – Comparison of Fin # 9 data with LBL Asymptote

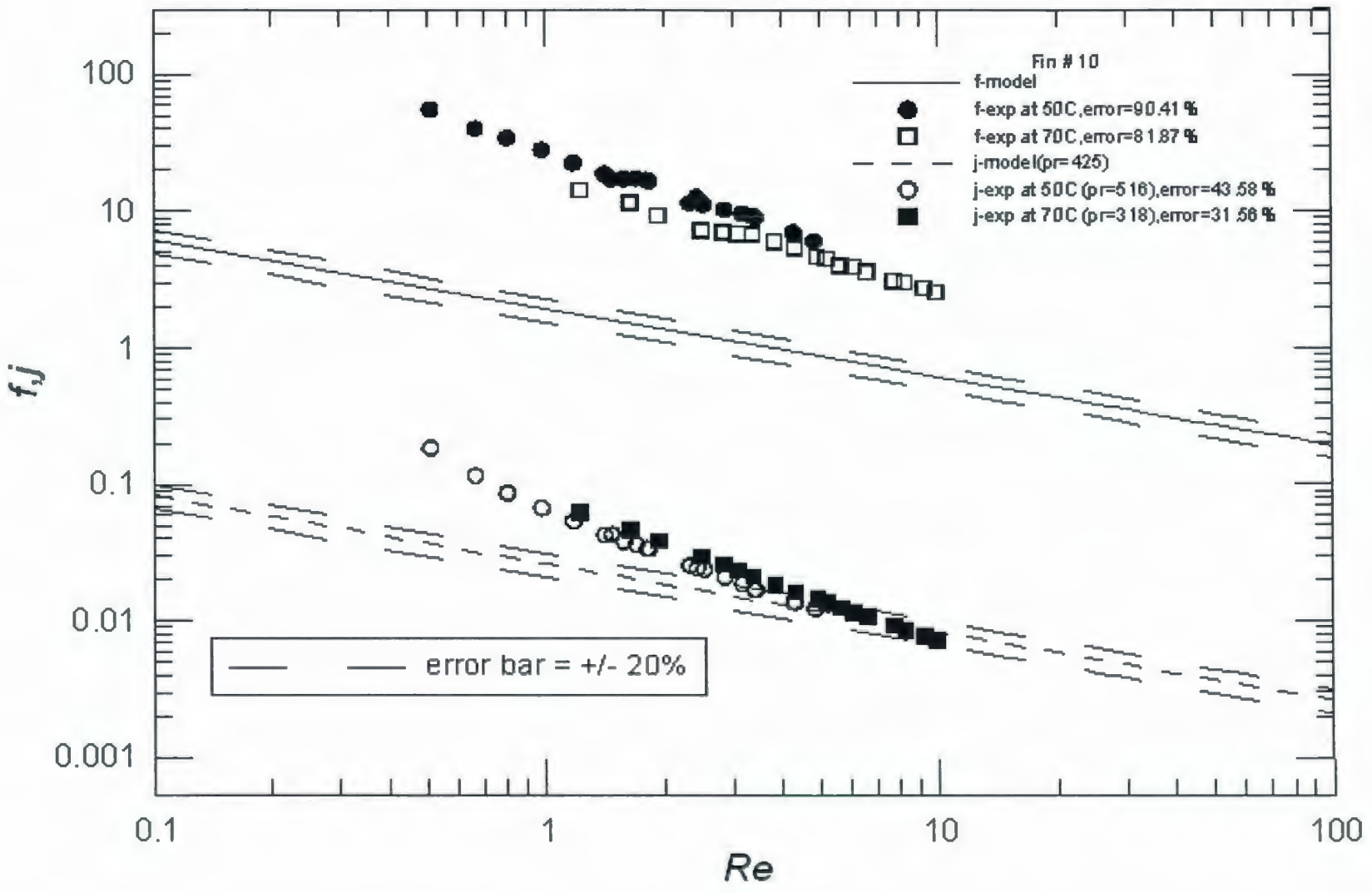

Fig. D.42 – Comparison of Fin # 10 data with LBL Asymptote

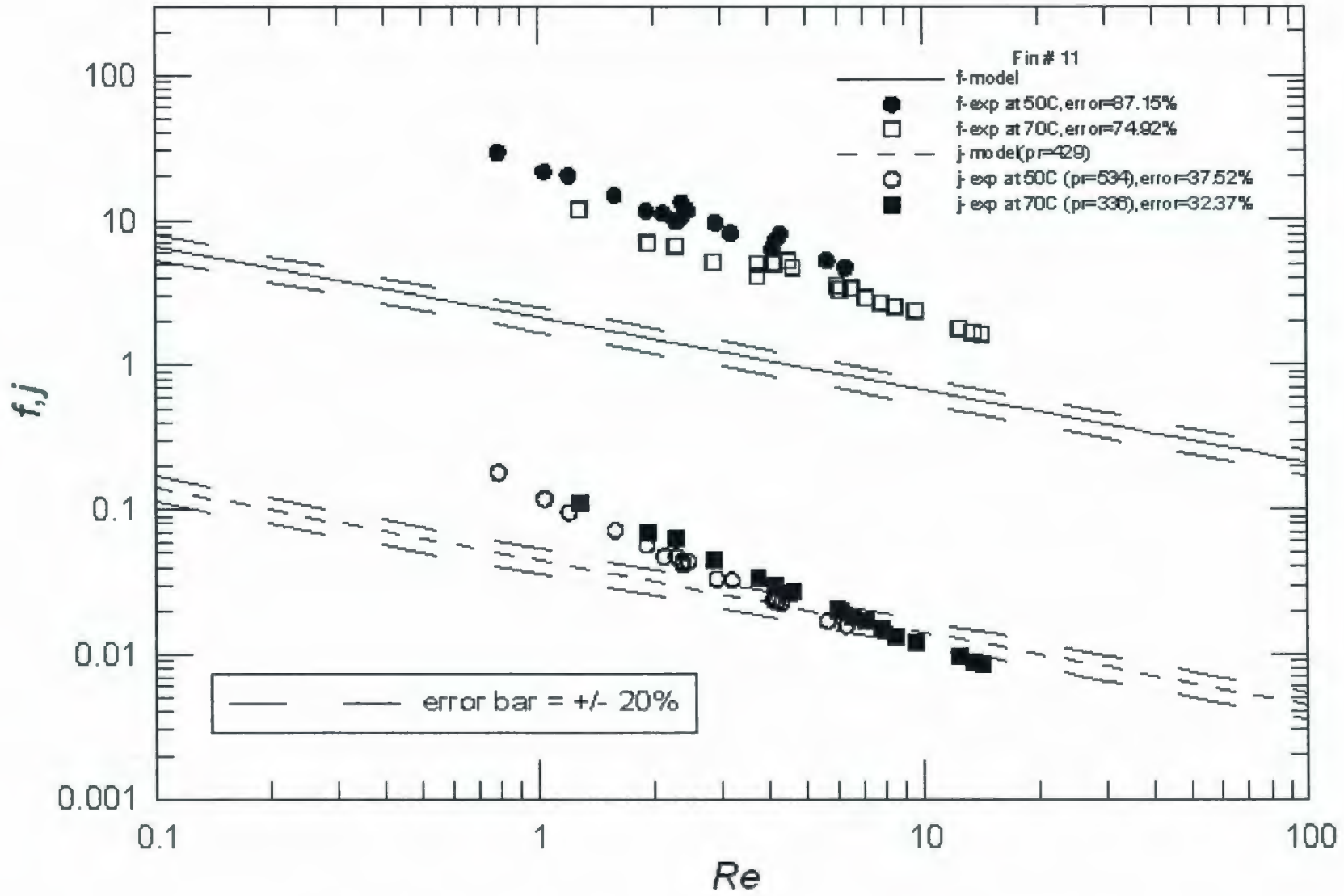

Fig. D.43 – Comparison of Fin # 11 data with LBL Asymptote

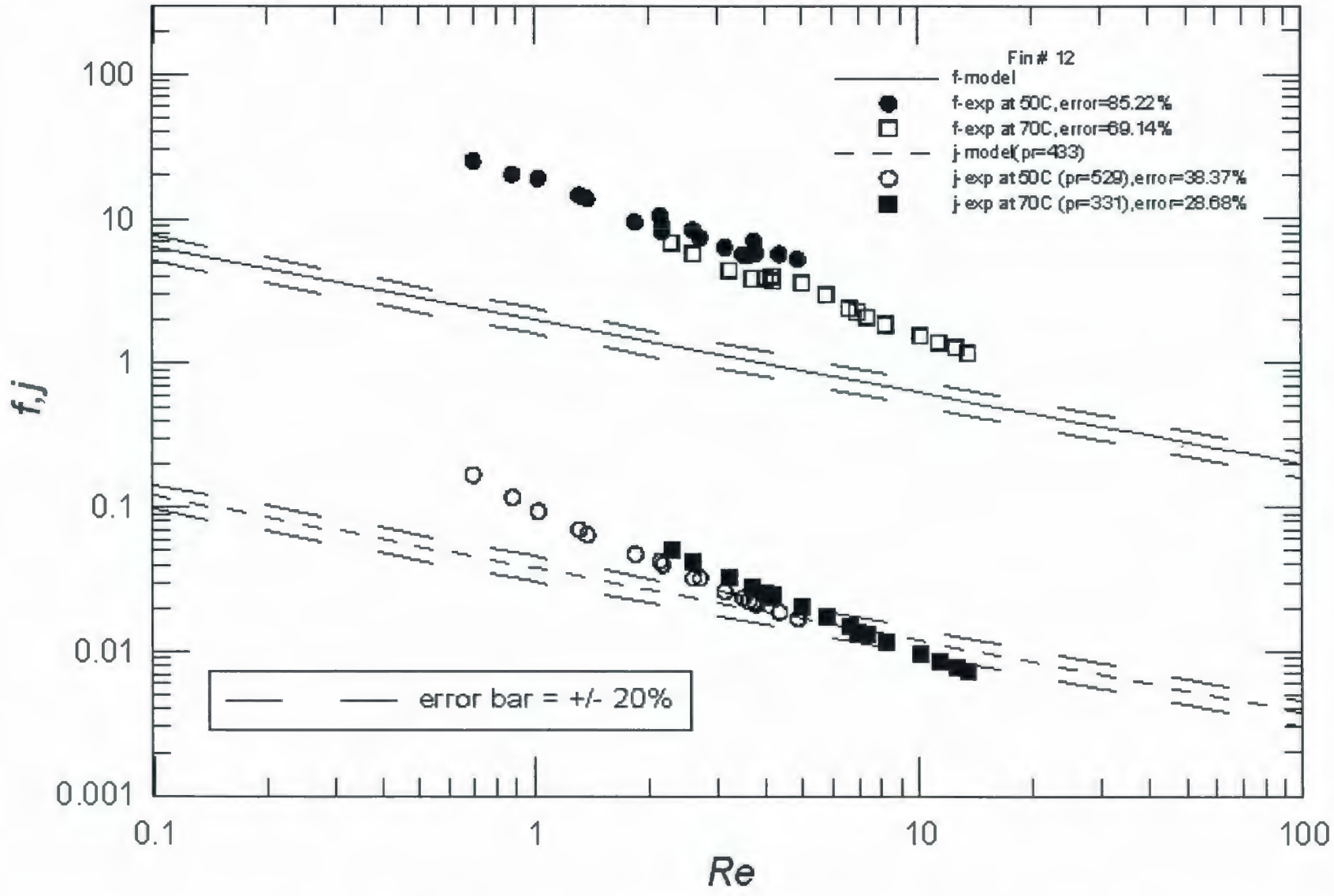

Fig. D.44 – Comparison of Fin # 12 data with LBL Asymptote

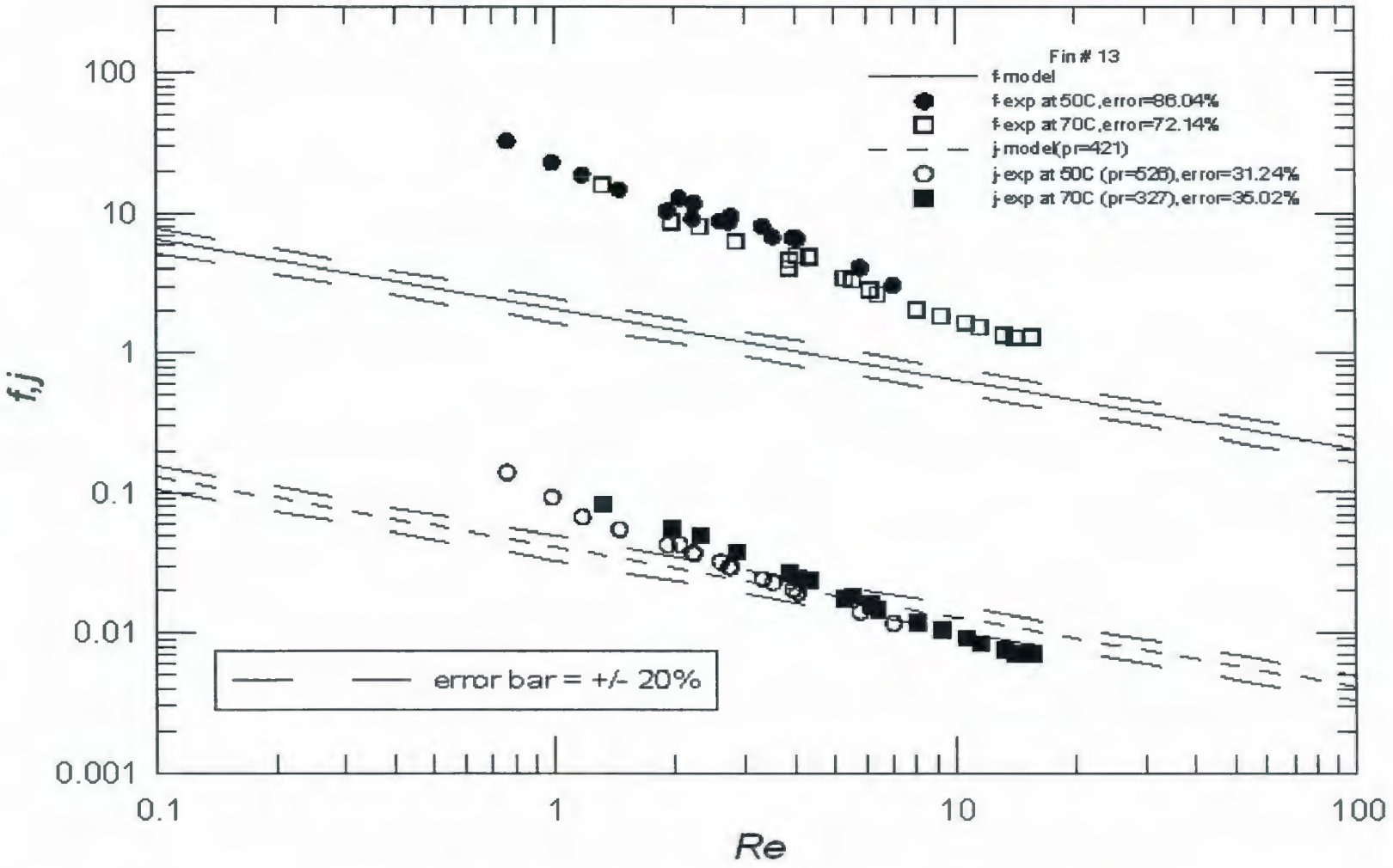

Fig. D.45 – Comparison of Fin # 13 data with LBL Asymptote

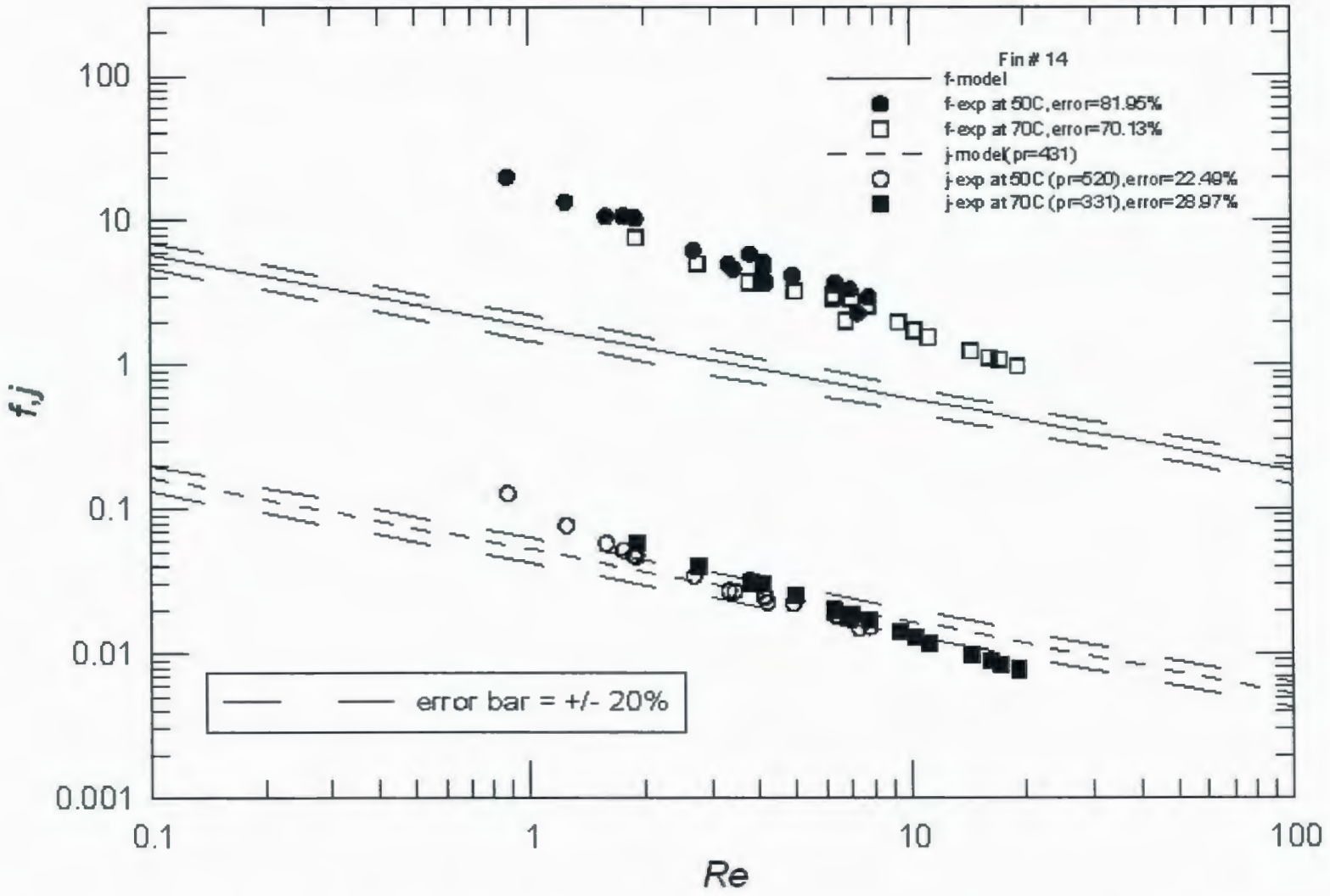

Fig. D.46 – Comparison of Fin # 14 data with LBL Asymptote

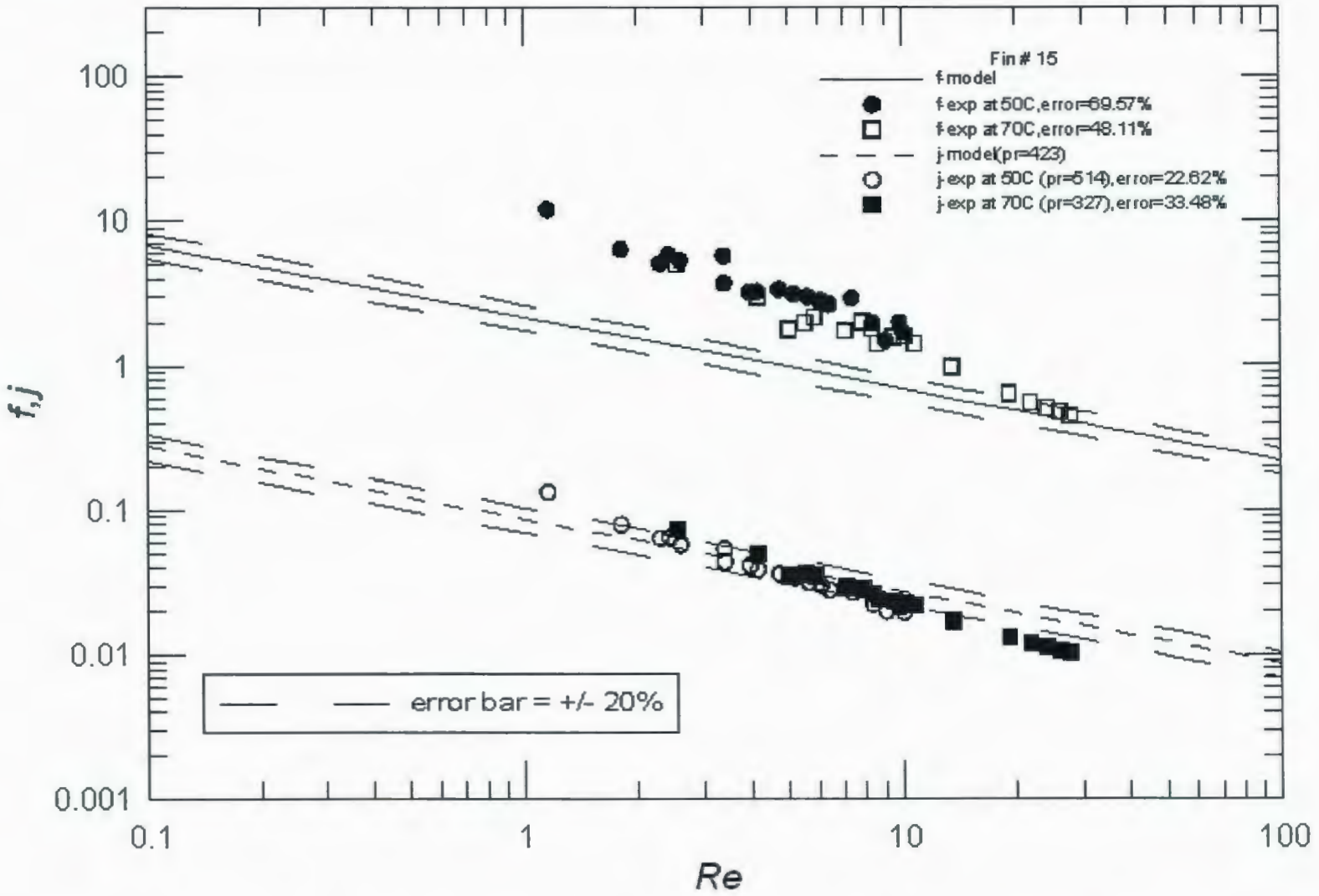

Fig. D.47 – Comparison of Fin # 15 data with LBL Asymptote

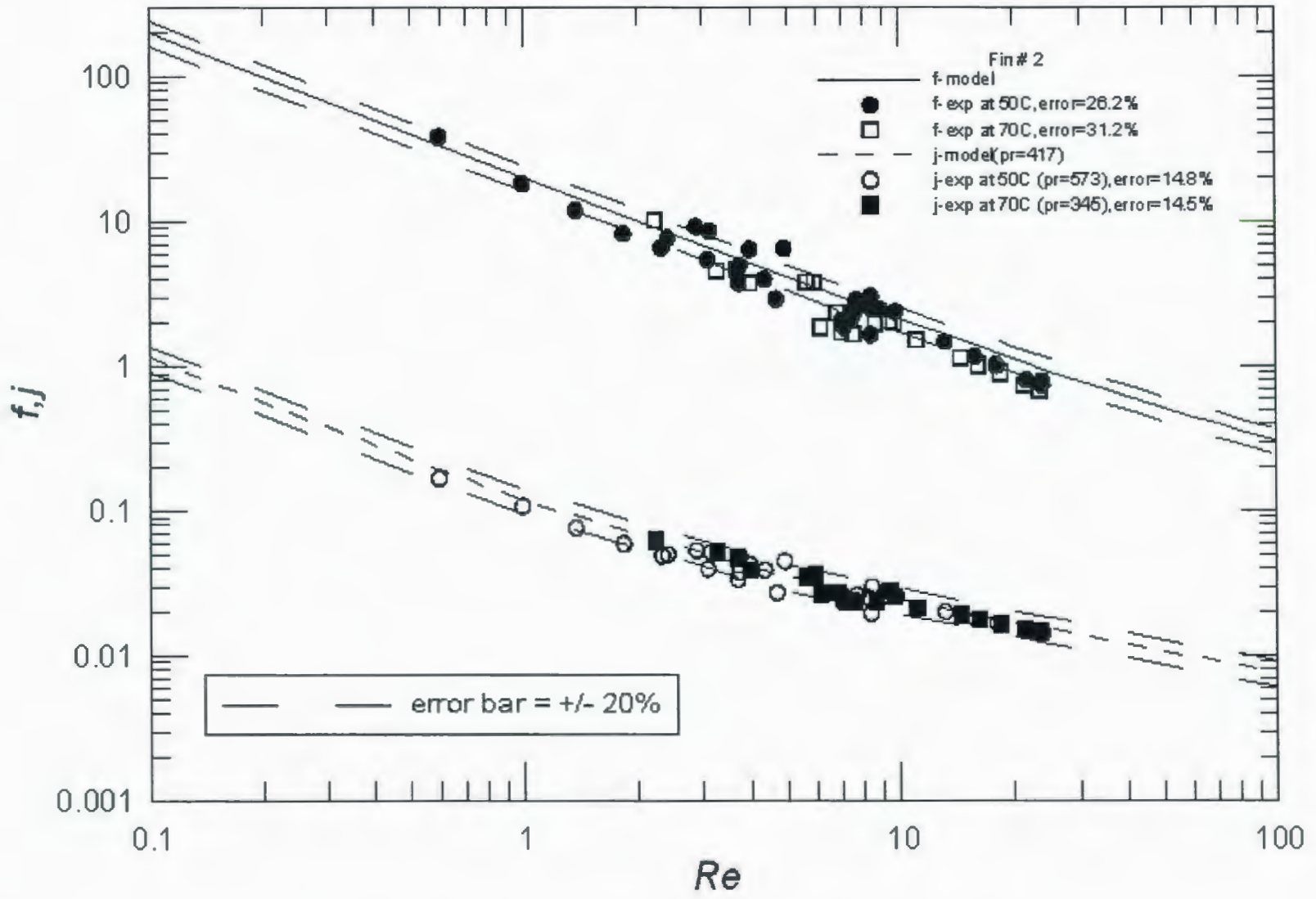

Fig. D.48 – Comparison of Fin # 2 data with models

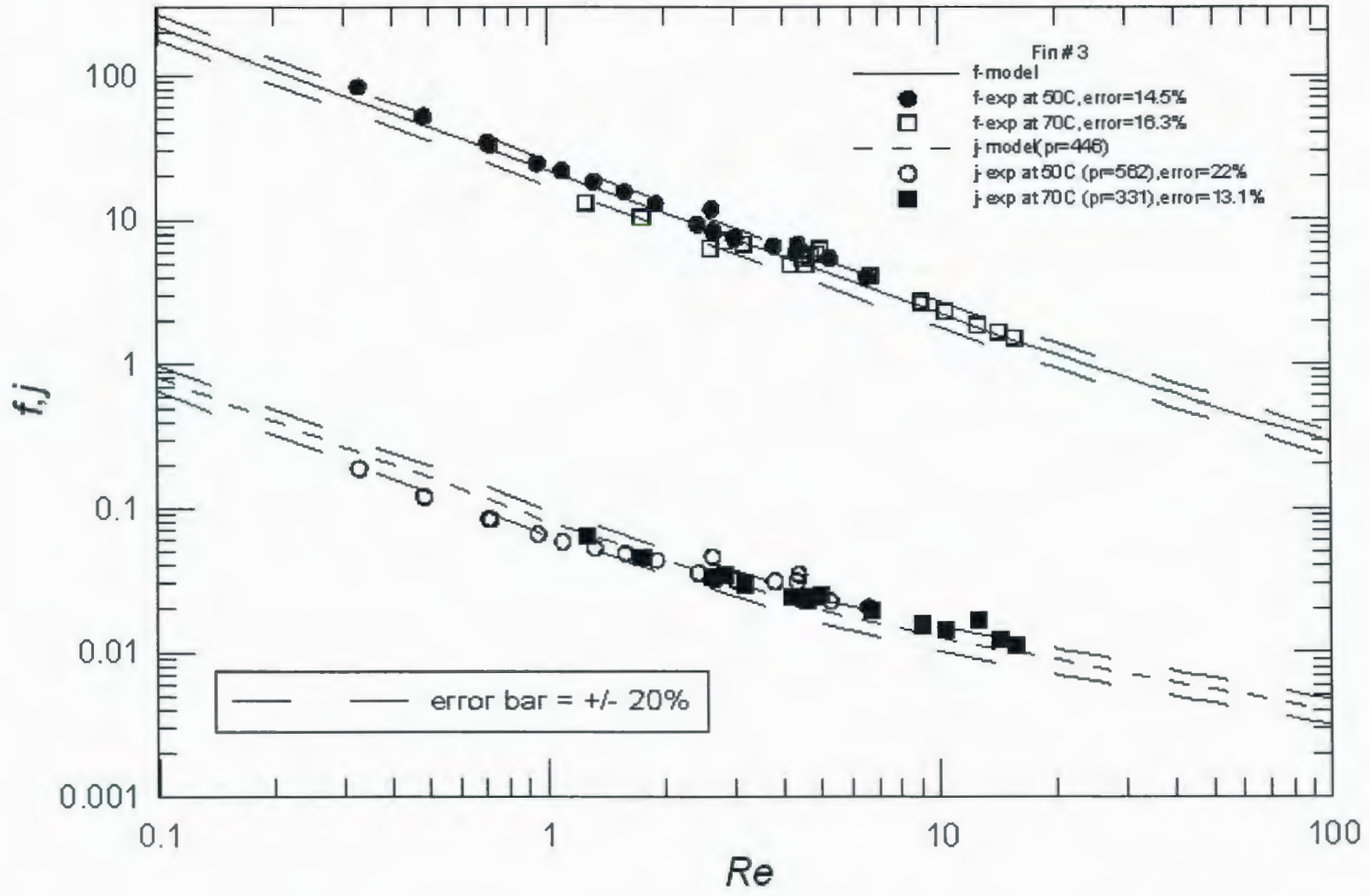

Fig. D.49 – Comparison of Fin # 3 data with models

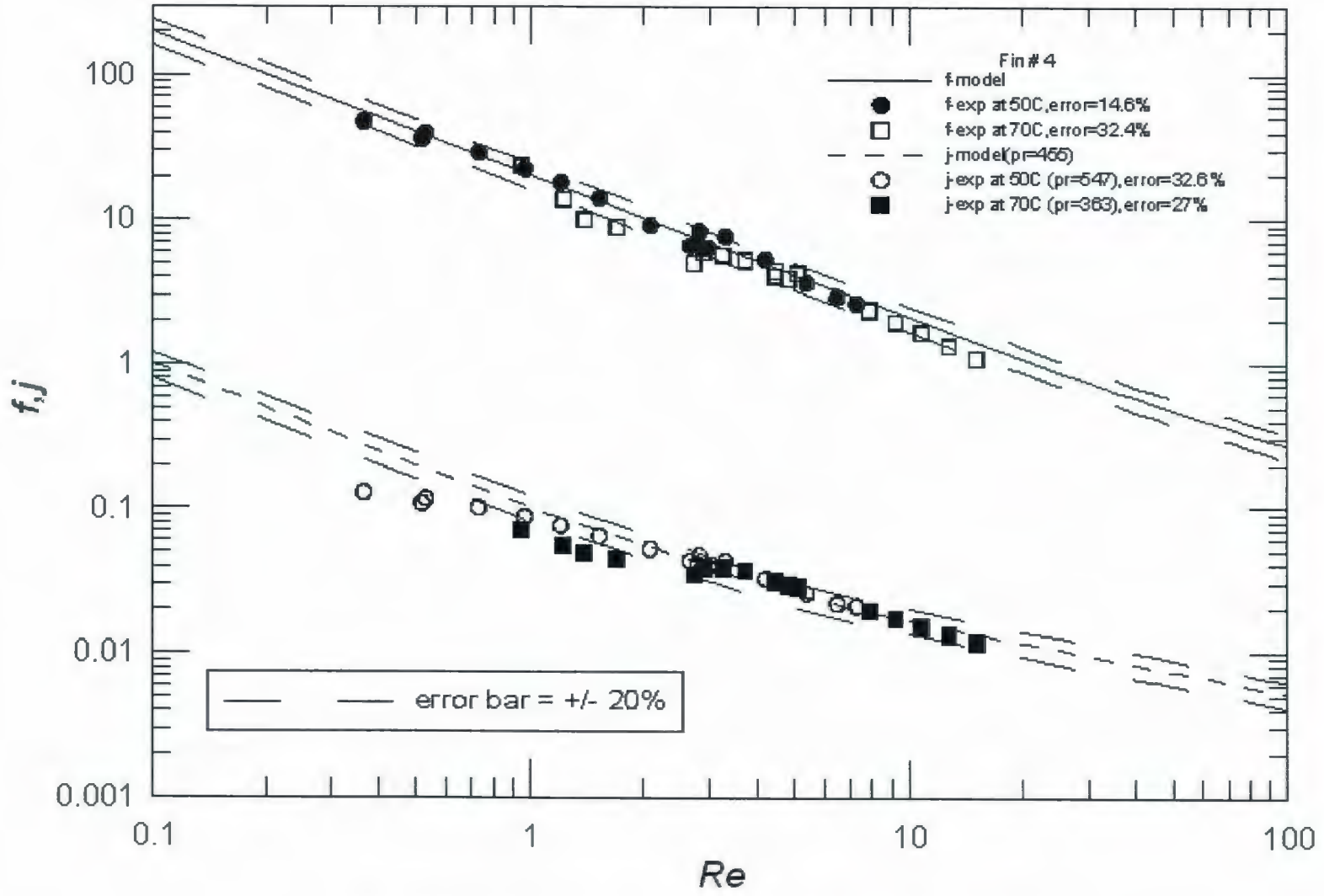

Fig. D.50 – Comparison of Fin # 4 data with models

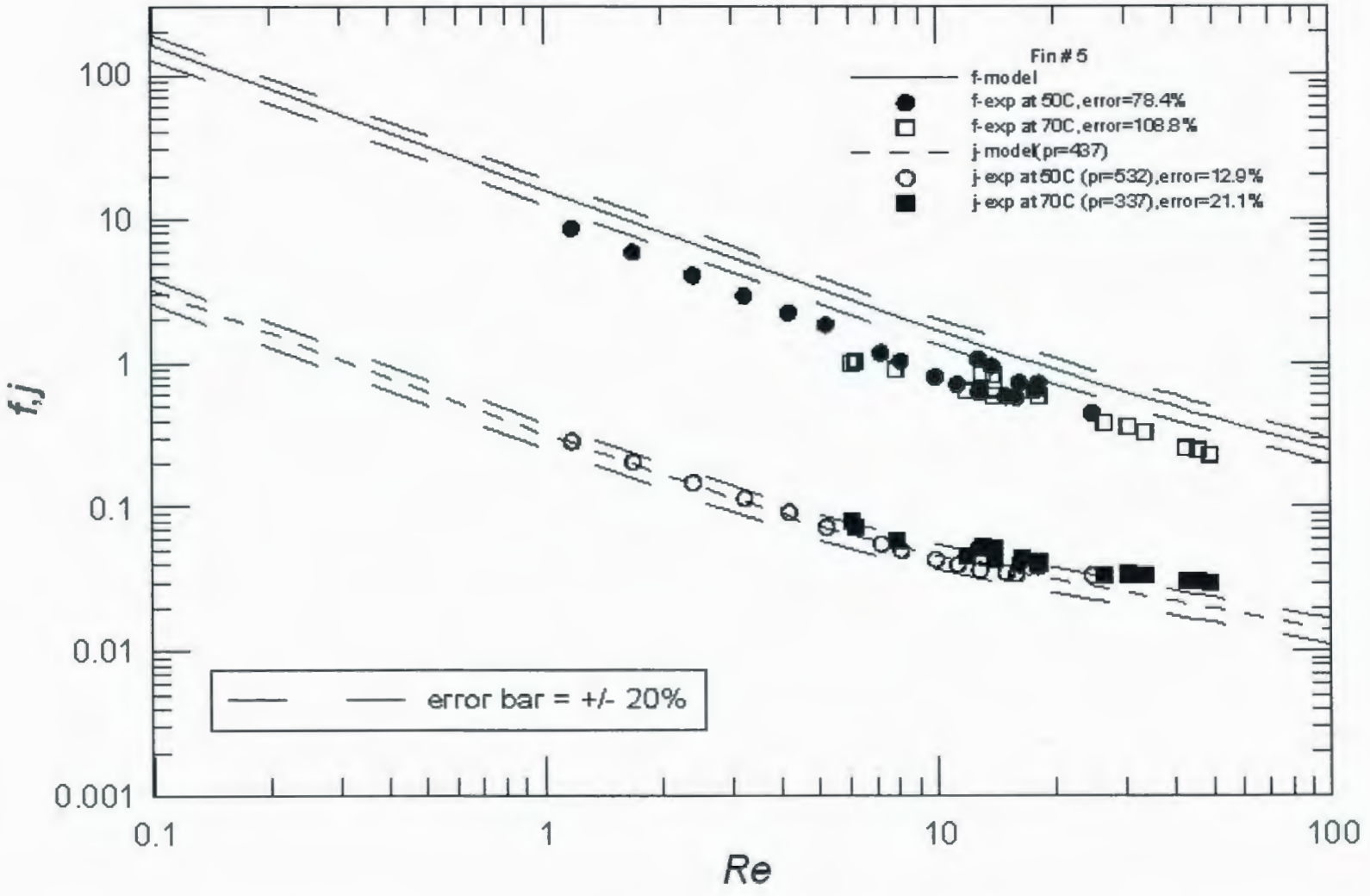

Fig. D.51 – Comparison of Fin # 5 data with models

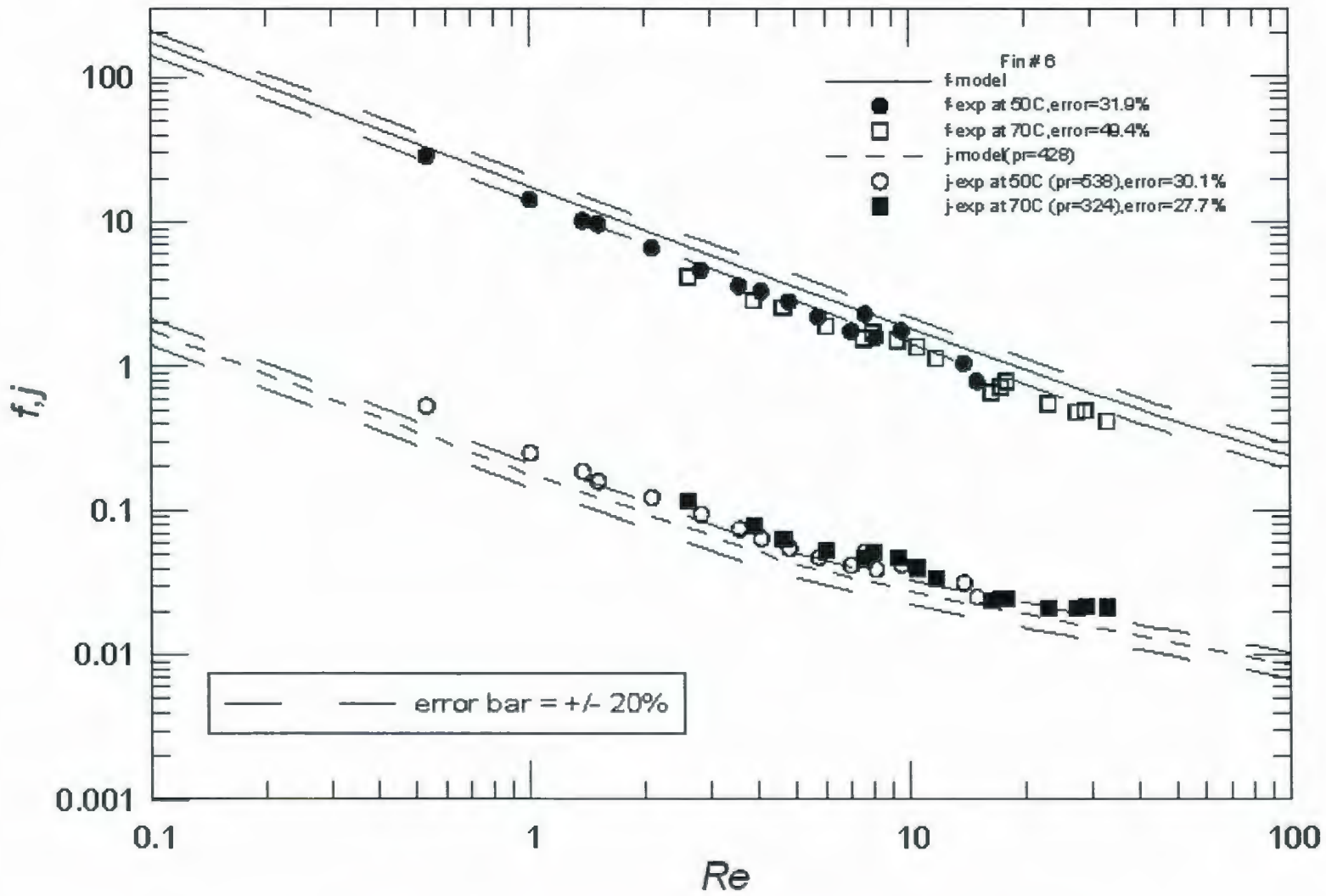

Fig. D.52 – Comparison of Fin # 6 data with models

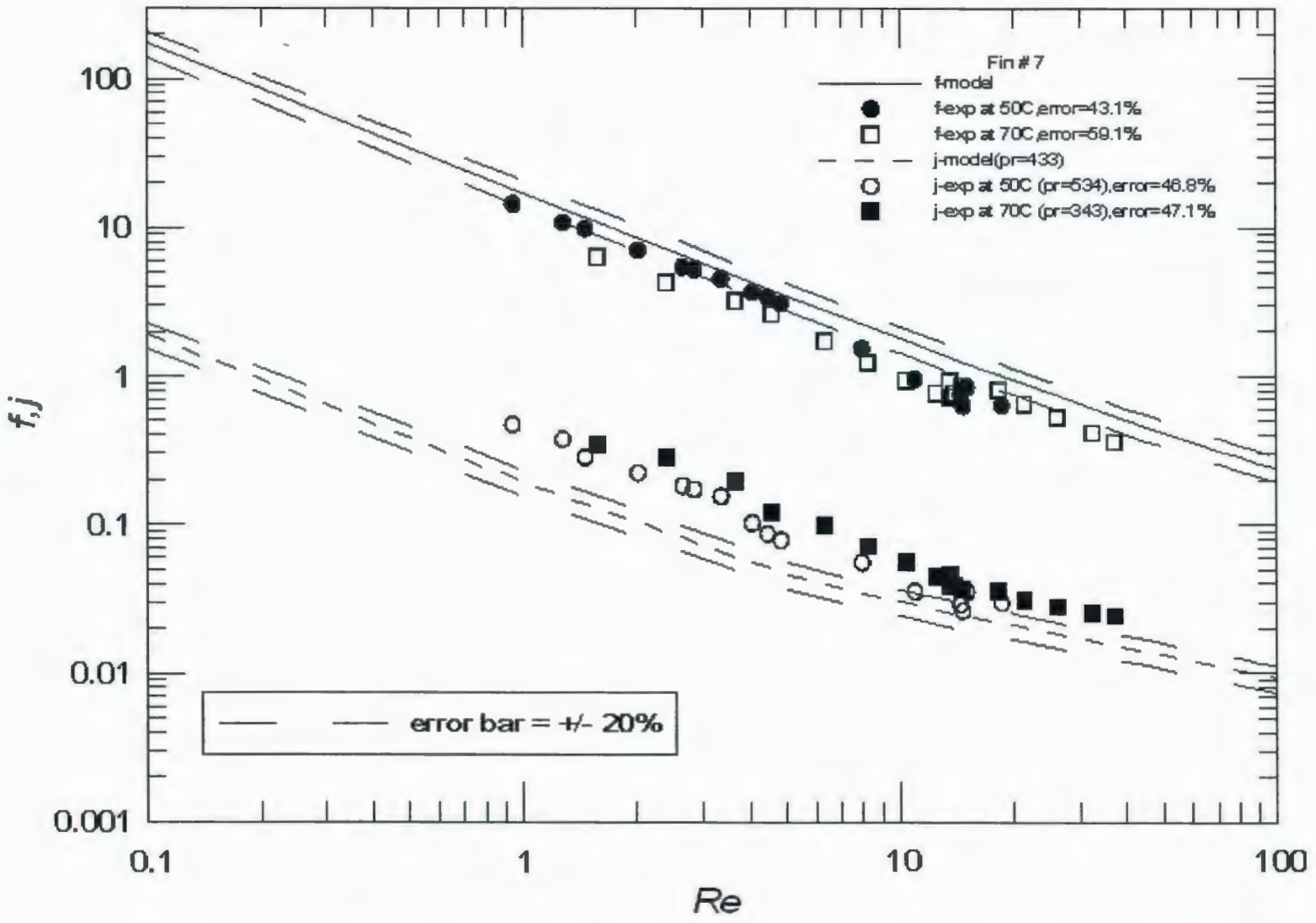

Fig. D.53 – Comparison of Fin # 7 data with models

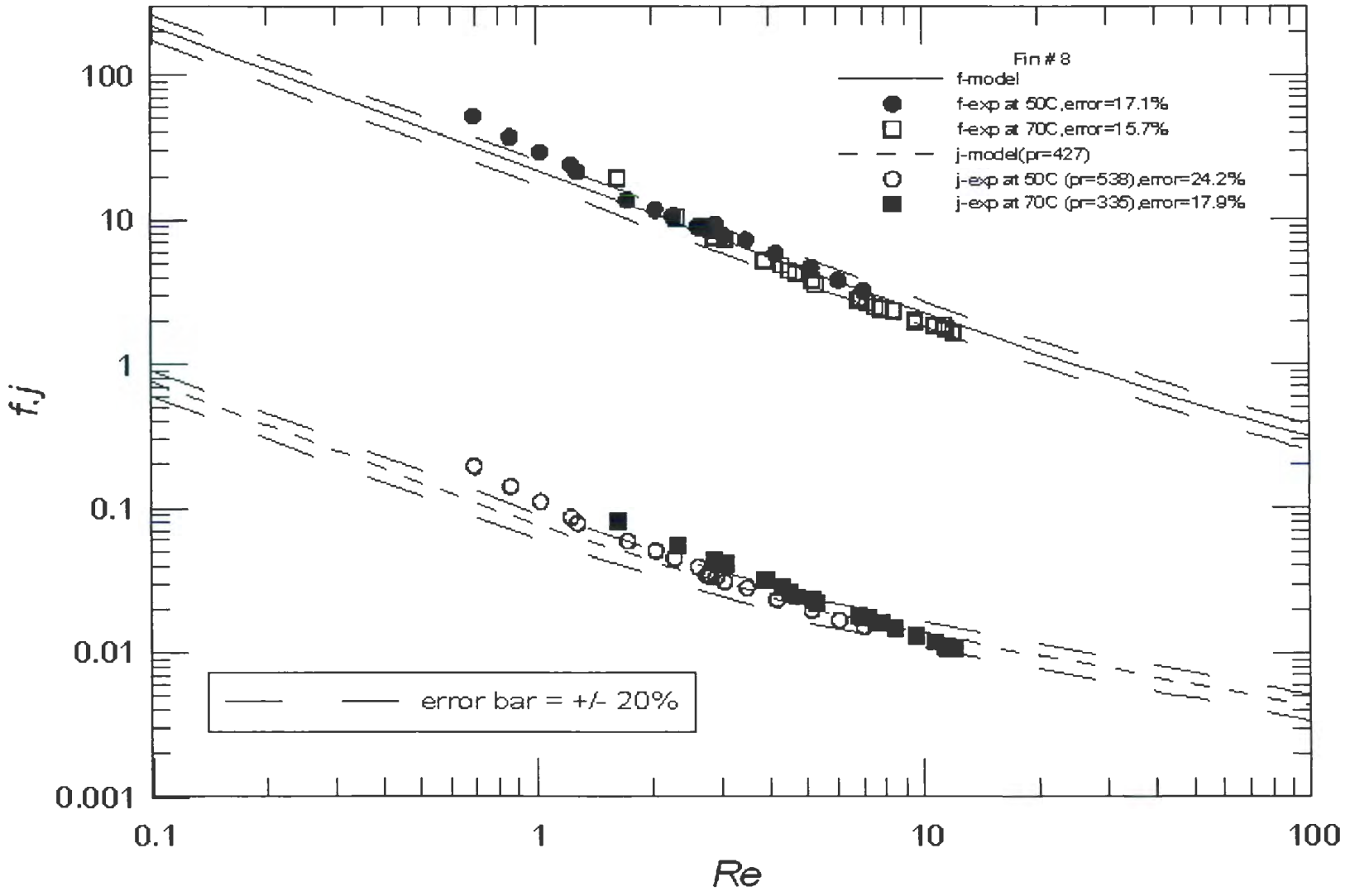

Fig. D.54 – Comparison of Fin # 8 data with models

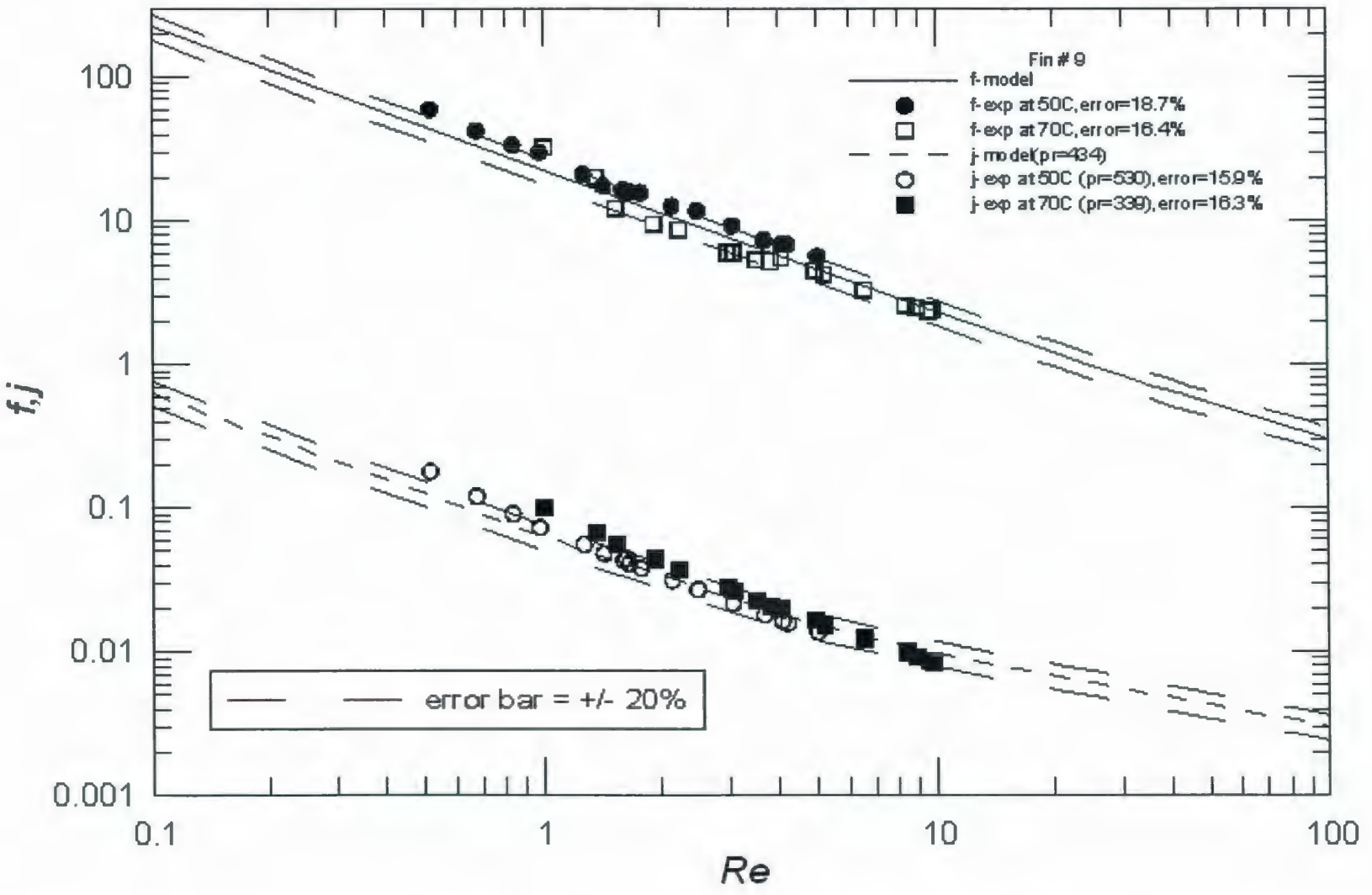

Fig. D.55 – Comparison of Fin # 9 data with models

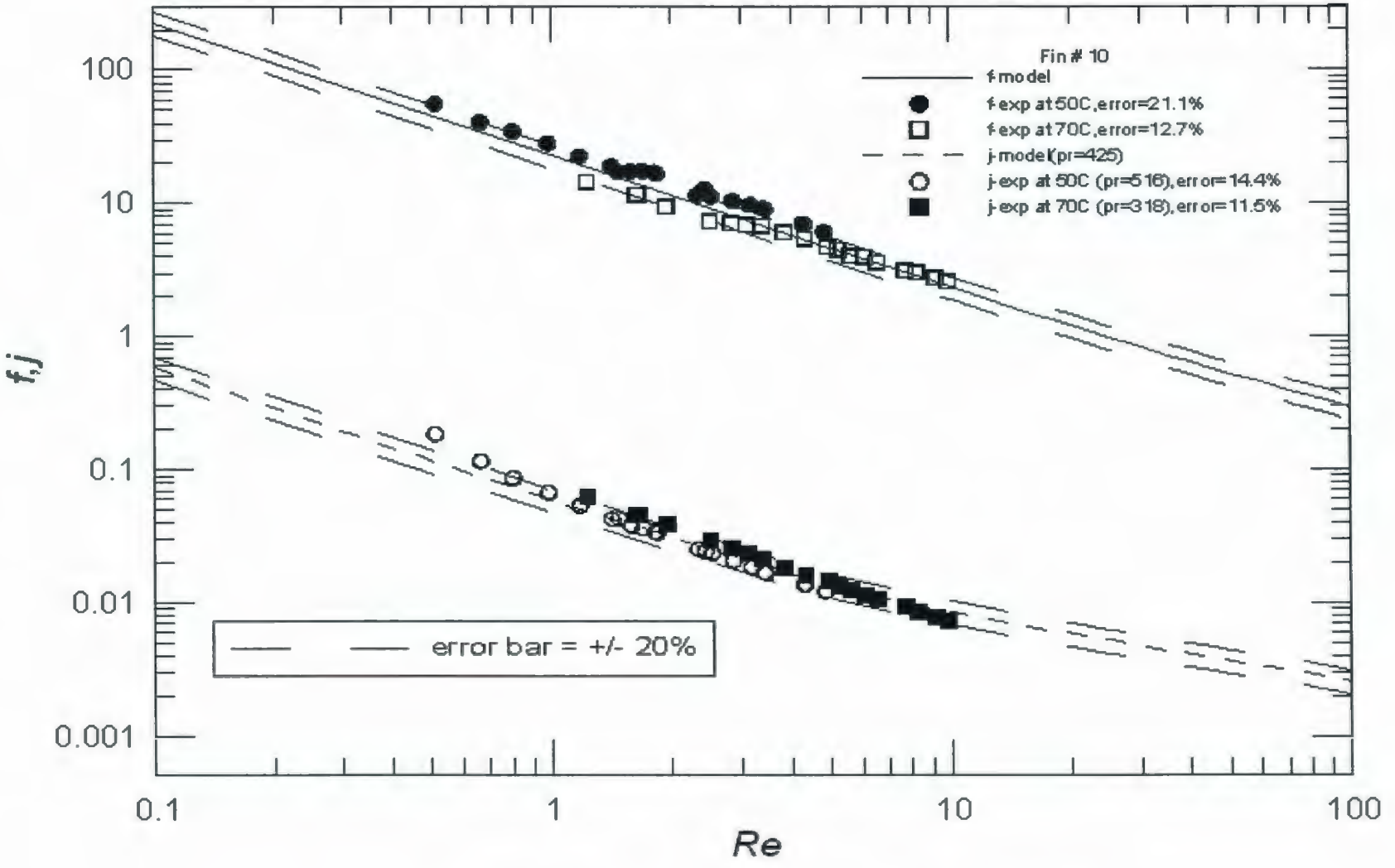

Fig. D.56 – Comparison of Fin # 10 data with models

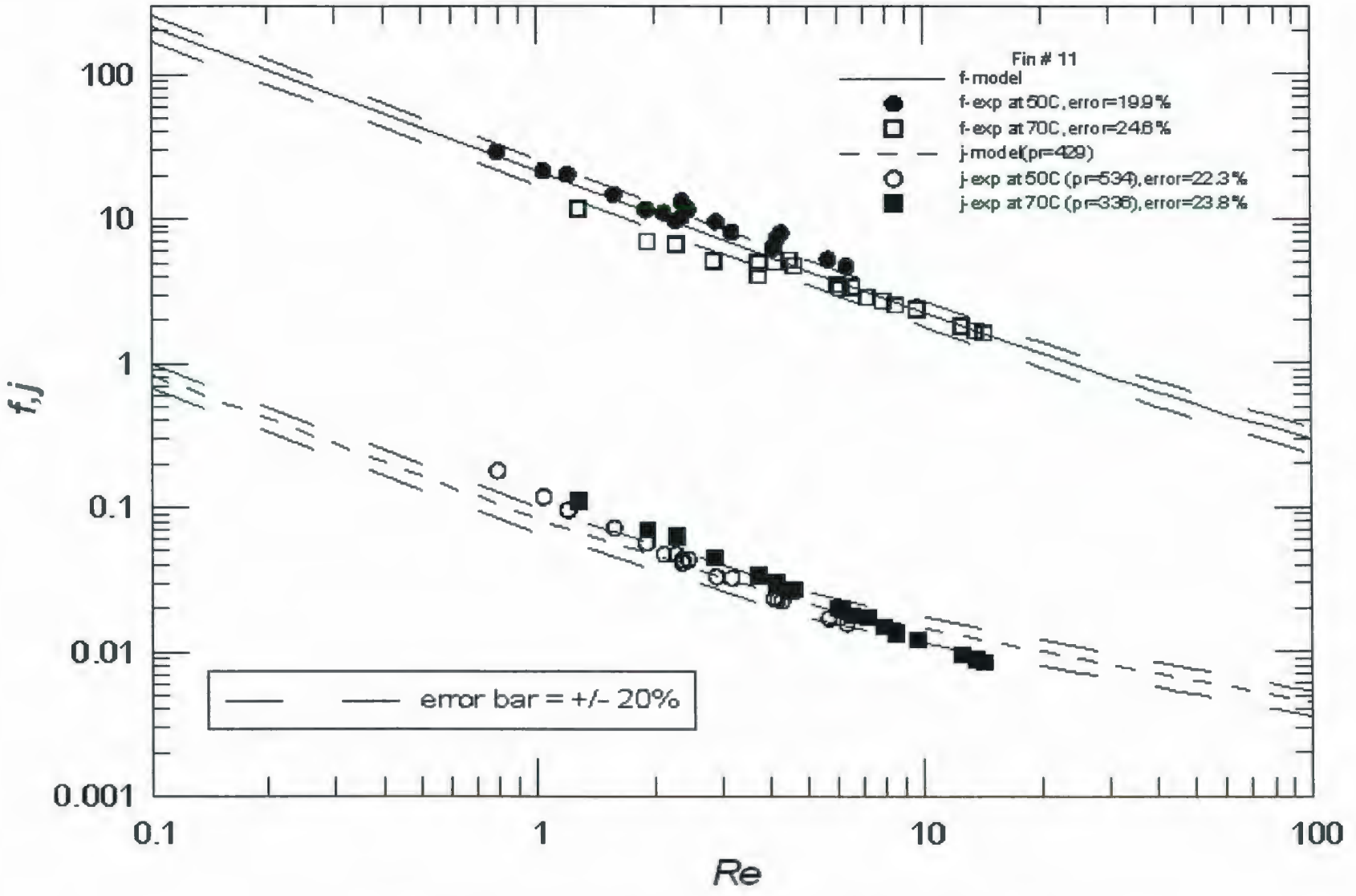

Fig. D.57 – Comparison of Fin # 11 data with models

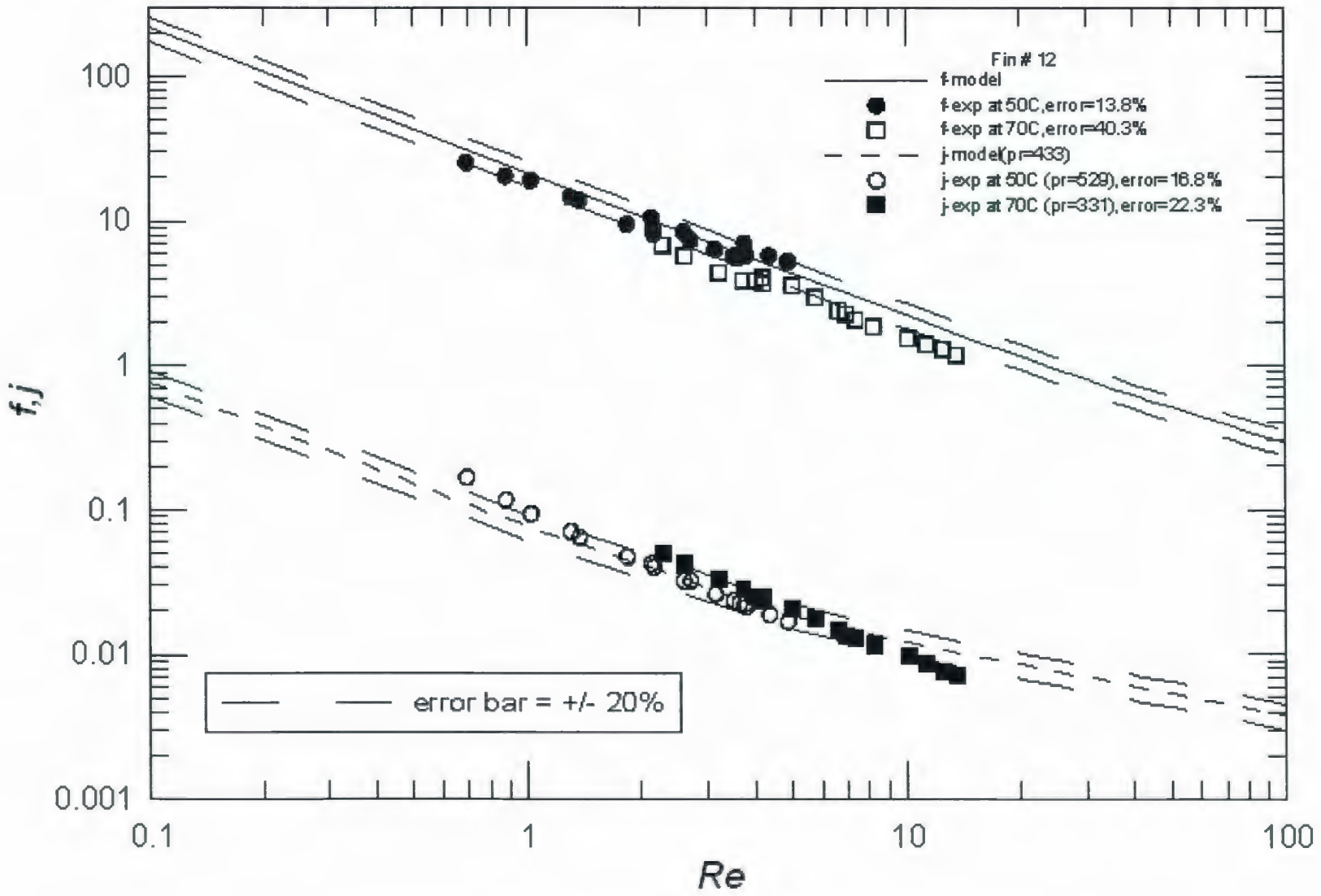

Fig. D.58 – Comparison of Fin # 12 data with models

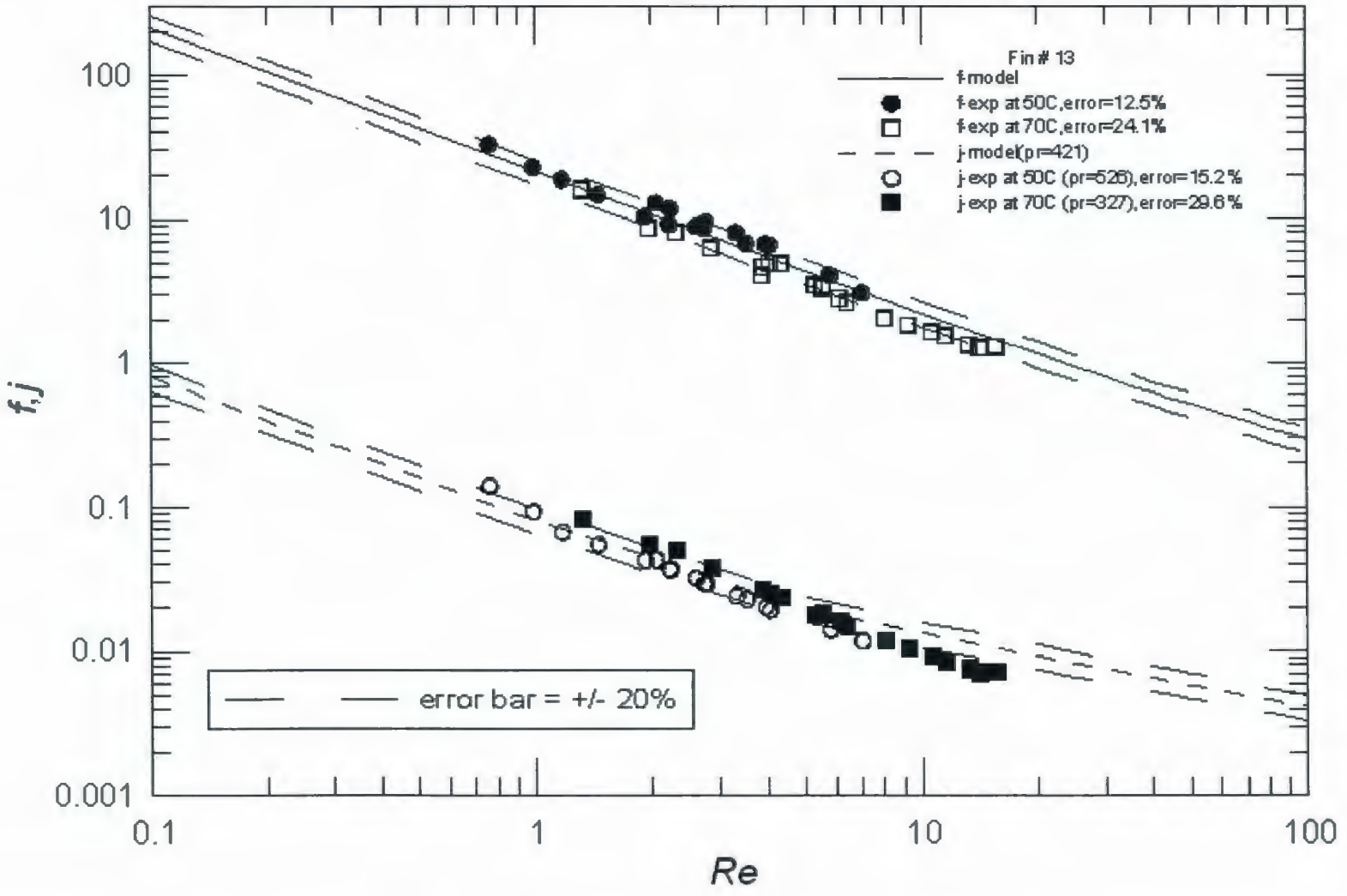

Fig. D.59 – Comparison of Fin # 13 data with models

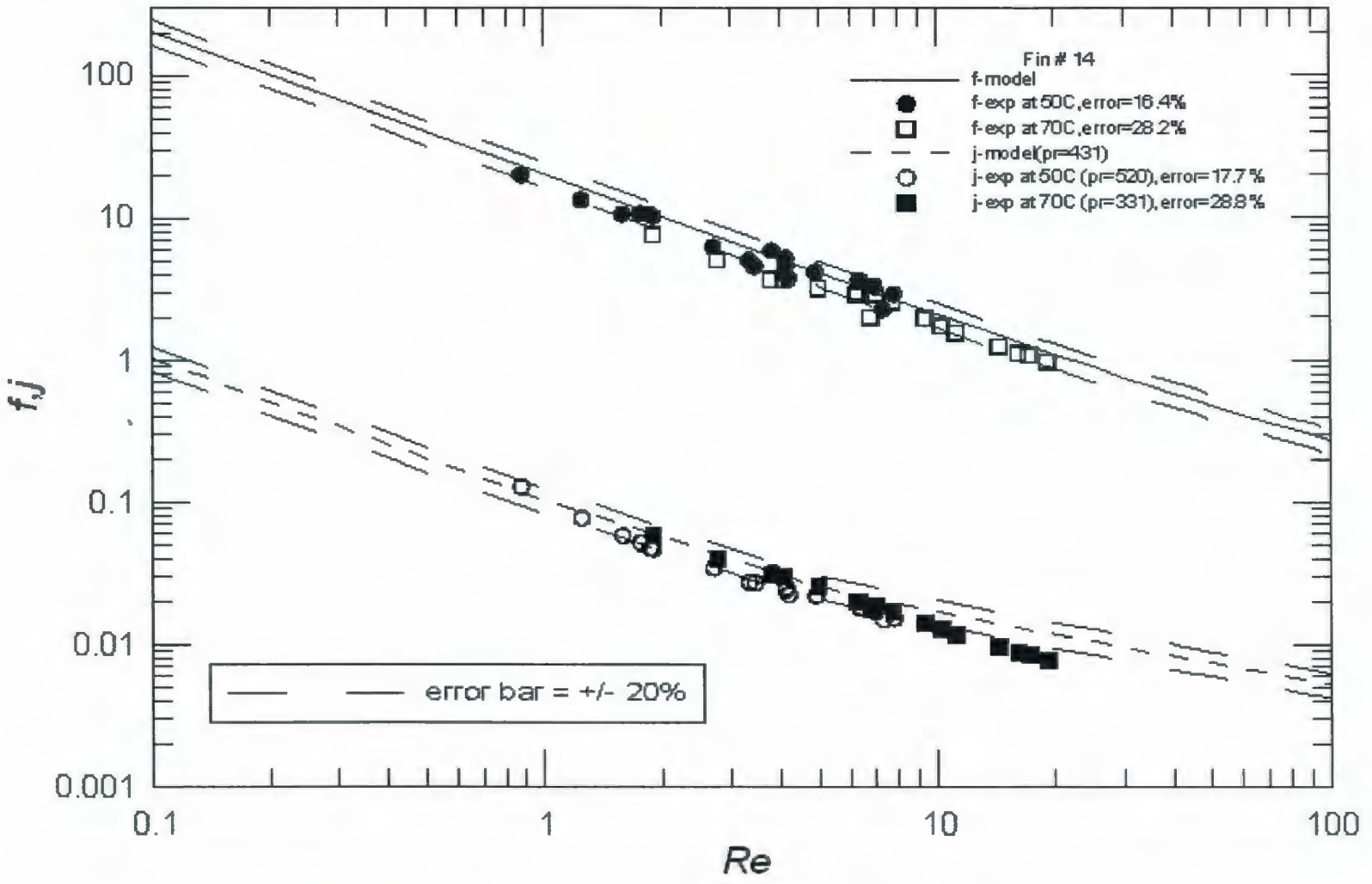

Fig. D.60 – Comparison of Fin # 14 data with models

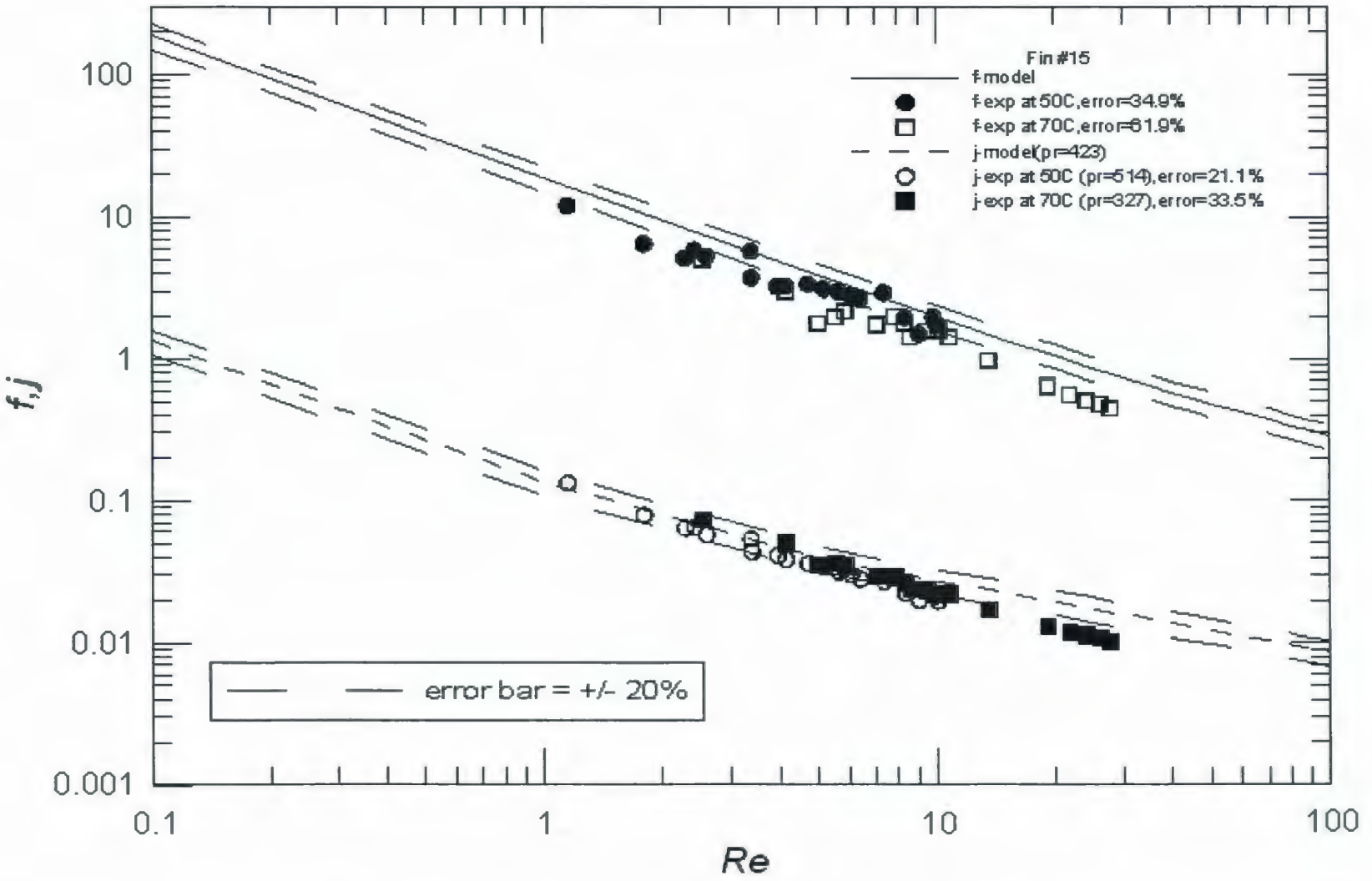

Fig. D.61 – Comparison of Fin # 15 data with models